A Muscular Response Model of the Human Lumbar Spine in the Performance of a Sagittal Plane Dead Lift

Albert R. Carbone

A Thesis

in

The Department

of

Electrical Engineering

Presented in Partial Fulfillment of the Requirements
for the Degree of Master of Engineering at
Concordia University
Montréal, Québec, Canada

April 1984

ABSTRACT

A Muscular Response Model of the Human Lumbar Spine in the Performance of a Sagittal Plane Dead Lift

Albert R. Carbone

A sagittal plane mathematical model of the lumbar spine has been developed. The model computes the resultant forces on the various spinal components as a function of the muscle activity, spinal geometry and external load. Keeping the spinal geometry and external load constant, the resultant forces are used to compute the musculo - skeletal stress as a function of muscle activity. The musculo - skeletal stress is then minimized with respsect to the muscle activity to yield muscle activity patterns.

The muscle activity patterns predicted by the model for low weight dead lifts are compared with available experimental results. Preliminary comparisons show the model able to predict gross muscle behavior. The model has been used to predict the muscle activity patterns required to subject the spine to equalized compression stress at all lumbar levels over a wide range of weights for different spinal geometries.

Acknowledgements

I would like to thank my advisors, Professor S. A. Gracovetsky and Dr. H. F. Fanfan for their many hours of discussion and valuable advice while I did my research.

Mr. Ed Wingrowicz and Mr. Kin Li deserve a heartfelt thanks for the help they gave me in typing the text and preparing the figures as my deadline approached! I would also like to thank Mrs. Madeleine Klein for typing the numerous equations in the text.

Dedication

I would like to dedicate this thesis to my parents and my sister for their love and support during the difficult and often trying times that I had while living the life of a graduate student.

Mom, Dad and Linda ... thanks for everything.

A Muscular Response Model of the Human Lumbar Spine in the Performance of a Sagittal Plane Dead Lift

Table of Contents

C. Derivation of Quadratic Objective Function

D. The Optimization Algorithm

List of Figures.

List of Tables

Chapter 1 Introduction

Low back pain is the leading cause of disability in the United States today, afflicting eight to nine million people [33, 34]. It is the most common disability in persons under the age of 45; in those over 45, it is third only after arthritis and heart disease [10, 33]. It is estimated that two out of three people will have low back pain at some time in their lives, usually between the ages of 20 and 50 [24 ,39]. The fact that back problems are so common in people of working age is not coincidental; most back problems are work-related.

The economic effects of back pain and injury are staggering. Back problems are second only to the common cold as a cause of absenteeism in industry [2, 20, 21, 26, 35]. It is responsible for 93 million lost workdays every year [9, 39] and is the leading cause of reduced work capacity [2, 34]. The average loss in income and benefits is $22,000 per person [34]. Back injury accounts for $1 billion annually in sick pay and wages [24]. Low back pain is the most common cause of workman's compensation payments [34]. In 1976, thirty eight percent of all compensation paid was for back injury [41]. Fifteen to 18 percent of all occupational injuries are back injuries [16]. All occupational injuries are increasing in frequency, but back injuries are increasing faster than any other [16, 41].

Attempts have been made to develop a screening method to identify those likely to develop back pain and to aid in planning prevention. Back X-rays once were touted as such a mechanism. However, extensive research has shown that the findings on X-rays do not correlate with

the development of back pain and are thus useless as predictors [1, 20, 35].

A recently developed screening mechanism is the exercise test, which is based on the premise that weakness of the low back, abdominal, and hip flexor muscles predisposes one to back pain. The exercise test measures the strength of these muscles as well as overall physical condition. Job placement and the need for an exercise program to strengthen muscles are determined by the test results. As yet there is little information as to the predictive and preventive value of this method [9, 24, 35, 40].

Another avenue towards understanding back pain is through the use of mathematical modelling. A useful spinal model would be one that enabled physicians to estimate the health of an individuals' back by analyzing that individuals' spinal geometry and muscular activity while the individual performed some light weightlifting task. This requires the derivation of mathematical relationships between observable data (spinal geometry, EMG signals) and the resulting forces acting on the various spinal components.

This thesis describes the development of a mathematical model of the lumbar spine in the performance of a sagittal plane dead lift. The relevant anatomy of the spine is presented. The types of spinal injuries that occur are discussed. Other mathematical models of the spine are reviewed and the functional requirements of a model are established. The components of the lumbar spine necessary to simulate a sagittal plane dead lift are represented mathematically to form a model

which computes the forces acting on the various spinal components. A control criterion is presented and implemented in a closed loop system to drive the model. Experimental results from an EMG study of subjects performing dead lifts are used for comparison against muscle activity patterns predicted by the model. Although the number of subjects tested is too small to make conclusive statements about the experimental results acquired, some patterns of muscle activity common to most subjects can be discerned. The model is used to predict muscle activity patterns necessary to maintain equalized compression stress at all lumbar levels for a wide range of weights and spinal flexion angles.

Chapter 2 Physiology of the Spine

2.1) Description of the Vertebral Column

The vertebral column is composed of 24 vertebrae, plus the sacrum and coccyx. The first 7 vertebrae constitute the cervical spine, the next 12 vertebrae constitute the thoracic spine and the last 5 vertebrae constitute the lumbar spine. The spine rests on the sacrum, which is composed of 5 fused vertebrae. The coccyx ("tail bone") is composed of between 3 and 5 small fused bones. The vertebral column exhibits 4 distinct curvatures: the cervical curve, the thoracic curve, the lumbar curve and the sacral curve (Figure 2.1).

This thesis deals primarily with the lumbar spine, thus the description will concentrate on those components relevant to the lumbar region.

2.2) Lumbar Vertebrae and Sacrum

The individual vertebrae in the lumbar region have a similar structure. A typical lumbar vertebra has a bony body (the centrum), and a posterior bony ring (the neural arch). The neural arch contains the articular, transverse and spinous processes. The centrum is an elliptical mass of cancellous bone surrounded by a thin shell of cortical bone. The neural arch is composed of two pedicles and two laminae. The seven processes are on these structures (Figure 2.2). Two typical lumbar vertebrae are illustrated in Figure 2.3.

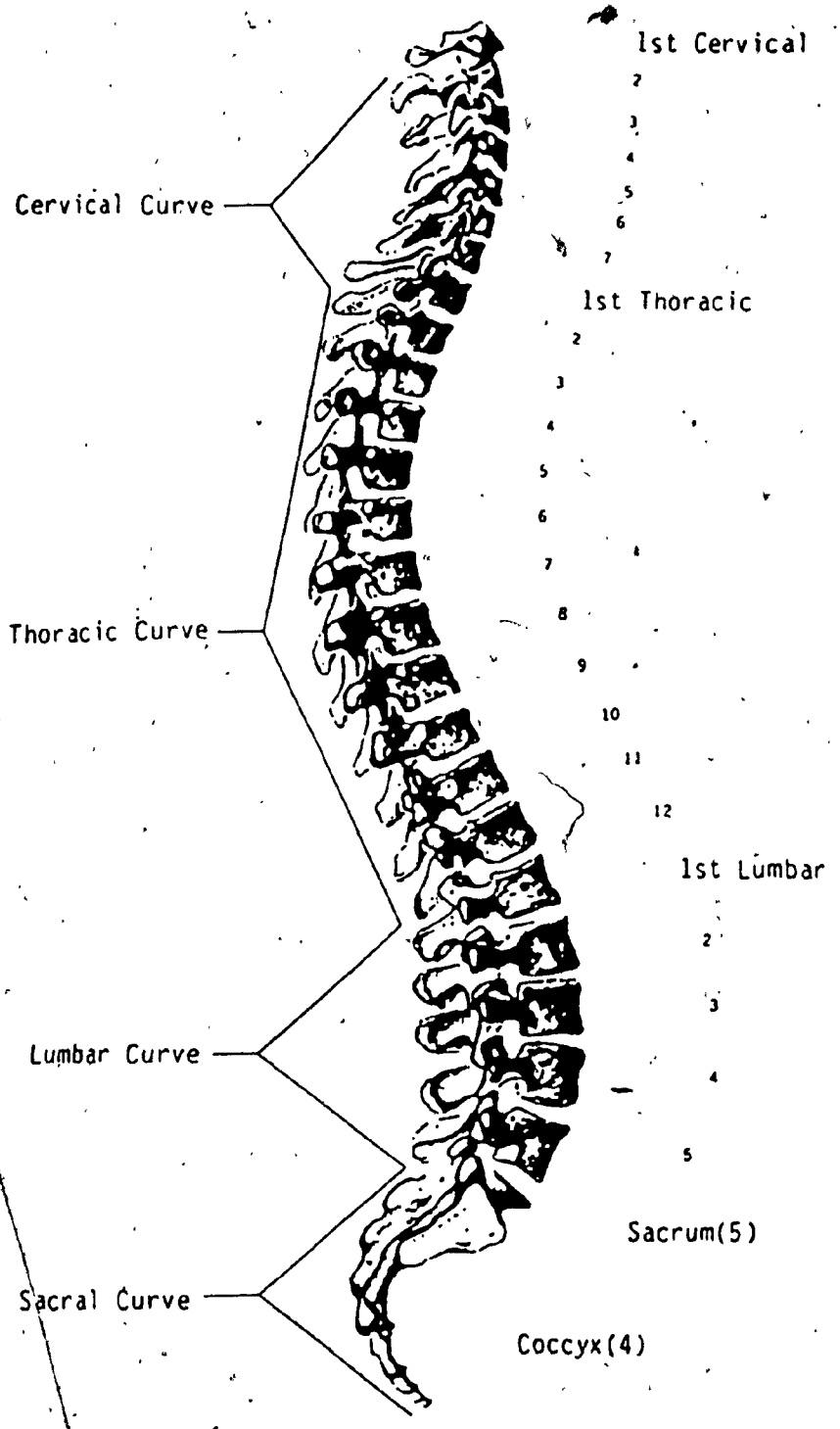

Lateral View of the Spinal Curvatures.
(from McClintic [30])

Figure 2.1

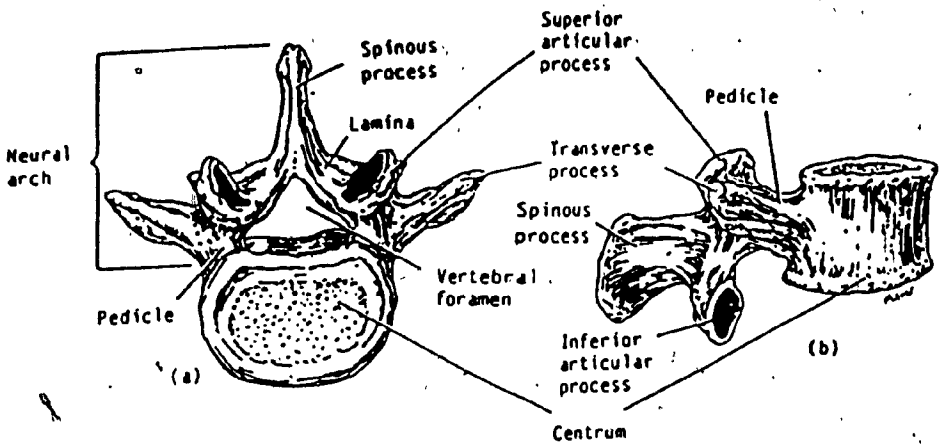

Two views of a lumbar vertebra.
(a) superior view. (b) lateral view.
(from Spence and Mason [37])

Figure 2.2

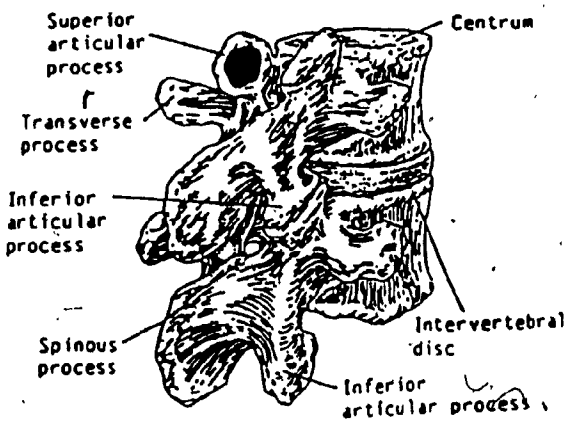

Two typical lumbar vertebrae.
(from Spence and Mason [37])

Figure 2.3

The sacrum is illustrated in Figure 2.4. It is responsible for transmitting any load on the spine to the hips and subsequently to the ground. The sacrum is somewhat wedge shaped and is stabilized in the pelvic gridle by the Auricular surfaces and reinforced by the sacroiliac ligaments. Gunterberg [19] has described the load bearing portions of the pelvic gridle as an arch with lateral pillars and a keystone (Figure 2.5).

2.3) Intervertebral Disc

The intervertebral discs separate the individual vertebrae from one another. The disc is comprised of 3 parts: the nucleus pulposus, the annulus fibrosus and the cartilaginous end plates (Figure 2.6). The nucleus is composed of a network of fine fibrous strands in a micro-protein gell. The lumbar nucleus accounts for between 30% and 50% of the total disc cross sectional area. The annulus fibrosus is made of concentric laminated bands of annular fibers. The fibers are oriented in opposite directions at $\pm$ 30 degrees with respect to the placement of the disc. The annulus fibrosus surrounds the nucleus and forms the outer boundary of the disk. The annular fibers are attached to the end plates. The end-plates in turn are attached to the centrum of the vertebrae sandwiching the particular disc.

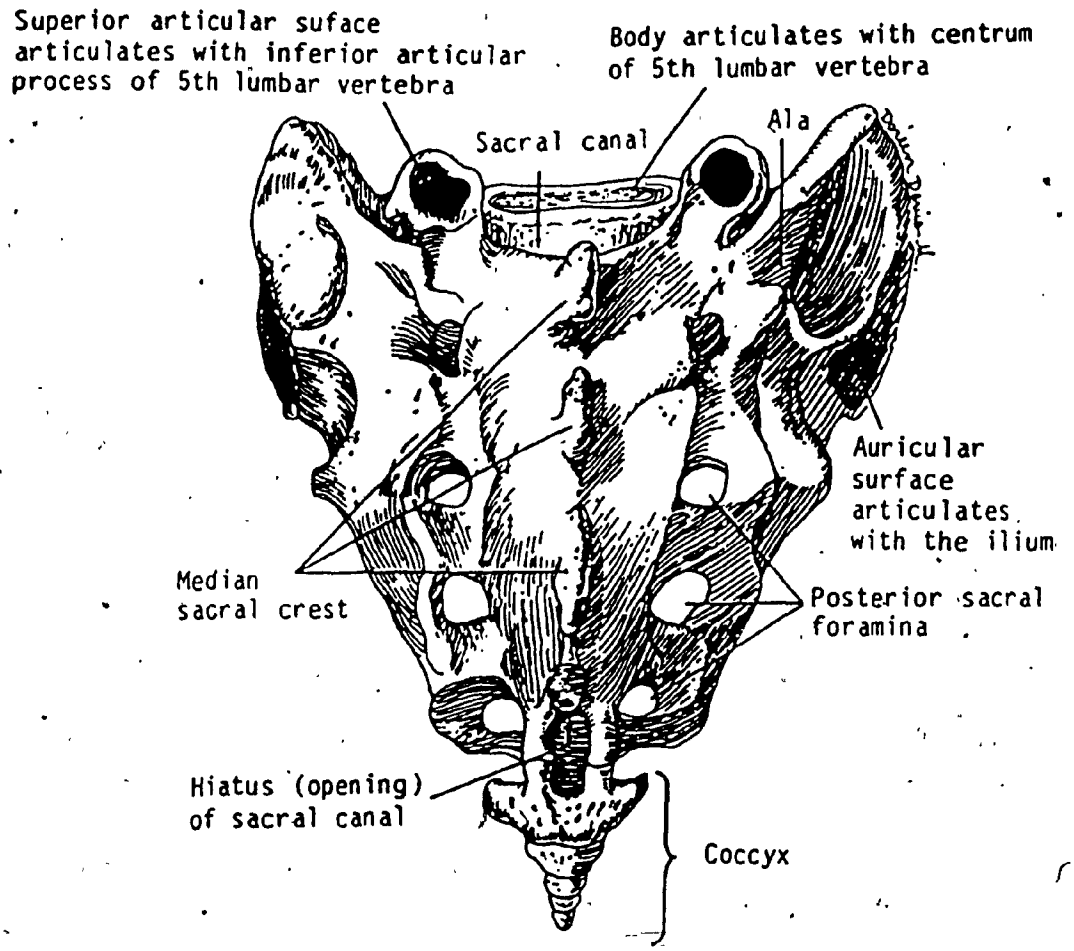

Posterior view of the sacrum and coccyx.
(from Spence and Mason [37])

Figure 2.4

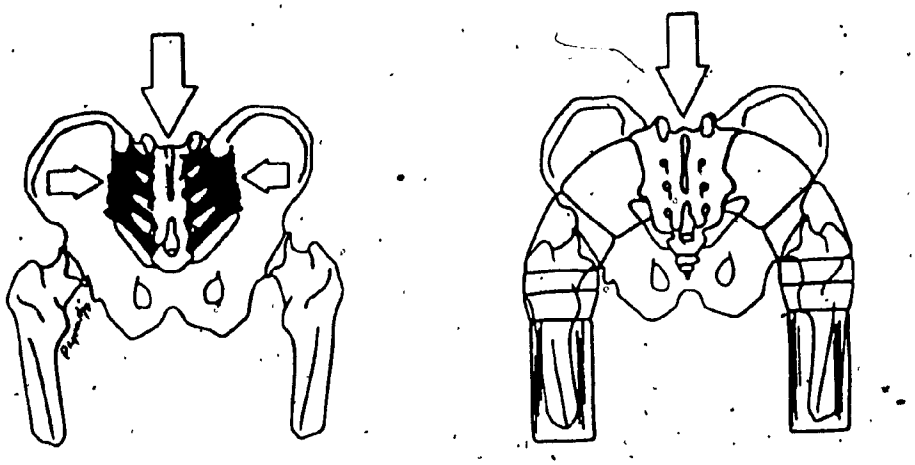

The sacrum as a load bearing member.
(Left) Reinforcement of the sacrum by the sacroiliac ligaments.
(Right) View of the sacrum as the keystone of an arch.
(from White and Panjabi [42])

Figure 2.5

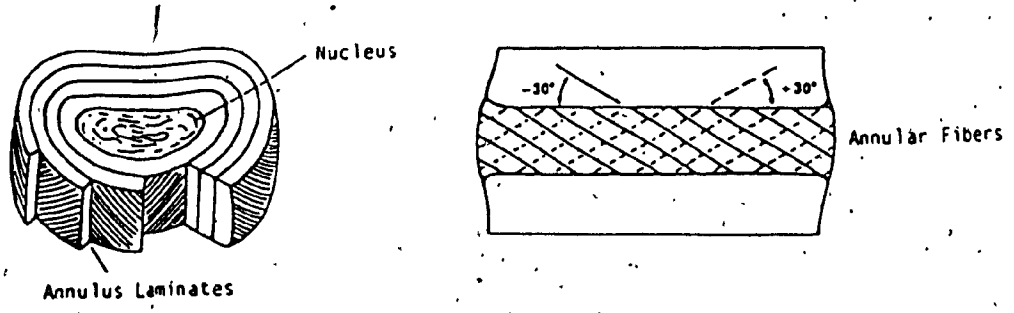

A typical intervertebral disc.
(from White and Panjabi [42])

Figure 2.6

2.4) Spine Ligaments

There are 7 spine ligaments as depicted in figure 2.7. The two important ligaments for this study are the interspinous and the supra-spinous ligaments. Collectively they will be called the midline ligament.

2.5) Lumbodorsal Fascia.

The lumbordosal fascia is a dense ligamentous sheet that surrounds the bulk of the Erector Spinae muscle bundle and joins the midline ligament. As the Erector Spinae muscles contract, they tend to push this ligamentous sheet in the posterior direction (Figure 2.8). The Transversus Abdominis and Internal Obliques muscles insert into the lateral edges of the fascia. When these muscles contract, they act on the fascia to extend the spine (Figure 2.9).

2.6) Muscles

A spine with ligaments but without muscles is an unstable structure. Lucas and Bresler [29] demonstrated that a fresh cadaveric spine without the rib cage that was fixed at the sacrum and oriented vertically could support a maximum load of 4 lbs. placed centrally on the first thoracic vertebra. Any load greater than 4 lbs. caused the spine to be permanently displaced from its central position.

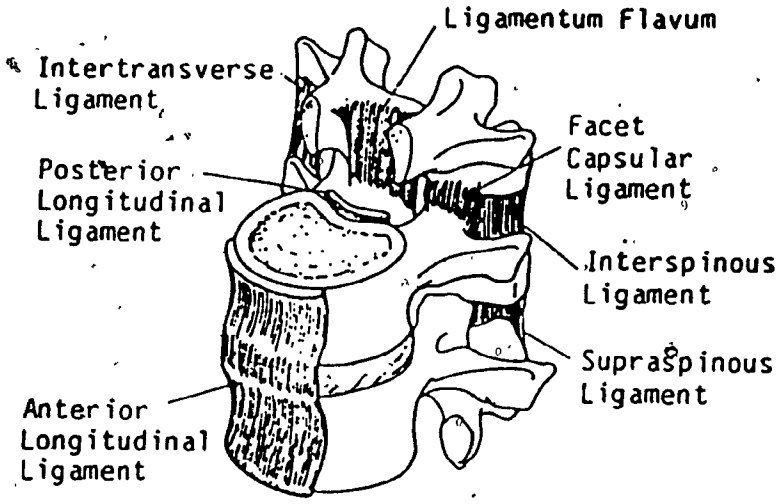

Spine Ligaments.
(from White and Panjabi [42])

Figure 2.7

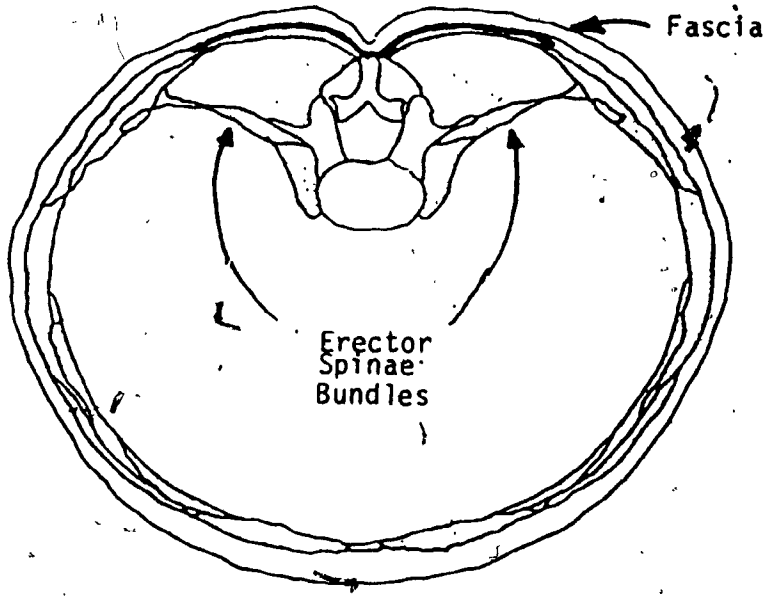

A transverse section through the trunk.
(Modified from Helleur [22])

Figure 2.8

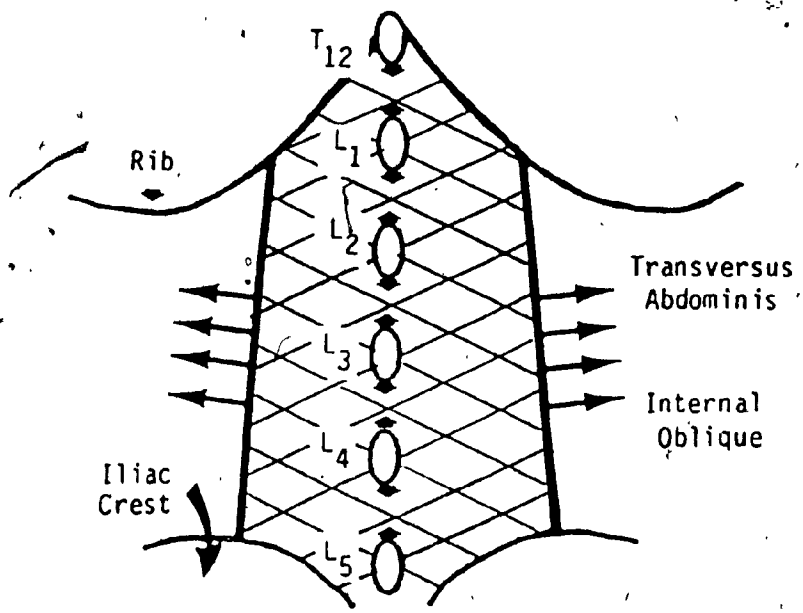

The Fascia arrangement.
(from Gracovetsky et al [17])

Figure 2.9

It is obvious that muscular action is needed for movement and maintenance of the upright posture of the spine. The muscles that control the motion of the lumbar spine can be identified by their location, either anterior or posterior to the spinal column. The anterior muscles are the four abdominal muscles: External Oblique, Internal Oblique, Transverus Abdominis and Rectus Abdominis. The posterior muscles are: Iliocostalis Lumborum, Sacrospinalis, Medialis Spinalis (these 3 constitute the Erector Spinae bundle), Multifidus, Quadratus Lumborum, Latissimus Dorsi. The Psoas muscle cannot be classified as an anterior or posterior muscle due to its unique location, but, none the less, it also controls the motion of the spine. The muscles considered in this thesis are illustrated in chapter 5.

Chapter 3 Types of Spinal Injuries

3.1) Compression and Torsion Injuries

Common back disorders are a result of the mechanical failure of the spine. Two common disk injuries have been identified which correspond to two different types of mechanical failure of the spine: the compression injury and the torsion injury.

The compression injury starts centrally with a fracture to the end plate, sometimes followed by injection of part of the nucleus into the vertebral body. Neither the annulus nor the facets are damaged (Figure 3.1).

The injured end plate permits the invasion of the avascular nucleus and the avascular inner portion of the annulus by granulation (healing) tissue. The effect of this is to dissolve or hydrolyse the avascular portion of the disk. With progression the disk loses its thickness while the outer layers of the annulus remain relatively well preserved. With loss of disk thickness the facet joint subluxates and becomes arthritic.

The fracture of the end plate is an undisplaced fracture of cancellous bone which heals rapidly. The symptoms are short lived, typically lasting two weeks. The facet joint arthritis appears late; at this stage symptoms may also arise from a reduction in size of the spinal canal (lateral and central spinal stenosis).

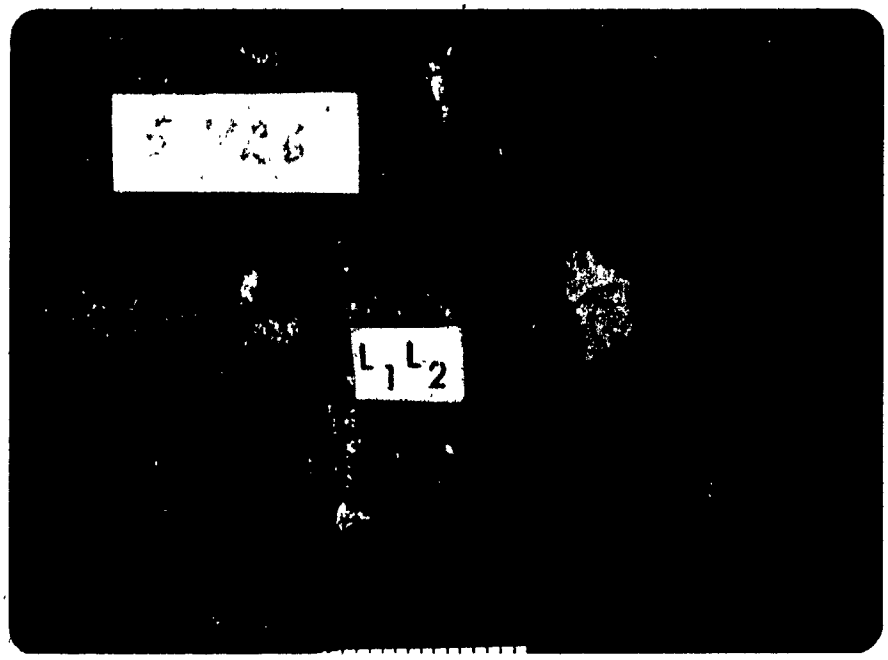

Compression Injury

Figure 3.1

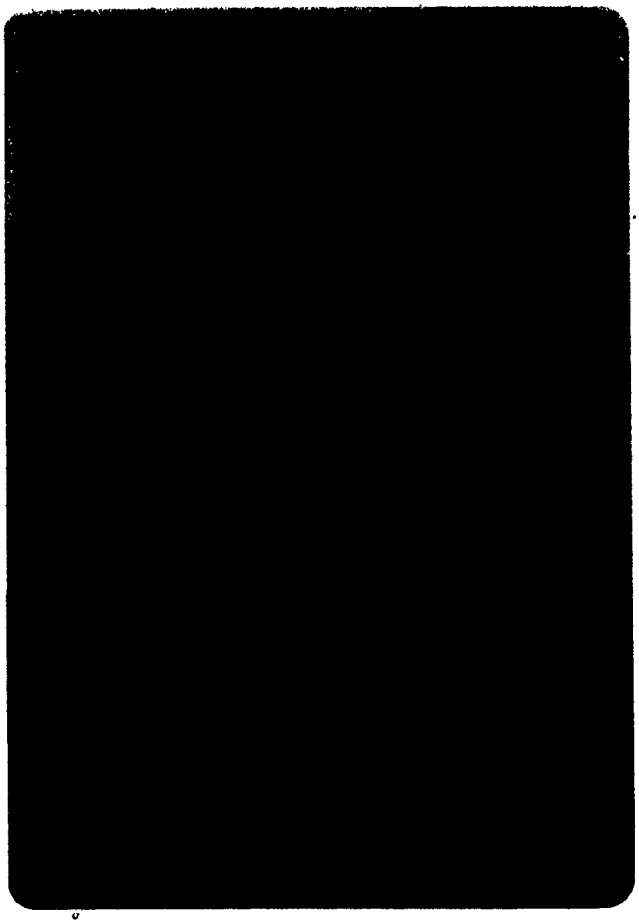

Torsion Injury

Figure 3.2

The torsion injury is characterized by damage of the annulus occurring simultaneously with damage to the facet joint. The outer rings of the annulus are torn off the vertebral end plate, and separation occurs between the laminations of the annulus. There is no damage to the nucleus or to the end plate. The facet joint shows subchondral fracture, with consequent collapse of the articular surfaces and chronic synovitis (Figure 3.2).

The basic injury here is to collagenous ligamentous tissue which requires six weeks to regain 80% of its strength. Because the injury involves both the disk and the facet joint, it is more difficult for the joint to stabilize itself and recurrence is frequent. The condition is progressive, and may lead to spinal stenosis, instability, and degenerative spondilolisthesis.

In the laboratory, a compression injury is easily produced by compressing the joint between 300 lbs/in^2 to 900 lbs/in^2 [36]. Given that an average vertebra has an area of 3.5 in^2, this translates into loads of between 1050 lbs and 3150 lbs. The torsional injury can be seen with as little as 2 to 3 degrees of forced rotation requiring only 195 to 300 inch-lbs of torque [14].

3.2) Relative Frequency of Injuries

In a series of 100 patients [13, 28] 64% exhibited torsional injuries and 35% exhibited axial compression injury. The torsional injury occurs mainly at the fourth level. Almost 100% of fourth joint

problems are torsional injuries. Almost 100% of the compression injuries occur at the L_5/S_1 level. Double injuries (that is, joint injured with both compression and torsion) occurred in 22% of the cases; these double injuries were invariably at the L_5/S_1 level.

Table 3.1 reflects the probabilities of injuries (any injury, compression, torsion) amongst patients complaining of backache and sciatica, or sciatica alone. The important frequency of torsional injury cannot be overlooked. This table suggests that the probability of a third type of injury giving symptoms is remote. A third type of injury has so far not been recognized in autopsy material.

It is to be noted from the above description of pathology that both types of injuries can give rise to identical symptomology. Hence symptoms cannot be used to diagnose a type of injury because identical symptoms may arise from different injuries.

Therefore the injury caused by a certain task cannot be identified from the patient's symptoms. Because of this basic difficulty it is not possible to relate directly tasks to the injury mode. Such a relationship is central to the definition of tasks that will not injure any given individual.

JOINT	P(injury)	P(compression)	P(torsion)
L_1/L_2	< 1 %	< 1 %	< 1 %
L_2/L_3	< 1 %	< 1 %	< 1 %
L_3/L_4	< 5 %	< 1 %	< 1 %
L_4/L_5	47 %	< 1 %	76 %
L_5/S_1	47 %	98 %	22 %
	100 %	100 %	100 %

Clinical Determination of the various probabilities of injury.

Table 3.1

Chapter 4 Modelling of the Spine

4.1) A Review of Spine Models

The evolution of spine models over the years can be followed in the literature. Early models by Latham [28] and Hess & Lombard [23] were of the continuum type. This approach assumed the spine to be a continuous rod or beam that had homogeneous material properties. Latham modelled the spine as a vertical weightless spring with two masses, one at either end. The top mass represented the body and the bottom mass represented a seat. This model was subjected to high accelerations in the axial direction in an attempt to obtain dynamic load factors for the spine as a function of the spring constant. The model could not deal with non-axial loads. The human spine has a natural curvature to it which causes the internal loads to be non-axial in nature. The Latham model is structurally inadequate to describe the response of the spine to axial acceleration. Hess & Lombard modelled the head and trunk as an elastic rod. They curve fitted experimental data of head displacement during impact accelerations and used this information to tune model parameters to yield the same results. But the spine is neither a beam nor an elastic rod. The continuum models cannot simulate physiological behavior.

The next type of model that became popular was the discrete parameter type. This approach treats the spine as a structure composed of various elements. These elements (vertebral bodies, intervertebral discs, ligaments) are assumed to have different material properties.

Toth [38] and Aquino [5] modelled the vertebrae as rigid bodies and the intervertebral discs as springs and dashpots. They ignored the muscles and ligaments. Belytscho et al [8] modelled the ligaments as springs and the contents of the abdominal cavity as stacked hydrodynamic elements. The main problem with these models is that they ignore the fact that muscles can exert forces.

The basic philosophy of the continuum and discrete parameter models is the simulation of the human spine through the study and modelling of the material properties of the constituent members of the spine. This is the fundamental flaw. These models are spring/dashpot or elastic rod representations of a living system capable of generating internal forces independent of external forces. The muscles, under the active control of the central nervous system, act on the spine. This constitutes a control system. Thus a control system approach should be used to model the spine.

The muscular response models incorporate the control system approach. In these models, the spine is represented as a series of rigid bodies (the vertebrae) that are hinged to each other by intervertebral joints and held together by muscles and ligaments. The muscles and ligaments are described by lines of action between their points of origin and insertion on the skeleton. The muscles are assumed to exert forces based on their activity level. Given a vector of muscle activity levels, the moments and rection forces are calculated at the joints. Some control criterion is formed based on these moments and reaction forces as a function of the muscle activity levels. This

control criterion is then expressed in terms of an objective function and minimized with respect to muscle activity levels through the use of optimization techniques. The output of the optimization is a muscle firing strategy that minimizes the objective function. Thus the control system.

Avrikar and Seireg [6] used this approach to model the spine of a seated individual. They formed a control criterion based on the sum of the muscle forces, the sum of the reaction forces at the joints and the sum of the moments at the joints. The resulting objective function was linearly dependant on the stress levels in the joints and muscles.

Gracovetsky et al [18] developed a sagittal plane model of the lumbar spine in the performance of a dead lift. The forces generated by the weight lifted are supported by the ligaments, muscles and IV joints. The range of motion of the lumbar spine and the measurements required to locate the various muscles and ligaments are obtained from sagittal plane radiographs of a subject performing an actual dead lift. The cross sectional areas of the muscles are obtained from cross sectional anatomical slices. This allows the representation of the muscles and ligaments as vector forces with the resultant of all these forces estimated at the bisector of the disc. The forces generated by the weight lifted are estimated at a line joining the hip and shoulder, the movement of which is followed in lateral photographs. The forces along this hip - shoulder line are then translated to each of the five lumbar segments and decomposed into their shear and compression components.

An objective function based on the resultant shear force at each lumbar segment, the muscular stress and the ligament moment induced all as a function of muscle activity is minimized through the application of an optimization technique. The result is the distribution of moments between ligaments and muscles which produce a minimum of shear at the bisector of the intervertebral joint. The hypothesis here is that the human uses a feedback mechanism to monitor the shear and thus select the best combination of muscles and ligaments to accomplish the given task. This constitutes the basis of a control system (Figure 4.1).

The Gracovetsky model database incorporates radiographs and measurements taken of a weightlifting champion. The choice of the weightlifter was deliberate, giving the researchers the opportunity to tune their model. They hypothesized that the weightlifter was a champion because he used his system in an optimal fashion: at his maximum lift all his biological resources were used to their maximum level, but the risk of injury at the same time was reduced to a minimum level.

While the hypothesis of shear minimization could not be tested by direct measurements, the deductions from theory were subjected to experimental verification. The Gracovetsky model was used to simulate certain measurements observed on volunteers performing light tasks. The following results were obtained.

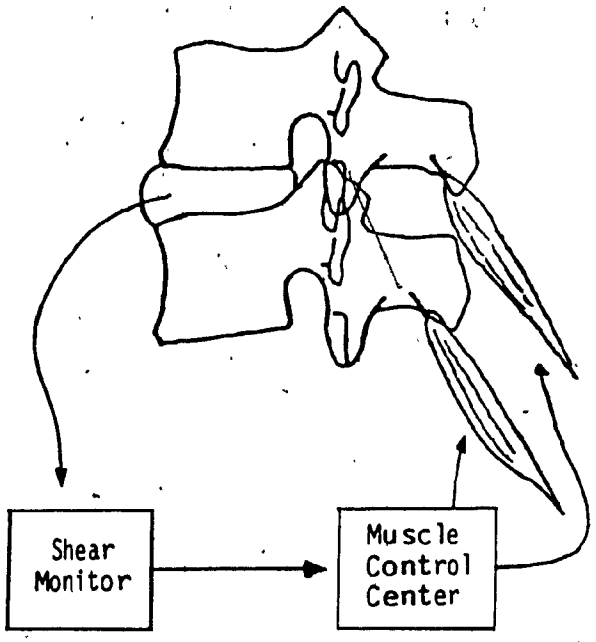

Feedback Monitor of
Intervertebral Joint Shear

Figure 4.1

1. Integrated EMG pattern.

The calculated integrated EMG value of the Sacrospinalis and the Multifidus was found to be substantially linear for a range of weight lifted between zero and 90 pounds. This linear relationship has been confirmed by Andersson [4]. In addition, it was found that by using a conversion factor of 1 μV = 1.28 lbs/in^2, the calculated muscle activity could be superimposed on the experimental data (Figure 4.2).

2. Disc pressure

As early as 1960, Nachemson [32] found experimentally a linear relationship between disc pressure (measured in the nucleus pulposus) and weight supported by the spinal column in the case of small weights. The calculations of the model confirm this finding.

The researchers did not place too much emphasis on the importance of disc pressure because they did not believe that the disc pressure truly described the instantaneous load carrying capacity of the joint.

3. Abdominal pressure

A linear relation between internal abdominal pressure (IAP) and weight lifted has been reported for small weights [3]. The calculations indicated that as the weight lifted increases, the IAP tended to a maximum not exceeding 9.7 to 11.6 lbs/in^2.

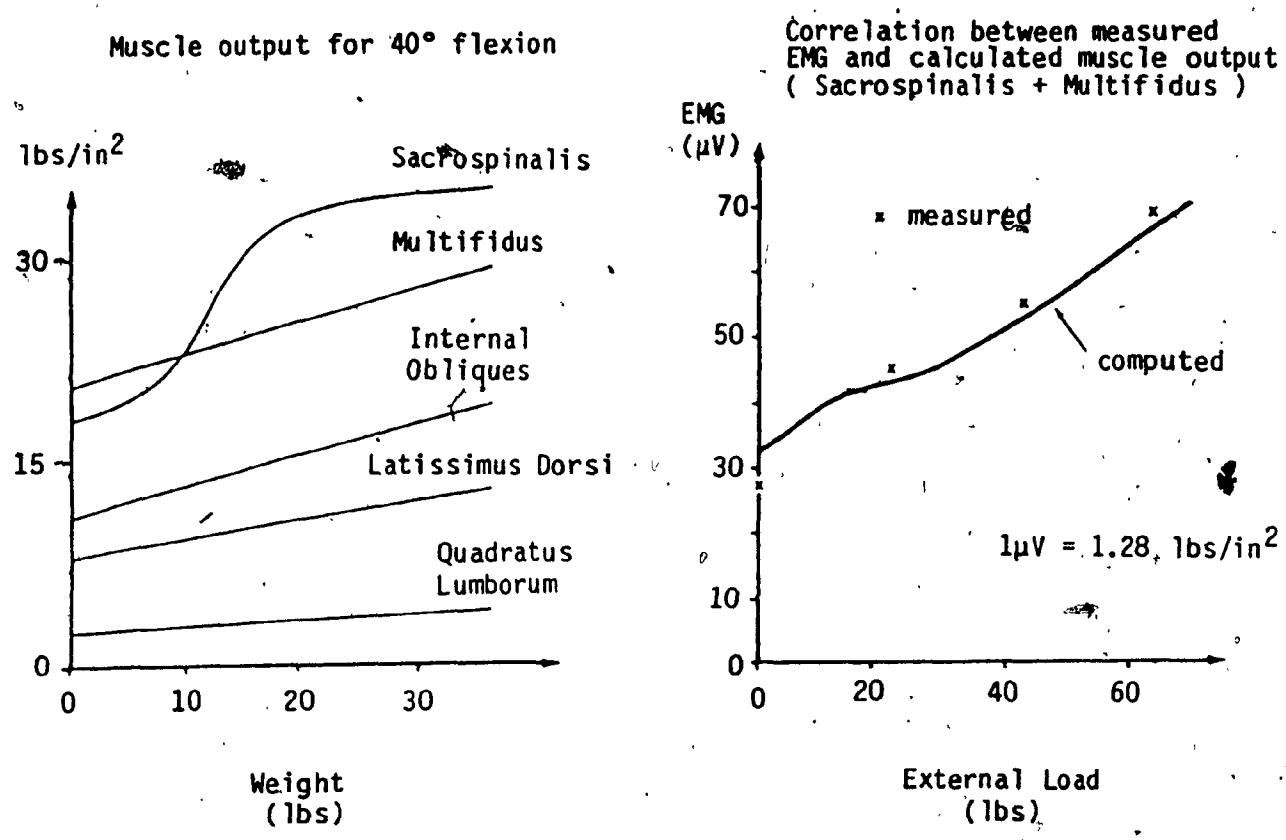

Comparison of calculated and measured EMG patterns.

(Left) Relationship between the muscle output as the external load increases for a spinal flexion angle of 40 degrees. (Right) The solid line is the summed Sacrospinalis and Multifidus output from the graph to the left. The measured points were acquired experimentally using EMG techniques by Andersson et al [4]. (Modified from Gracovetsky et al [18]).

Figure 4.2

4- Moment of the erectores.

The maximum extension moment required for weightlifting has been estimated by McNeill et al to be 2250 in-lbs at L5/S1 [31]. Gracovetsky et al predicted this value with their own calculations. The model calculated that the moment value of 2250 in-lbs occured at two points: the maximum static lift of 120 lbs, and the maximum dynamic lift of 400 lbs.

5- The $ALPHA_0$ position.

An important feature of the model is the $ALPHA_0$ angle. This is the angle of spine flexion, the hip-shoulder angle, at which the midline ligament is first brought under tension (Figure 4.3). At this significant point in the motion, the moment may be balanced by either ligament or muscle, and is accompanied by a change in EMG output. In full forward flexion with all muscles relaxed, ligament tension is just sufficient to support the moment due to bodyweight. This angle was measured in the weightlifter to be 45 degrees compared to a model prediction of 47 degrees.

Despite the fact that the model appeared to calculate results in the physiological range, the researchers were unsatisfied with certain aspects of its behaviour. They are:

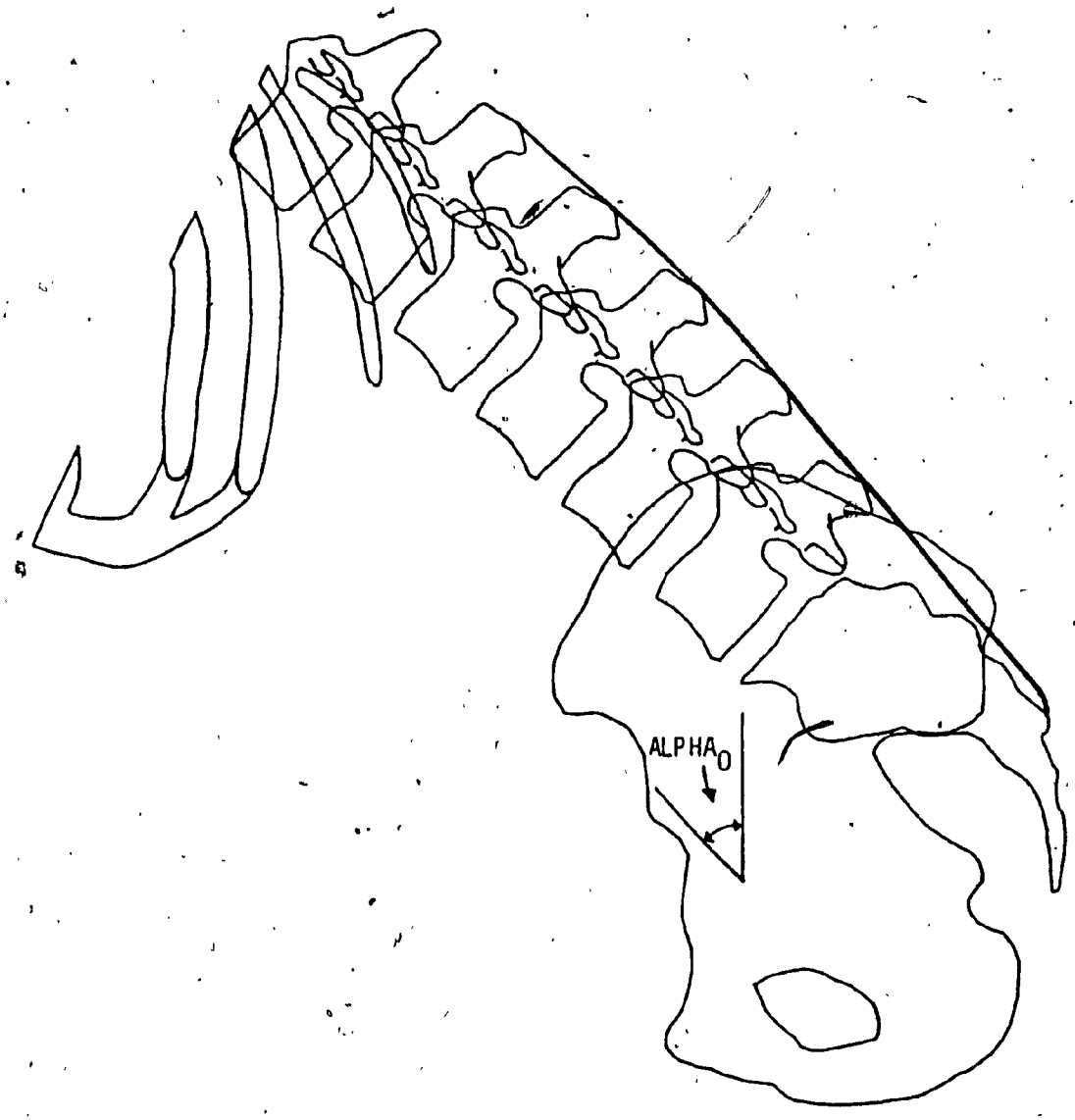

Definition of the ALPHA$_0$ angle

The angle of forward flexion at which the midline ligament is first brought under tension is defined ALPHA$_0$.

Figure 4.3

1) The pattern of EMG calculated from the force of muscle contraction did not exhibit the muscle relaxation noted by Floyd and Silver to occur in full forward flexion [15].

2) For weights below 120 lbs the model could not equalize the compression stress at all levels whereas for weights above 120 lbs, the model gave equalized stress at all levels.

3) The switchover mechanism from muscle to ligament strategy appeared abrupt rather than smooth as was expected.

Acquiring the database was a long and laborious task. Computer implementation of the model was clumsy due to the size and structure of the database and the generation of simulation results used inordinate amounts of computer time. Four areas that could be improved were recognized. They are outlined below:

1) The motion of the dead lift was approximated by taking eight sagittal plane radiographs of a subject performing a dead lift. The radiographs recorded the spinal geometry in the upright position and at forward flexion angles of 10 to 70 degrees (in increments of 10 degrees). Measurements were then taken from each of the eight radiographs to build the database for the model. Building a database for a new subject required a whole new set of radiographs and associated measurements.

2) Locating the same point on eight different radiographs was difficult due to the low quality and resolution of the radiograph images. Muscle and ligament attachment points had to be averaged over the resulting cluster of points measured on the eight radiographs. Because of this, the descriptions of the muscle and ligament lines of action obtained from the radiographs were rough approximations.

3) The anatomy was described according to the understanding of its function at the time. Low weight simulation results of the model indicated that the functions of some anatomical components had to be reassessed.

4) The structure of the control system equations did not permit the use of a specialized optimization algorithm. The algorithm employed was slow and sometimes did not converge.

4.2) The Functional Requirements of a Mathematical Model.

In the performance of any task, normal individuals will exhibit changes in many parameters such as spinal geometry, muscle activity (EMG), blood pressure, pulse rate and the like. The sum total of all these changes may be defined as normal physiological behaviour.

The measurable physiological behaviour of the lumbar spine may be defined as those pertinent parameters which have been measured in the living. These include:

1- The internal abdominal pressure.

2- The disc pressure.

3- The muscle activity patterns as monitored by EMG.

4- The maximum extensor moment.

5- The change in spinal geometry.

Taking X-Rays and the measurement of internal abdominal pressure, disc pressure and EMG with needle electrodes are invasive techniques. Avoiding invasive techniques leaves two non-invasive techniques:

1- Monitoring muscle activity with surface electrodes.

2- Measuring geometrical changes using external skin markings (although skin motion introduces some error).

A mathematical model should relate measurable physiological parameters to the forces developed in the joint, and evaluate the compression and shear induced by a given task.

To ascertain the applicability of a model to healthy individual performance, the model must be able to assess the effect of individual variations of spinal structures on overall function. Because spinal injury leaves its stigmata on the measured physiological behaviour of the individual, the model should assess the differences between injured and normal individuals.

The basic philosophy of the Gracovetsky model (the control system approach) has been used to develop a new model that satisfies these requirements by incorporating the following features:

1) The motion of the Lumbar Spine during flexion is computed given a subject's $ALPHA_0$ angle and one sagittal plane radiograph in the erect stance.

2) A coordinate frame of reference is used for the muscle and ligament attachment points. This gives accurate descriptions of the muscle and ligament lines of action.

3) The descriptions of the muscles and ligaments have been refined. For example, Sacrospinalis has been modified to recognize the differences in the mechanical behaviour of its medial portion (Medialis Spinalis) as compared to its deep and superficial portions.

4) The control system criterion has been structured as a positive - definite quadratic optimization problem with linear constraints. A robust optimization algorithm tailored to this type of problem has been implemented. (In this context, 'robust' means an algorithm that is successful in obtaining an optimal solution for a wide range of problems.)

Chapter 5 Quantization of the Relevant Spinal Anatomy

5.1) Introduction

As described in Chapter 2, the human back is a complex structure of muscle, bone, ligament and cartilage. To model all of the constituent components would be a near - impossible task. Rather, the components that have been modelled are those which are thought to be the most important for the performance of a dead lift, along with others that could not be omitted without sacrificing completeness. In all, 11 muscles and 2 ligament structures have been modelled.

The modelling of a muscle requires a description of its points of origin and insertion on the skeleton, how it is distributed among its attachment points (lines of action) and the cross - sectional area of the muscle. The cross - sectional area of a muscle determines the magnitude of force it exerts for some level of muscle activity. Muscle activity is defined in units of pressure. Thus muscle activity multiplied by muscle cross - sectional area gives force. Modelling a ligament requires all of the above except the cross - sectional area. This is because a ligament is a passive member (acting like a cable) and knowledge of its cross - sectional area is not necessary to compute the tensile force it supports when tightened. The muscles and ligaments are modelled as vectors given a magnitude (muscle force or tensile force) and direction (line of action).

The muscles and ligaments modelled follow three types of attachment patterns. Some run from the thorax to the pelvis and sacrum, completely skipping the lumbar vertebrae; some run from the thorax to the lumbar vertebrae and some run from the lumbar vertebrae to the sacrum and pelvis. The three regions of attachment can be identified as thoracic, vertebral and pelvic - sacral. The attachment points of the muscles and ligaments modelled in these regions were determined by consulting appropriate anatomy books [25, 30, 37]. A cross sectional anatomy book was used to determine the muscle areas [11].

The resulting attachment points are illustrated in Figures 5.1, 5.2 and 5.3. Note that the attachment points are represented by points whereas in vivo the attachment points are usually attachment areas. The attachment points used are at the centroids of the attachment areas found in anatomy books (Figure 5.4). In this way a muscle or ligament force induced over the attachment area or at the attachment point will yield the same net global effect.

5.1) The Muscles

PSOAS

The Psoas inserts into the lesser trochanter of the femur, curves around the anterior part of the pelvis and fans out to attachments at T12 and L1 through L4. The Psoas is assumed to skip L5, as it often does in vivo. The cross - sectional area of the muscle is 2.46 in^2 and each of the five strands is assumed to have 1/5 of the muscle area (Figure 5.5).

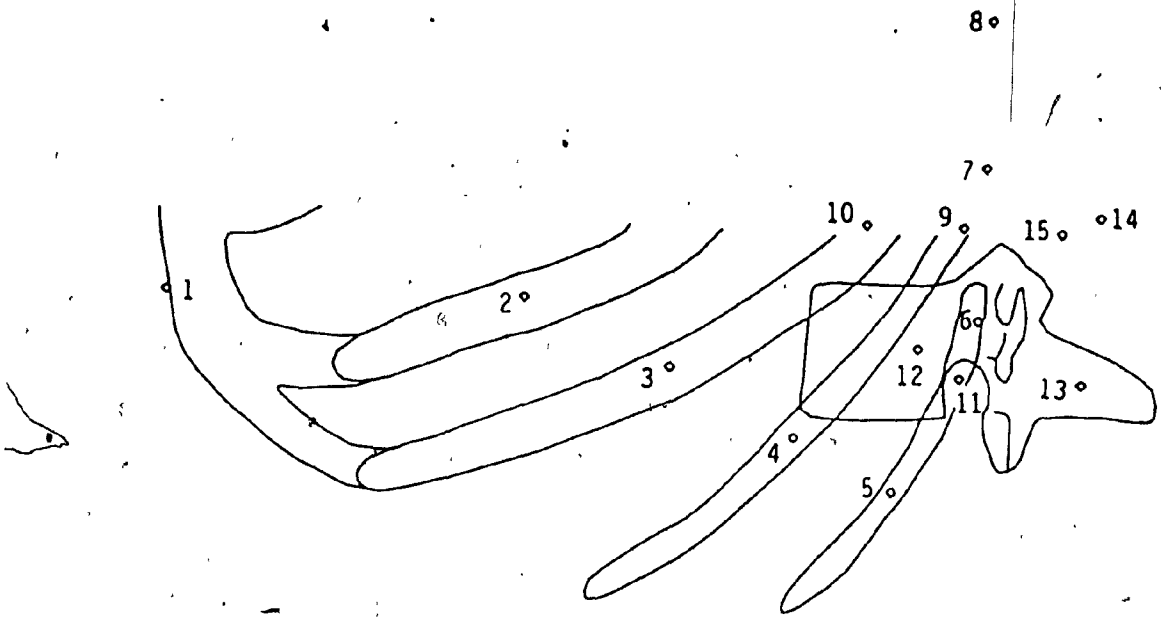

Rectus Abdominis	1
External Obliques (Posterior part)	2, 3, 4, 5
Iliocostalis Lumborum (Superficial part)	6, 7, 8
Medialis Spinalis	9
Latissimus Dorsi	10
Quadratus Lumborum	11
Psoas	12
Multifidus	13, 14
Sacrospinalis (Superficial part)	15

Thoracic Attachment Points.

Figure 5.1

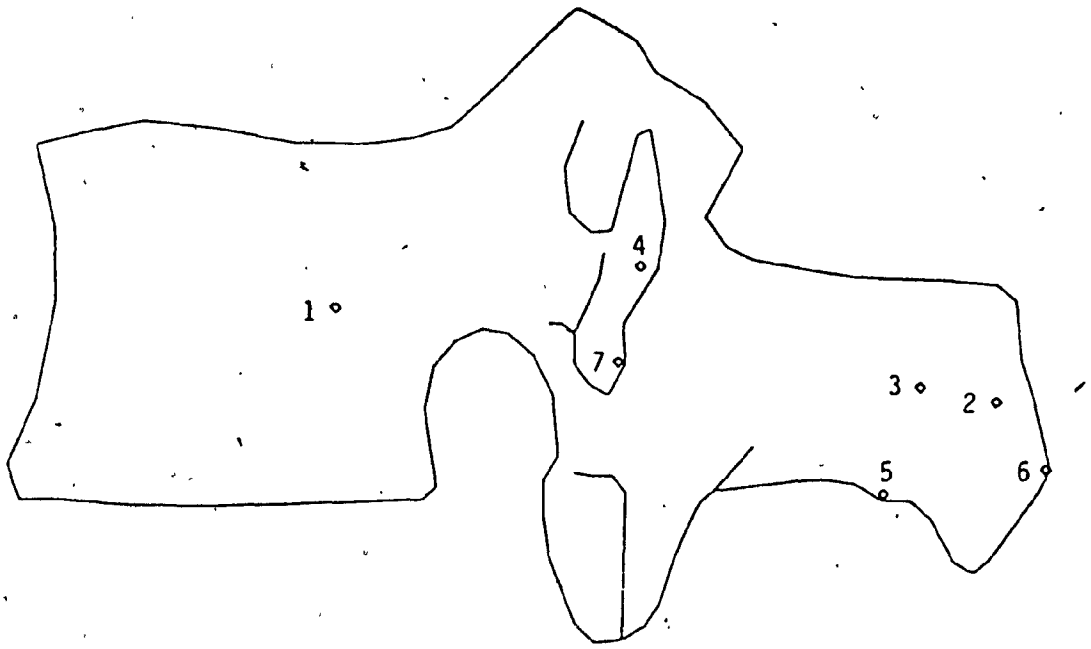

Psoas	1
Medialis Spinalis	2
Multifidus	3, 4
Latissimus Dorsi (Spinal part)	5
Midline, Fascia	6
Sacrospinalis (Deep part)	7

Vertebral Attachment Points.

Figure 5.2

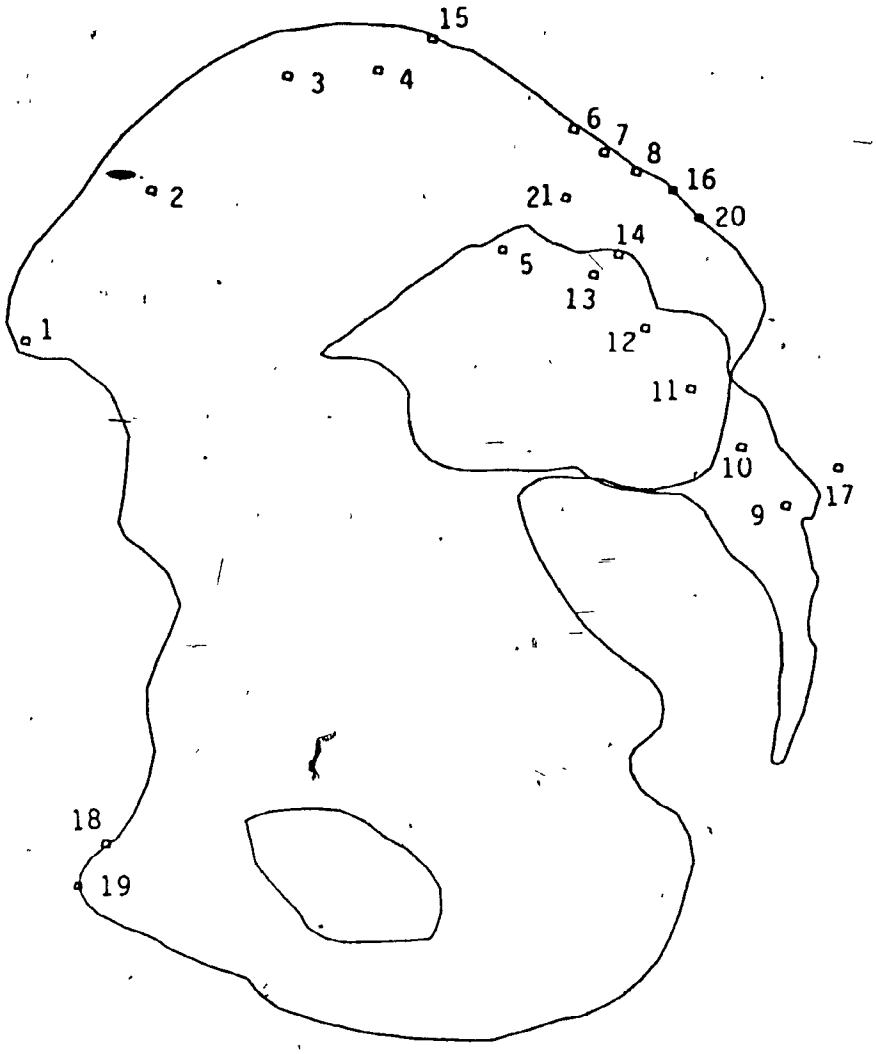

External Obliques (Posterior part)	1, 2, 3, 4
Quadratus Lumborum	5
Iliocostalis Lumborum (Superficial part)	6, 7, 8
Multifidus	9, 10, 11, 12, 13
Latissimus Dorsi (Spinal part)	14
Latissimus Dorsi (Superficial part)	15
Midline	17
Psoas	18
Rectus Abdominis	19
Fascia	20
Sacrospinalis (Deep part)	21

Pelvic - Sacral Attachment Points.

Figure 5.3

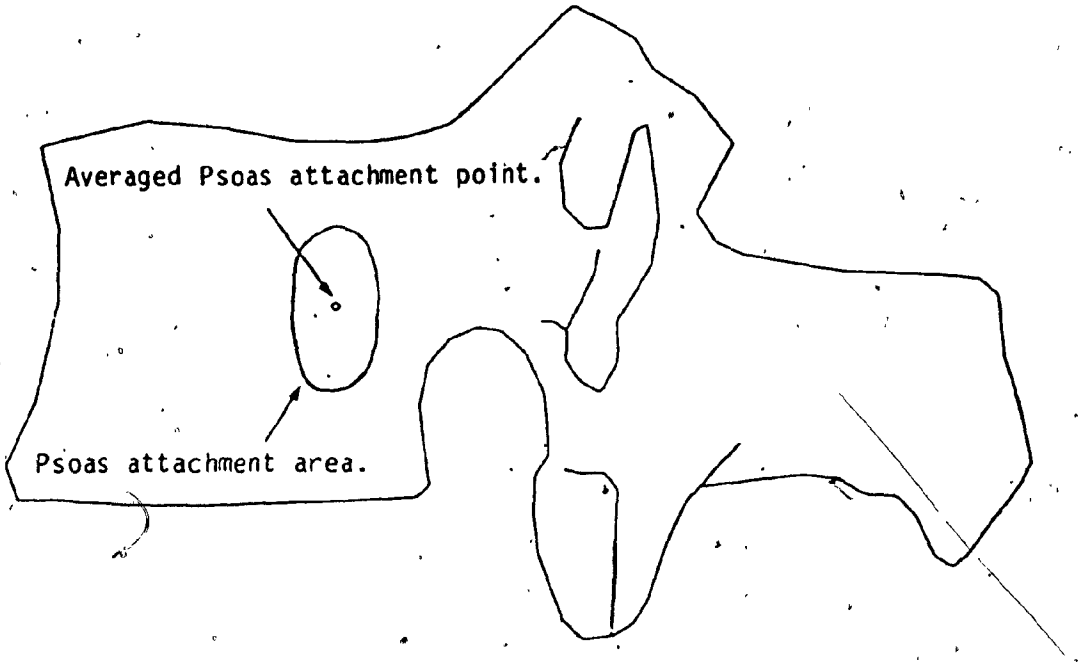

Averaging of a muscle attachment area
to a muscle attachment point.

Figure 5.4

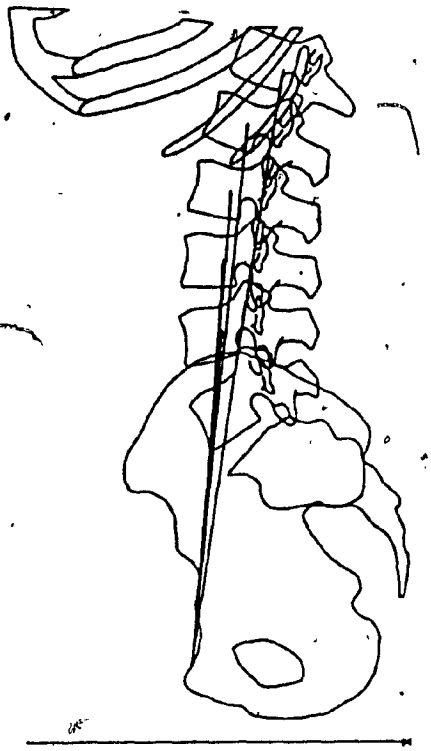

Psoas
Figure 5.5

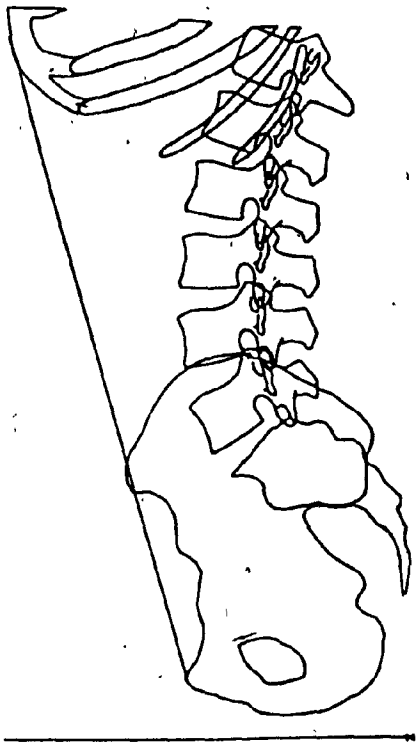

Rectus Abdominis
Figure 5.6

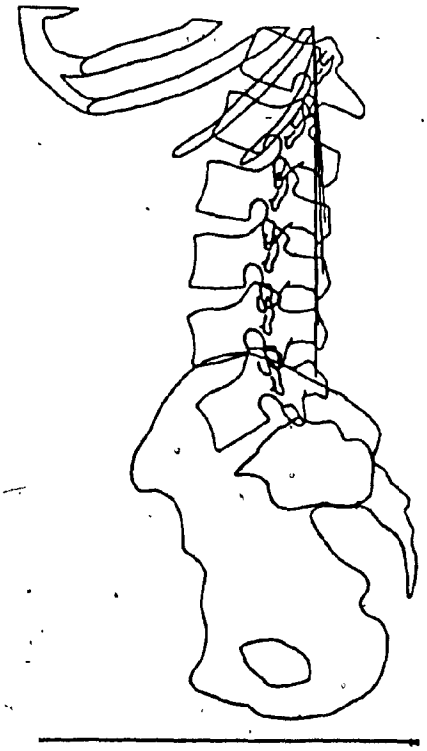

Medialis Spinalis
Figure 5.7

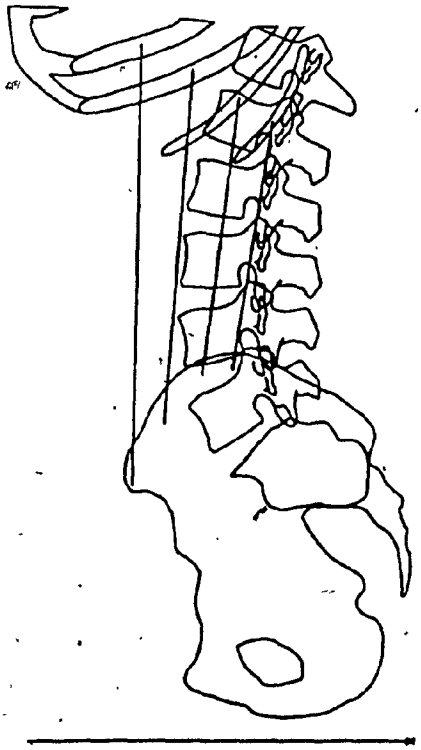

External Obliques
(Posterior part)
Figure 5.8

RECTUS ABDOMINIS

The Rectus Abdominis is modelled as a single strand from the pubic arch to the Xiphoid process. It has a cross - sectional area of 0.9 in^2 (Figure 5.6).

MEDIALIS SPINALIS

The Medialis Spinalis has digitations from its thoracic attachment point to the spinous processes of L1 to L5. The attachment at L1 is ignored because it does not exert any force on the Lumbar IV joints. The muscle has a cross - sectional area of 1.8 in^2 at L2. Each of the four strands from L2 to L5 are assumed to have 1/4 of this area (Figure 5.7).

EXTERNAL OBLIQUES (Posterior part)

This part of the muscle is a broad sheet that extends down from the ribs to the Iliac crest. Modelling the External Obliques as a single strand is inappropriate. Thus it is modelled as four strands. The muscle has a cross - sectional area of 4.375 in^2 and each strand is assumed to have 1/4 of the area (Figure 5.8). The anterior part of the muscle has been ignored.

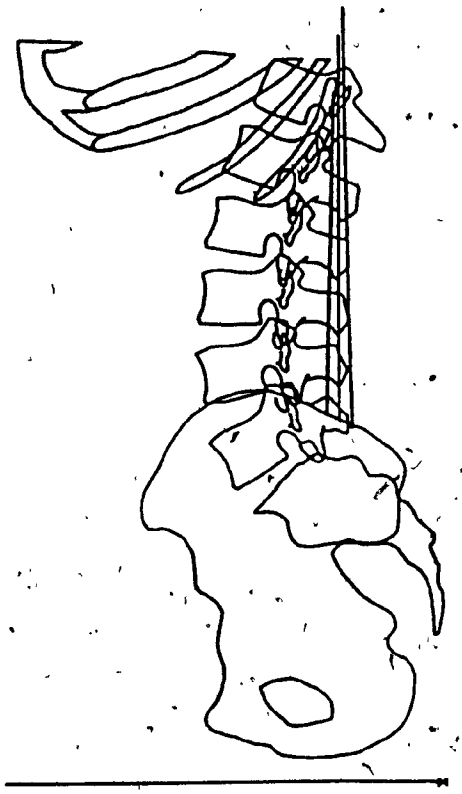

Iliocostalis Lumborum
(Superficial part)
Figure 5.9

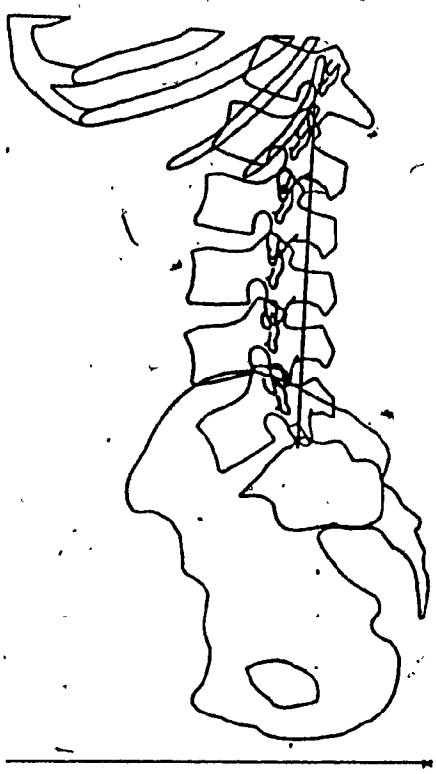

Quadratus Lumborum
Figure 5.10

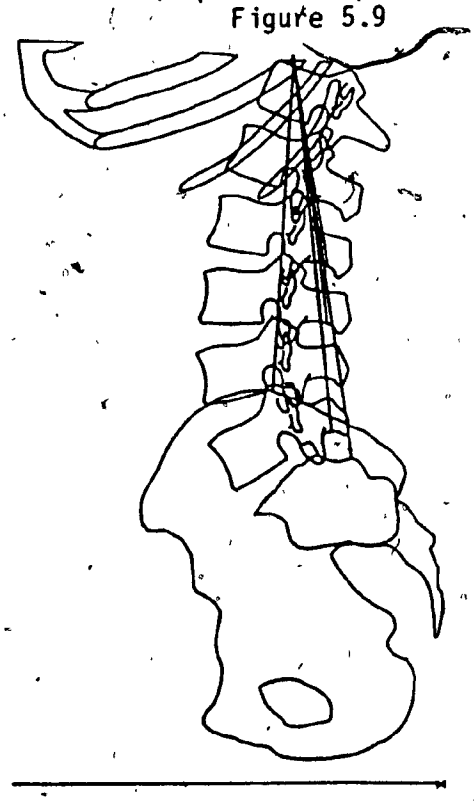

Latissimus Dorsi
Figure 5.11

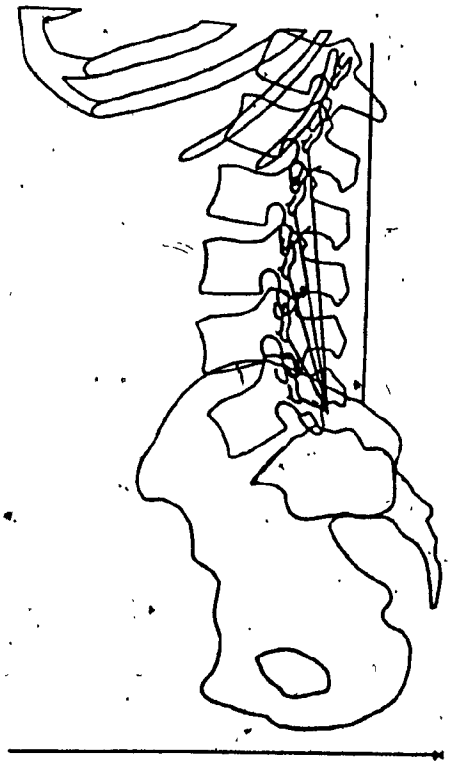

Sacrospinalis
Figure 5.12

ILIOCOSTALIS LUMBORUM

The superficial part Iliocostalis Lumborum originates on the Iliac crest and inserts into the angles of the ribs. Since the attachment points at the ribs are spread out, Iliocostalis Lumborum (superficial) is modelled with three strands to better represent the structure of the muscle. It has a cross - sectional area of 1.89 in^2, with each strand having 1/3 the area (Figure 5.9). The deep part of Iliocostalis Lumborum is lumped with the deep part of Sacrospinalis.

QUADRATUS LUMBORUM

The Quadratus Lumborum originates on the Iliac crest and the Iliolumbar ligament and inserts into the lower border of the twelfth rib and transverse processes of the upper lumbar vertebrae. The vertebral attachments are negligibly small and so ignored. The muscle is modelled as a single strand from the twelfth rib to an averaged location of the Iliac crest and Iliolumbar ligament. The muscle has a cross - sectional area of 1.4 in^2 (Figure 5.10).

LATISSIMUS DORSI

The Latissimus Dorsi originates on the Iliac crest and along the spinous processes of the lumbar vertebrae and the sacrum. It runs up the lateral wall of the thorax to insert into the upper humerus. The muscle is divided into two parts, the pelvic part that originates on the Iliac crest and the vertebral part that originates on the spinous

processes of the lumbar vertebrae and the sacrum. Because of its position on the back, the line of action of the Latissimus Dorsi can be assumed to act on the tenth rib near the spine. The pelvic part is modelled as a single strand with a cross - sectional area of 1.22 in^2. The vertebral part is modelled as five strands going from L2 to L5 and the sacrum with a cross - sectional area of 2.65 in^2. Each strand of the vertebral part is assumed to have 1/5 the area (Figure 5.11).

SACROSPINALIS

The Sacrospinalis is divided into a superficial portion and a deep portion. The superficial portion is modelled as a single strand running from the posterior part of the ribs to the posterior part of the Iliac crest. This strand has an area of 1.8 in^2. The deep portion has strands running from the lower posterior parts of the transverse processes to the dorsal segment of the iliac crest. The deep part of Iliocostalis Lumborum is similar in structure and function to the deep part of Sacrospinalis and thus the two muscles are lumped together. Each strand of the two lumped muscles has an area of 1.73 in^2 (Figure 5.12).

MULTIFIDUS

The Multifidus is a complex muscle. The origins are on the posterior surface of the sacrum and the transverse processes of the vertebrae. The insertions are in the spinous processes of the vertebrae. A

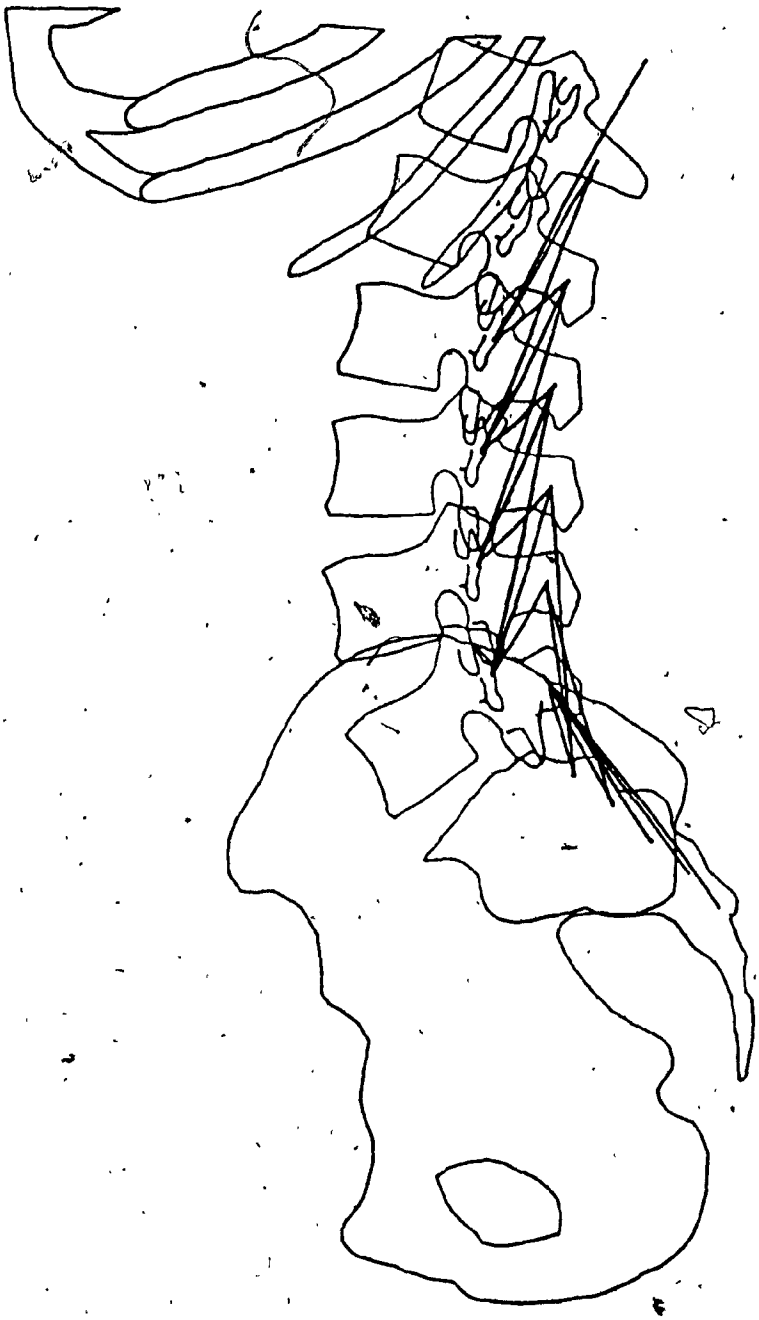

Multifidus

Figure 5.13

given origin on the transverse process of a vertebra has three strands going to the spinous processes of the three vertebrae immediately above it. There are five strands from the origins on the sacrum. These five strands run to the spinous process of L5. Two of these strands run to the spinous process of L4 and one strand runs to the spinous process of L3. The muscle area at any level is a constant 2 in^2 and is assumed divided evenly among the strands active at that level (Figure 5.13).

MIDLINE

This ligament has attachments on the tips of the spinous processes and in the sacrum. The structure of the midline from L1 to L2 to L3 can be modelled as a single strand. From L3 to L4 to L5 to the sacrum the midline is distributed between the three vertebrae to the sacrum. This structure is best modelled as a strand from each spinous process to the sacrum (Figure 5.14).

FASCIA

The lumbodorsal fascia inserts into the tips of the spinous processes and into the iliac tuberosity. The Transversus Abdominis and Internal Obliques both act on its lateral edges. A lateral pull on the edges of the fascia induces forces on the spine that bring the spinous processes closer together, thus extending the spine. The fascia covers the Erector Spinae muscle bundle which gives it an angled insertion into the spinous processes at L3 and L4 depending on the size of the Erector Spinae. The combined muscle cross-sectional area of the

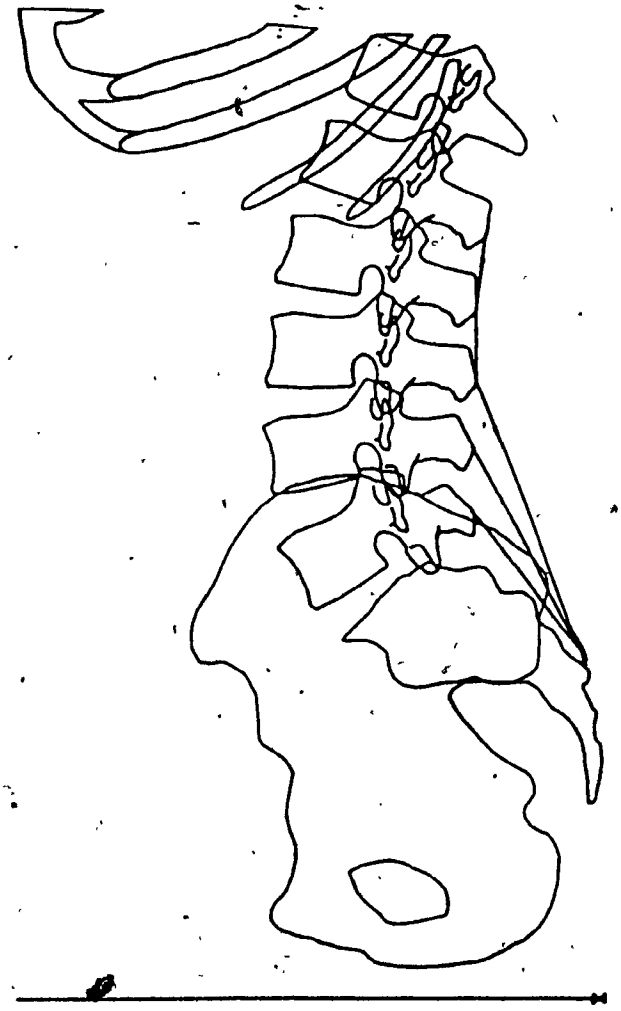

Midline

Figure 5.14

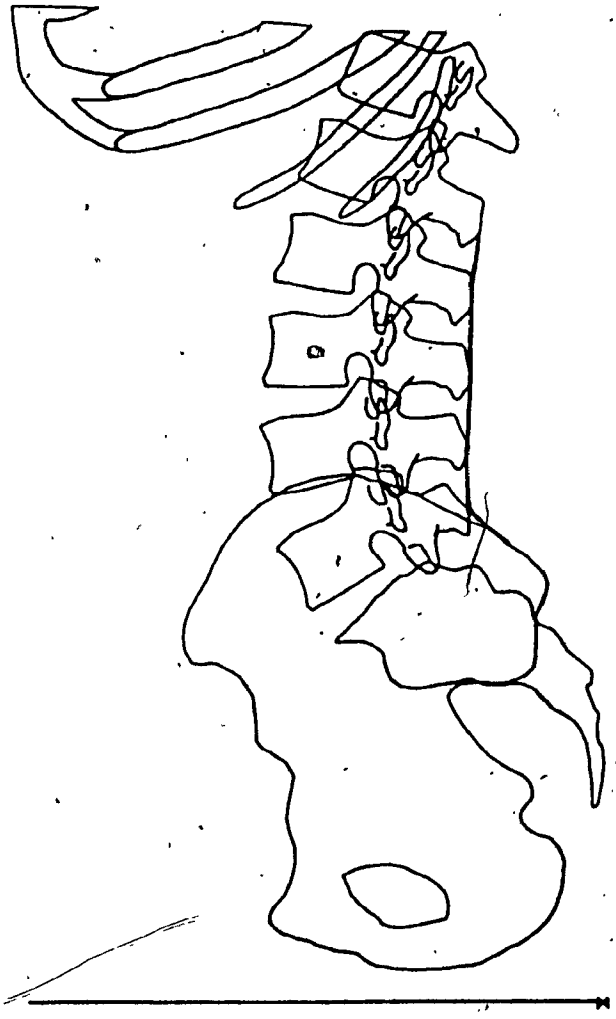

Fascia

Figure 5.15

Transversus Abdominis and Internal Obliques as they act on the fascia is 3.37 in^2 (Figure 5.15).

5.3) Grouping of the muscles.

Several of the muscles modelled are seen to act as a single functional unit. That is to say that when one particular muscle in the functional unit (group) is active, the other muscles in that group will exhibit similar activity. A given group is assumed to be able to exhibit activity independently of other groups.

The Iliocostalis Lumborum, the Medialis Spinalis and the Sacrospinalis constitute such a group (the Erector Spinae). Some abdominal muscles - the External Obliques, the Internal Obliques and the Transversus Abdominis also constitute a group. The remaining muscles are each considered as individual groups. The muscle groups are numbered in table 5.1.

5.4) The Hip Extensors.

The hip extensors are not explicitely modelled. These muscles act on the pelvis & sacrum and are the principal muscles used to maintain the position of the pelvic girdle in reaction to moments induced by external loads, lumbar muscle activity and ligament tension on the spine. Farfan [12] has calculated the maximum moment the hip extensors can support to be 14000 in-lbs.

Group Number	Constituent muscles in group
Group 1	Medialis Spinalis, Iliocostalis Lumborum, Sacrospinalis
Group 2	Multifidus
Group 3	Latissimus Dorsi
Group 4	Quadratus Lumborum
Group 5	Psoas
Group 6	Rectus Abdominis
Group 7	External Obliques (Posterior part), Internal Obliques, Transversus Abdominis

Numbering of the Muscle Groups.

Table 5.1

5.5) Motion of the Lumbar Spine in the Sagittal Plane.

Computation of the directions and magnitudes of the internal and external forces acting upon the various intervertebral joints of the Lumbar Spine requires the relative positions in space of all the force vectors, as well as the geometry of the Lumbar Spine itself. The geometry is obtained from a sagittal plane X-Ray of the spine in the upright position. The data defining the geometry are: 1) the coordinates of the centers of rotation of each lumbar intervertebral joint (taken to be located at the intersection of the line through the posterior third of the disc and the disc bisector)(Figure 5.16), 2) the disc inclination angle of each joint (Figure 5.17) and the initial disc wedge angle (Figure 5.18).

The motion of the unloaded Lumbar Spine (i.e. only bearing the body weight) flexing in the sagittal plane is divided into two separate arcs: 1) From the erect stance to a forward flexion angle of between 35 & 50 degrees the spine unfolds about an essentially stationary pelvis (spine flexion). During spine flexion the pelvis will rotate about 3 degrees, which is negligible whan compared to the rotation of the spine. The disc inclination angle varies for this motion. 2) From this forward flexion angle to full flexion, the rotation of the entire Lumbar Spine is determined by the rotation of the pelvis around the hips (hip flexion). The disc inclination angle stays constant for this range of motion. The forward flexion angle which marks the transition between the two arcs of motion is denoted $ALPHA_0$ (see Figure 4.3). As a load is applied to the spine, the

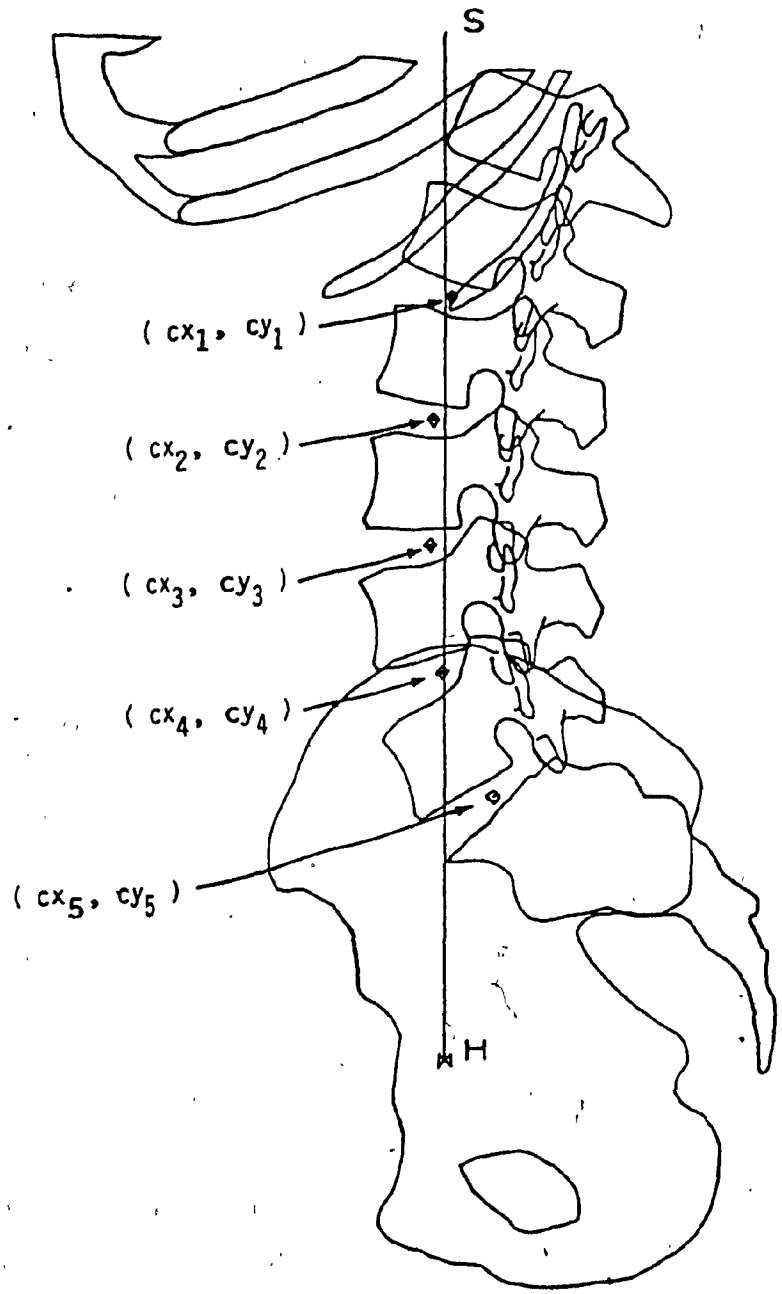

The Centers of Rotation

Figure 5.16

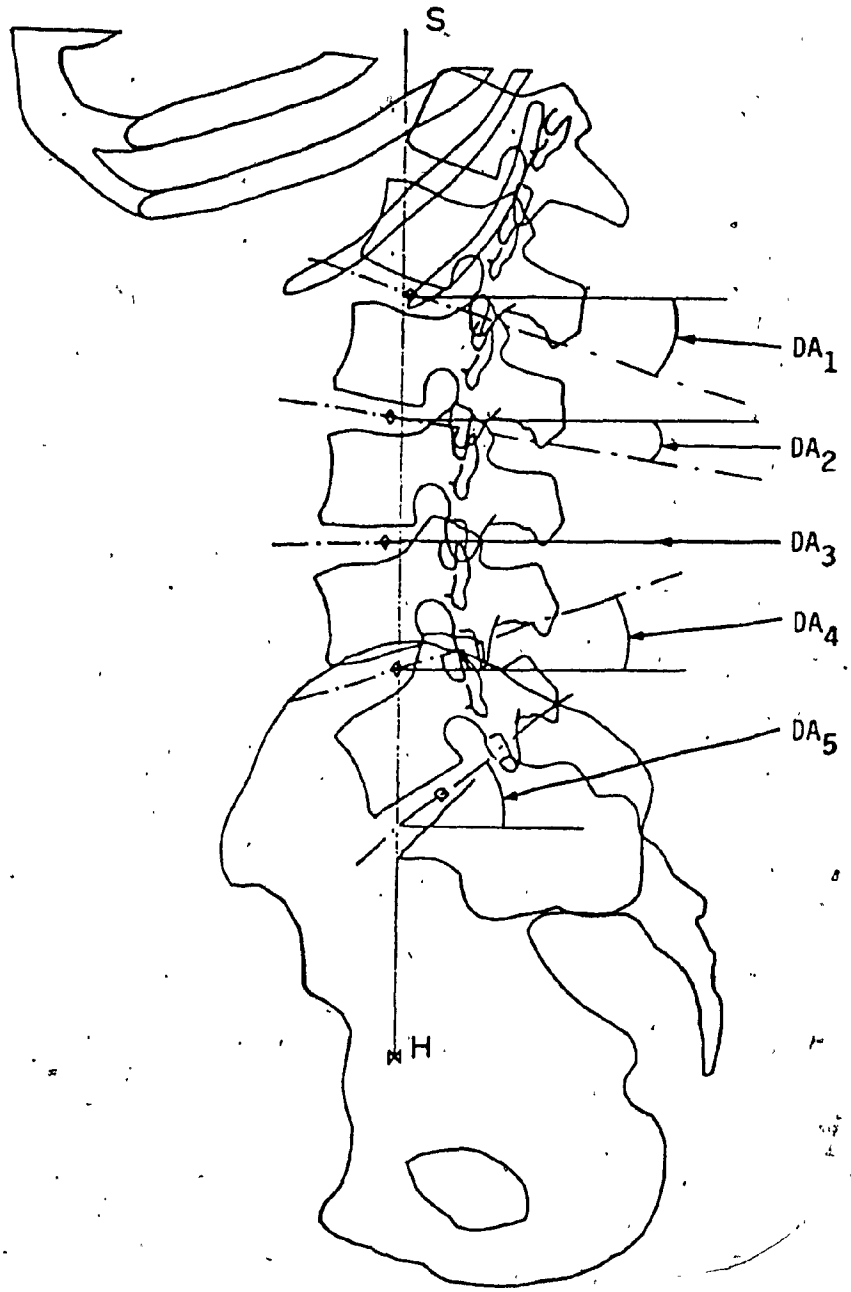

The Disc Inclination Angles

Figure 5.17

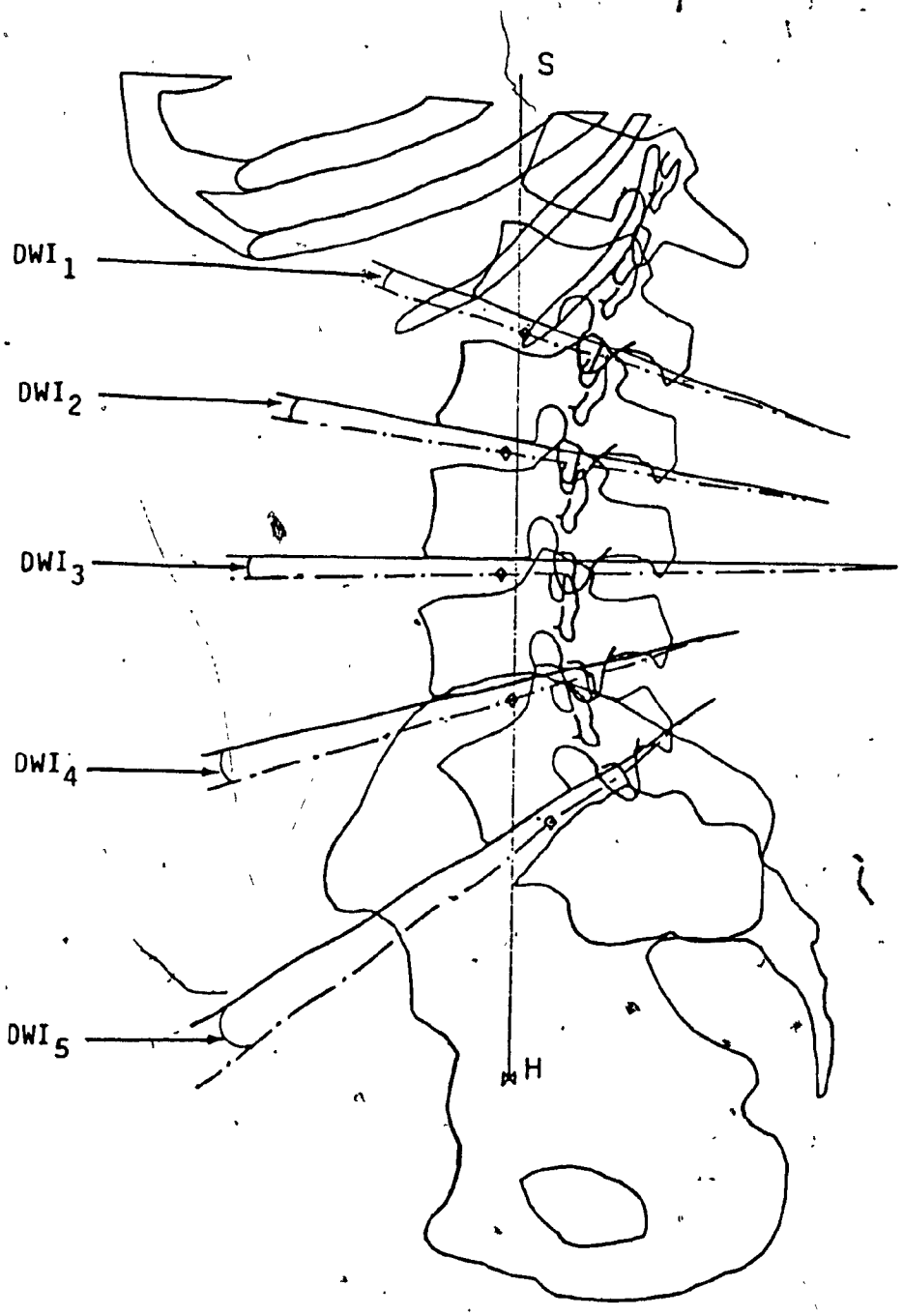

The Initial Disc Wedge Angle

Figure 5.18

pelvis is 'tucked' (rotated is such a way as to straighten the lumbar curve) which decreases the $ALPHA_0$ angle (Figure 5.19).

Given the spinal geometry for the upright position and the $ALPHA_0$ angle, it is possible to generate the spinal geometry for any angle of forward flexion. The motion of a dead lift is modelled by eight images of the spine at flexion angles of 0 to 70 degrees (Figure 5.20). A full description of the mathematics involved in the computation of the motion of the spine is given in APPENDIX A.

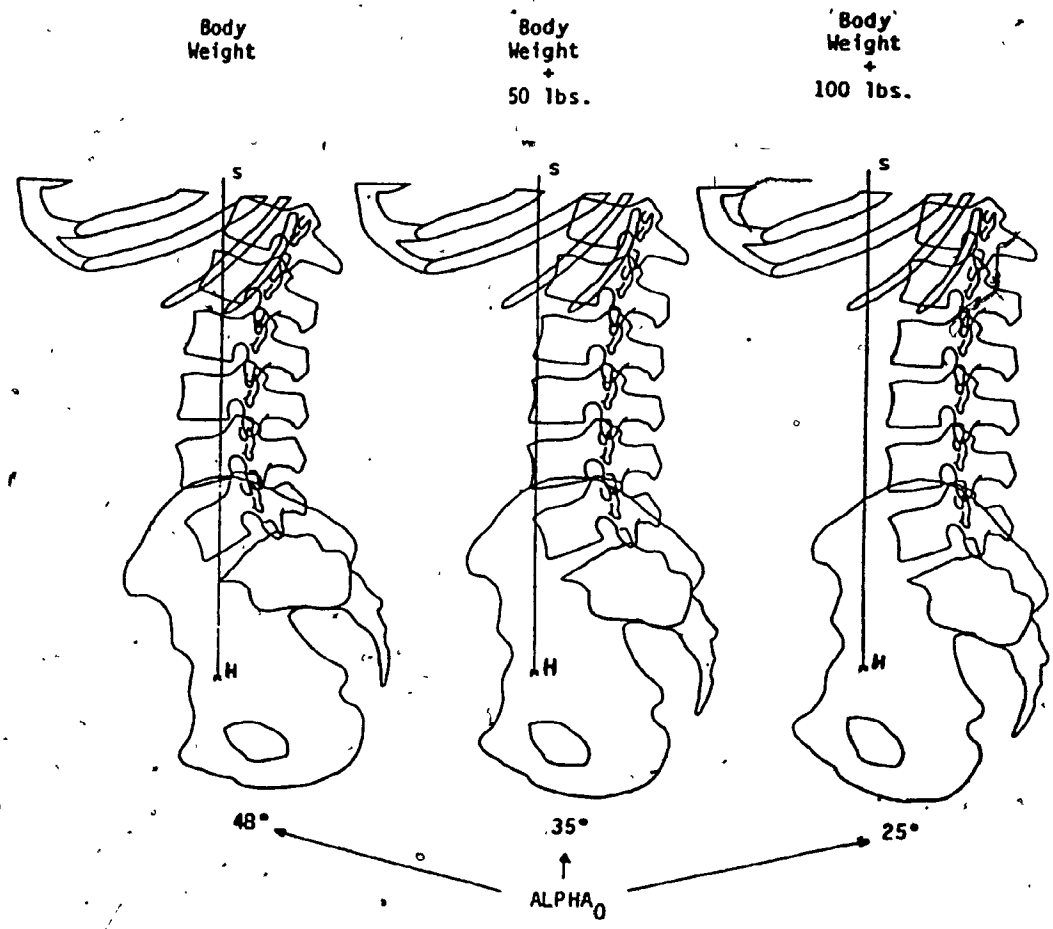

Change in pelvic orientation as spinal load increases.

Figure 5.19

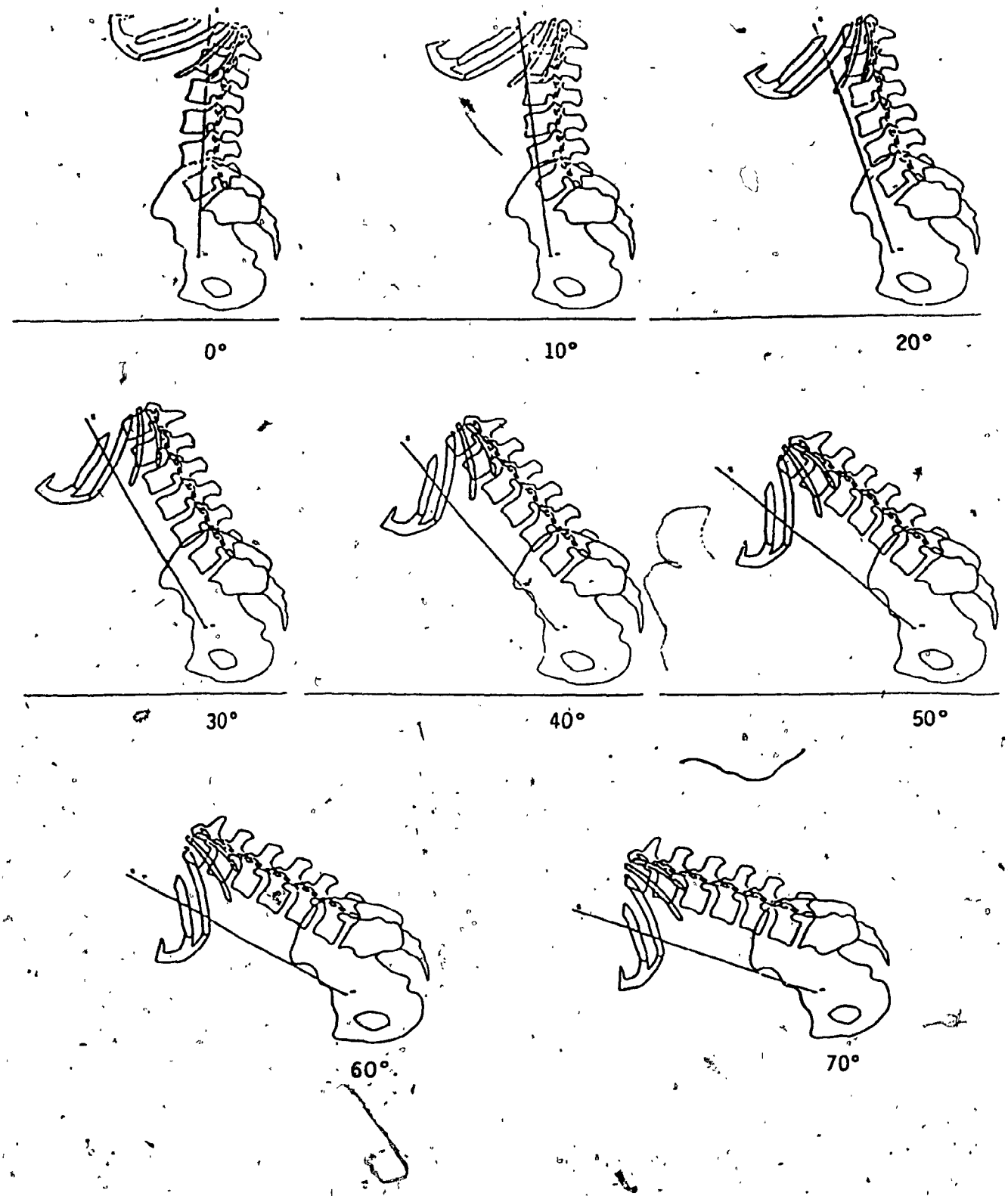

Images used to describe the motion of a dead lift.

Figure 5.20

Chapter 6 Derivation of the System Equations

6.1) Forces acting on the Spine

The force induced when lifting a load is transmitted to the ground via the spine, the pelvis and the legs. The total force exerted at any IV joint of the lumbar spine can be divided into 3 constituent forces: The force due to the load and body weight, the summed force due to muscular activity and the summed force due to ligament tension. These forces also induce moments at the IV joints (Figure 6.1).

6.2) Definition of Center of Reaction and Shear & Compression

Summing the three constituent forces yields the net force exerted at each IV joint. This net force can be decomposed into two orthogonal forces exerted on each IV joint, shear force and compression force, as shown in Figure 6.2. The positive shear direction for each IV joint is defined by a unit vector parallel to the disc bisector pointing in the anterior direction. The positive compression direction for each IV joint is defined by a unit vector perpendicular to the disc bisector pointing towards the IV joint below it (Figure 6.3). Prior to computing the moments at each IV joint (Figure 6.4), an axis about which the moments act upon for each IV joint must be determined. The axis (center of reaction) can be arbitrarily placed on the disc bisector between the anterior and posterior edges of the disc. The center of reaction can range $\pm 40\%$ of the size of the disc, from the center of the disc. The shear and compression unit vectors have their origins at these centers of reaction.

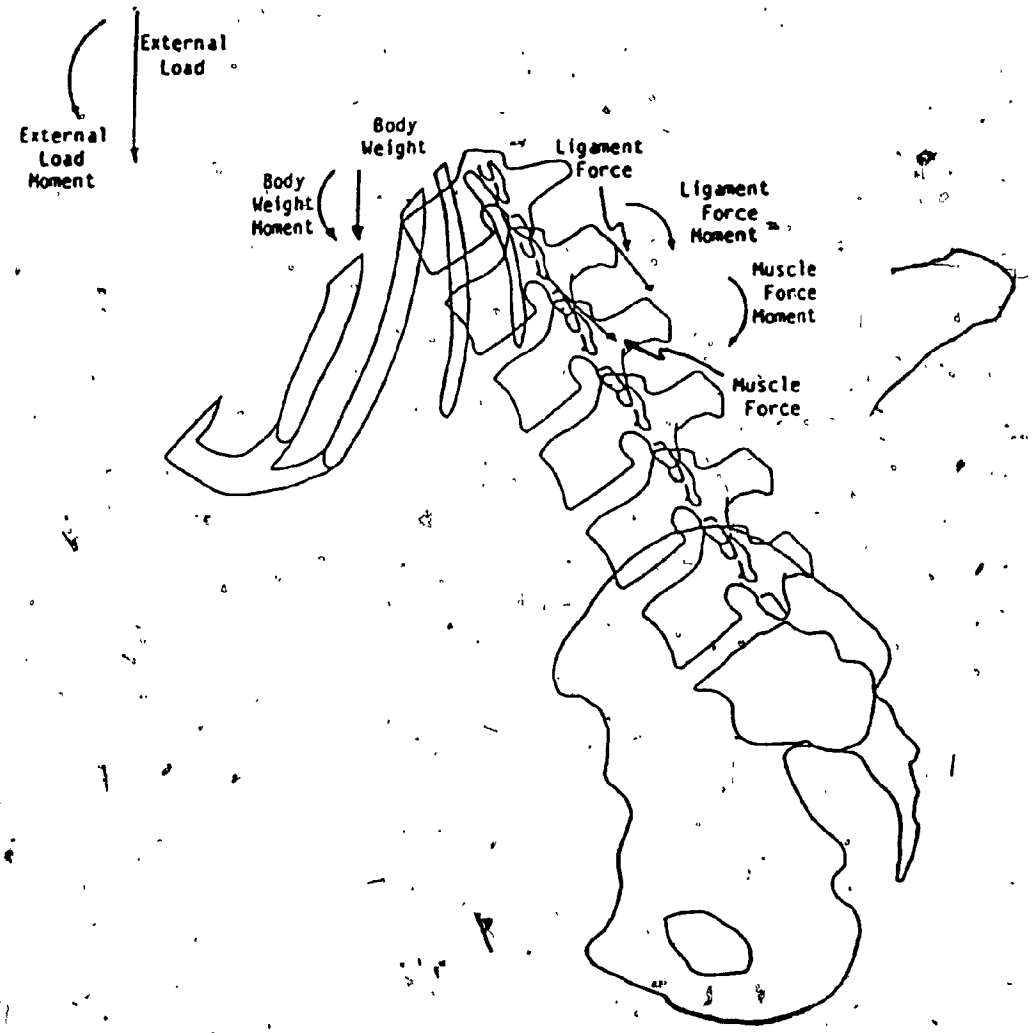

Forces acting on the Spine

Figure 6.1

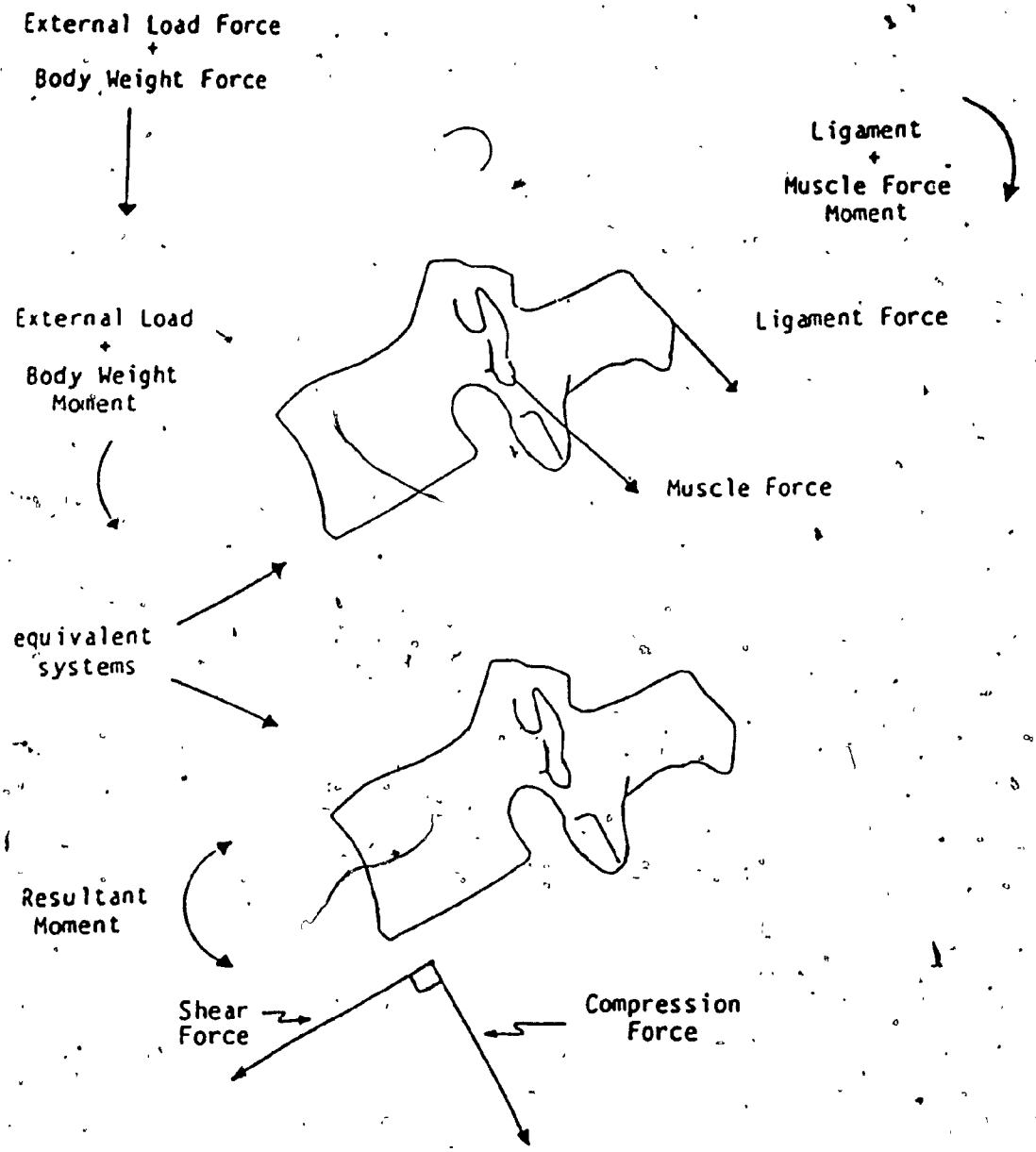

Translation of Force Vectors
to yield two orthogonal forces
and a resultant moment

Figure 6.2

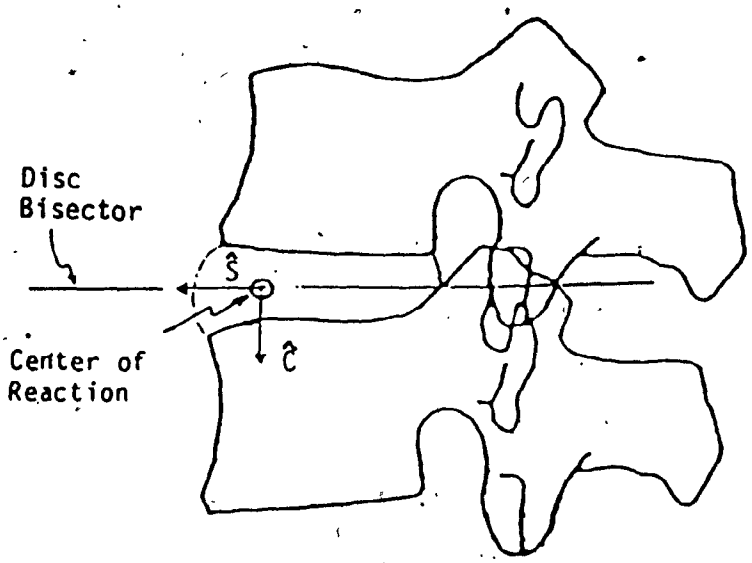

$\hat{C}$ is the unit vector defining the positive compression direction

$\hat{S}$ is the unit vector defining the positive shear direction

Definition of Shear and Compression directions

Figure 6.3

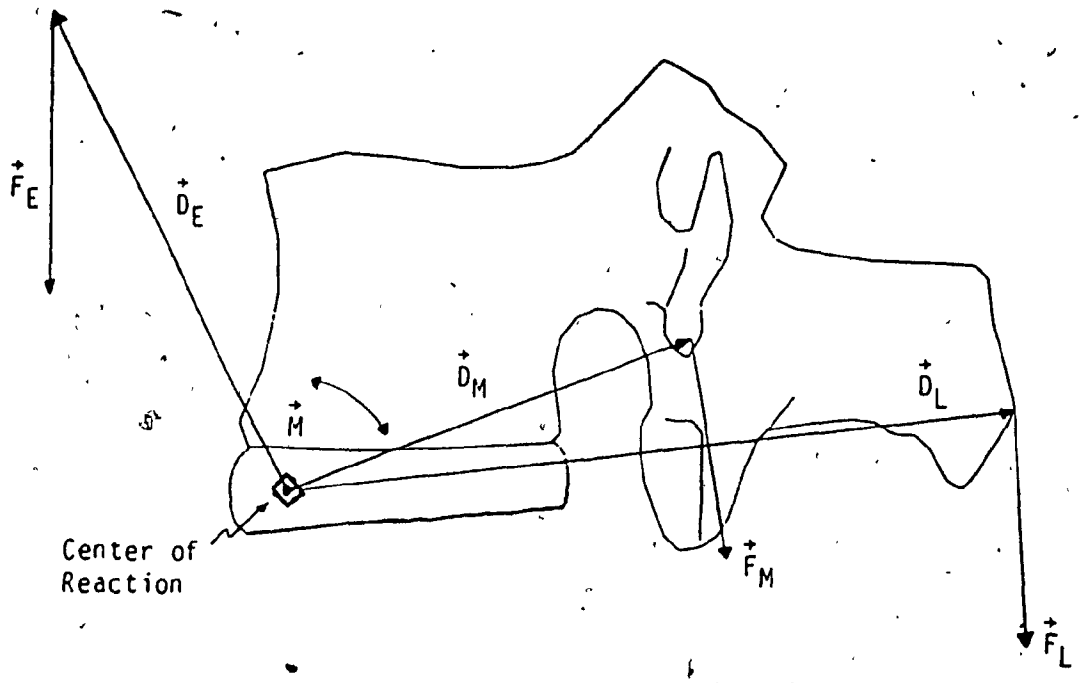

$$\vec{M} = (\vec{D}_E \times \vec{F}_E) + (\vec{D}_M \times \vec{F}_M) + (\vec{D}_L \times \vec{F}_L)$$

$\vec{M}$ is the resultant moment

$\vec{D}_E$ is the effective lever arm of the external load & body weight

$\vec{F}_E$ is the force due to the external load & body weight

$\vec{D}_M$ is the lever arm of the muscle line of action

$\vec{F}_M$ is the muscle force vector

$\vec{D}_L$ is the lever arm of the ligament line of action

$\vec{F}_L$ is the ligament force vector

Computation of Moments
about Center of Reaction

Figure 6.4

6.3) Equilibrium Condition

Static equilibrium at each IV joint requires that the net force at each level be balanced, as well as the net moment at each level be zero. The IV joints resist the shear and compression forces acting on them, thus balancing the net force. The resistive forces of the IV joints are assumed to have their lines of action through the center of reaction so they do not induce any moment. The moment equilibrium equation about every center of reaction is

$$\text{Load and Body Weight moment} + \text{Muscle moment} + \text{Ligament moment} = 0 \qquad (6.1)$$

This equation must be satisfied at each lumbar level for the load to be balanced.

6.4) Muscle Moment Matrix

Muscular activity exerts forces on the lumbar spine. For a given muscle, the magnitude of the force it exerts is given by the product of that muscles' cross - sectional area and its activity (firing pressure). The direction of the force is given by the muscles' line of action. Thus given a magnitude and direction, the muscle forces can be described by force vectors (Figure 6.5).

These muscle force vectors induce moments about the centers of reaction. The derivations of muscle moment at each center of reaction

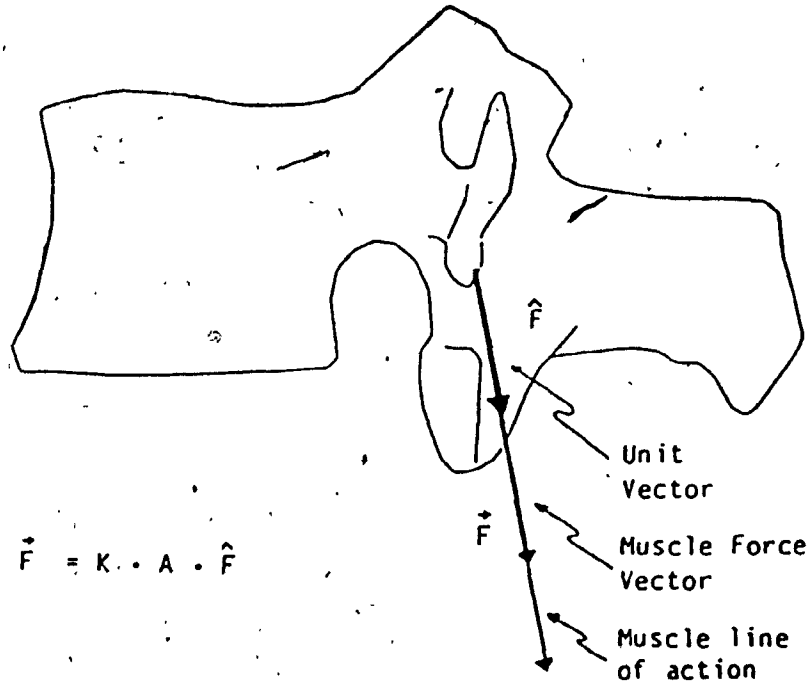

$$\vec{F} = K \cdot A \cdot \hat{F}$$

$\vec{F}$ = muscle force vector

$\hat{F}$ = unit vector along muscle line of action

A = muscle cross sectional area

K = muscle activity

Definition of the
Muscle Force Vector
Figure 6.5

as a function of muscle activity for all the muscles are given in APPENDIX B.

As described in Chapter 5, the 11 muscles modelled can be seen to act as 7 distinct groups. This leads to the creation of a muscle moment matrix. The muscle moment matrix is a [5 x 7] matrix whose rows represent the 5 IV centers of reaction and whose columns represent the individual muscle groups. The i,j^{th} entry in the muscle moment matrix is the muscle activity to muscle moment scaling factor for level 'i' of group 'j'. Thus if the muscle moment matrix is multiplied by a [7 x 1] muscle activity vector, the result is a [5 x 1] vector containing the muscle induced moment at each lumbar IV joint.

6.5) Ligament Tension, Resultant Shear & Compression as functions of Muscle Activity

As stated in section 6.3, for equilibrium to be obtained the net moment at each IV joint must be zero. Refering to equation 6.1, the load and body weight moment are constant and so are independent of muscle activity. However the muscle moment is a function of muscle activity. Isolating the ligament moment on the left hand side of equation 6.1 yields

$$\text{Ligament moment} = - (\text{Load and Body Weight moment} + \text{Muscle moment}) \qquad (6.2)$$

The ligament moment is a function of the muscle moment and is therefore a function of muscle activity. Given the ligament moment, it is

possible to derive the ligament tension in each strand as a function of muscle activity.

The external load and body weight forces can be decomposed into shear and compression forces at each IV joint (Figure 6.6). Since these forces are constant, so are the shear and compression forces that they induce. Similarly the muscle force and ligament strand tension can also be decomposed into shear and compression forces at each IV joint. Because both the muscle force and ligament strand tension are functions of muscle activity so are the shear and compression forces that they induce.

6.6) Net Ligament Tension Matrix

The ligament strand tension equations are based upon the external load moment, the body weight moment, the muscle moment matrix and the lines of action of the ligaments. The net ligament tension at each level follows from the ligament strand tension equations. The derivations are performed in APPENDIX B. The result of the derivations is the following system of linear equations:

$$\begin{bmatrix} HMTN_{1,1} & \cdots & HMTN_{1,7} \\ \vdots & & \vdots \\ HMTN_{5,1} & \cdots & HMTN_{5,7} \end{bmatrix} \begin{bmatrix} K_1 \\ K_2 \\ K_3 \\ K_4 \\ K_5 \\ K_6 \\ K_7 \end{bmatrix} + \begin{bmatrix} HMTNK_1 \\ HMTNK_2 \\ HMTNK_3 \\ HMTNK_4 \\ HMTNK_5 \end{bmatrix} = \begin{bmatrix} T_{N_1} \\ T_{N_2} \\ T_{N_3} \\ T_{N_4} \\ T_{N_5} \end{bmatrix} \quad (6.3)$$

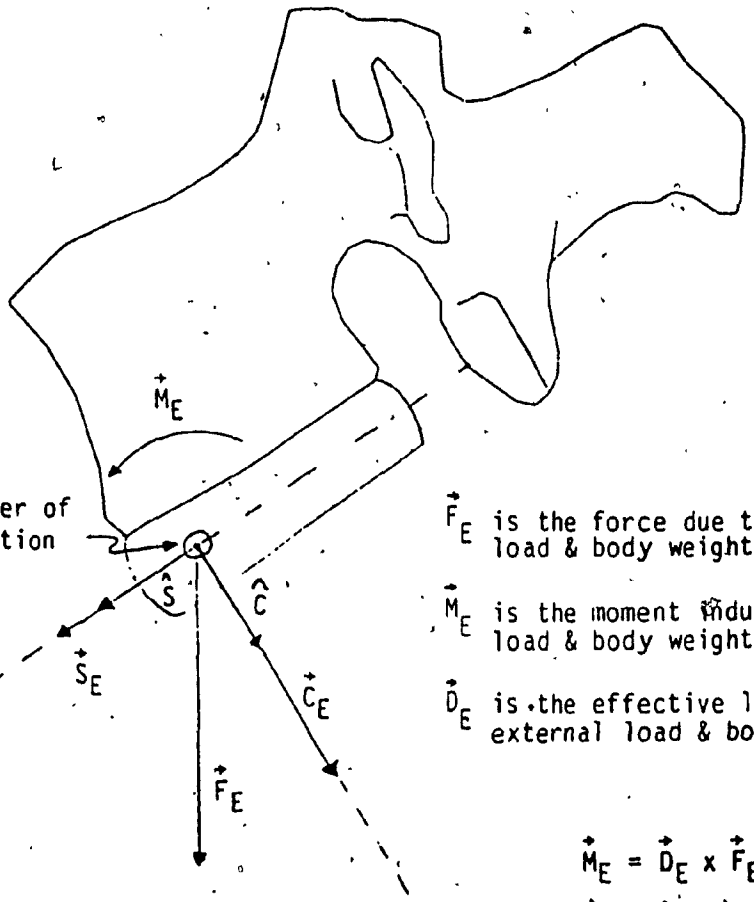

$\vec{F}_E$ is the force due to the external load & body weight

$\vec{M}_E$ is the moment induced by the external load & body weight

$\vec{D}_E$ is the effective lever arm of the external load & body weight

$$\vec{M}_E = \vec{D}_E \times \vec{F}_E$$

$$\vec{S}_E = \hat{S} \cdot \vec{F}_E$$

$$\vec{C}_E = \hat{C} \cdot \vec{F}_E$$

Translation of External Load and Body Weight to the Center of Reaction as a couple

Figure 6.6

where:

$HMTN_{i,j}$ is the muscle activity to net ligament tension scaling factor for level 'i' of group 'j'.

$HMTNK_i$ is the net ligament tension at level 'i' due to an external load and the body weight.

K_j is the muscle group activity of group 'j'

T_{N_i} is the net ligament tension at level 'i'

6.7) Resultant Shear & Compression Matricies

It is possible to derive the resultant shear and compression at each IV joint as a function of muscle activity. These derivations are performed in APPENDIX B. The resulting linear systems of equations are similar in form to the net ligament tension equations. The Shear equations are:

$$\begin{bmatrix} SHR_{1,1} & \cdots & SHR_{1,7} \\ \vdots & & \vdots \\ SHR_{5,1} & \cdots & SHR_{5,7} \end{bmatrix} \begin{bmatrix} K_1 \\ K_2 \\ K_3 \\ K_4 \\ K_5 \\ K_6 \\ K_7 \end{bmatrix} + \begin{bmatrix} SHRK_1 \\ SHRK_2 \\ SHRK_3 \\ SHRK_4 \\ SHRK_5 \end{bmatrix} = \begin{bmatrix} S_1 \\ S_2 \\ S_3 \\ S_4 \\ S_5 \end{bmatrix} \quad (6.4)$$

where:

$SHR_{i,j}$ is the muscle activity & ligament tension to shear force scaling factor for level 'i' of group 'j'.

$SHRK_i$ is the shear force at level 'i' due to an external load and the body weight.

K_j is the muscle group activity of group 'j'

S_i is the resultant shear at level 'i'

The compression equations are:

$$\begin{bmatrix} CMP_{1,1} & \cdots & CMP_{1,7} \\ \vdots & & \vdots \\ CMP_{5,1} & \cdots & CMP_{5,7} \end{bmatrix} \begin{bmatrix} K_1 \\ K_2 \\ K_3 \\ K_4 \\ K_5 \\ K_6 \\ K_7 \end{bmatrix} + \begin{bmatrix} CMPK_1 \\ CMPK_2 \\ CMPK_3 \\ CMPK_4 \\ CMPK_5 \end{bmatrix} = \begin{bmatrix} C_1 \\ C_2 \\ C_3 \\ C_4 \\ C_5 \end{bmatrix} \qquad (6.5)$$

where:

$CMP_{i,j}$ is the muscle activity & ligament tension to compression force scaling factor for level 'i' of group 'j'.

$CMPK_i$ is the compression force at level 'i' due to an external load and the body weight

K_j is the muscle group activity of group 'j'

C_i is the resultant compression at level 'i'

Equations 6.3, 6.4 and 6.5 are functions of muscle activity that give the resulting forces acting on the various spinal components. The equations are not intended to be used to solve for the muscle activity given a shear, compression or tension value. The equations are structured in this fashion for use in the implementation of the model, as described in the next chapter.

Chapter 7 Formation of the Spinal Control System

7.1) Feedback Hypothesis and Control Criterion.

As discussed in Chapter 4, there are numerous models in which muscles, ligaments, and joints are represented by springs and dashpots. Such models respond blindly to external forces or loads. The joints act as passive elements in which internal stresses are fully determined by external forces and the mechanical properties of its components. This approach ignores the fact that the joint is deformed and damaged when overloaded. Preservation of the spine as a functional unit requires that each IV joint remains undamaged. It reasonable to hypothesize that for its own protection, the joint reacts to its internal stress to control the force exerted upon it by the applied load. A feedback mechanism monitoring the stress at each IV joint could modify muscular activity in such a way as to minimize stress at the joints and therefore reduce the risk of injury. The ligaments could be connected to this feedback mechanism to minimize their stress through the control of muscular activity. Finally, the stress induced in the muscles by their activity could also be monitored and controlled by the feedback mechanism.

The hypothesis implies that the central nervous system can monitor musculo - skeletal stress levels in the spine and use this information to coordinate muscular activity in order to perform a task with the minimum musculo - skeletal stress possible. No such monitoring system has been recognized by neurophysiologists, but this is not a reason to deny a priori its existence.

System theory is used to describe the spinal structure and control theory is used to describe the role of musculo - skeletal stress information in the determination of muscular activity during the performance of a task.

The model of the lumbar spine presented in this thesis computes the resultant shear and compression at the intervertebral joints and the ligament tension as a function of spinal geometry, external load and muscle activity. Given the spinal geometry (flexion angle) and an external load allows the model to be described as a system with constant inputs (external load and flexion angle), variable inputs (muscle activity), and outputs (shear, compression and ligament tension). This open loop system is illustrated in Figure 7.1. Simulation of the feedback loop requires the muscular stress, the ligament stress and the joint stress. This information is then input to a control system whose output is muscle activity. This closed loop system is illustrated in Figure 7.2.

7.2) Transformation of the Control Criterion to an Objective Function.

Computer implementation of the feedback loop requires numerical representation of muscular stress, ligament stress and joint stress. Muscular stress is assumed to be proportional to the square of the muscle activity level. The ligament stress is the square of the ligament tension. The joint stress is the Euclidean norm of the joint shear and

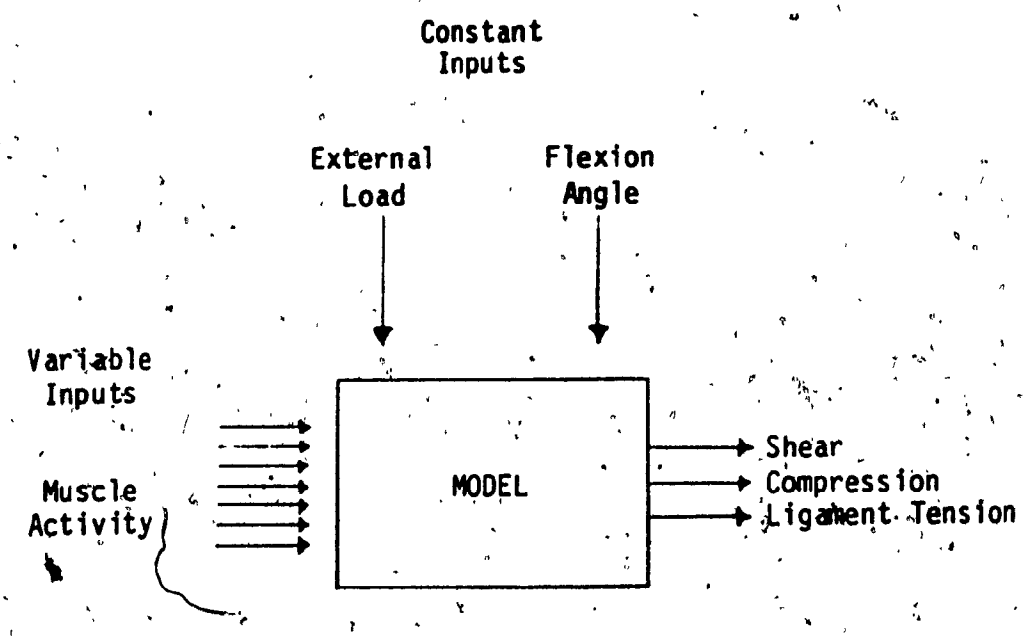

Open Loop System

Figure 7.1

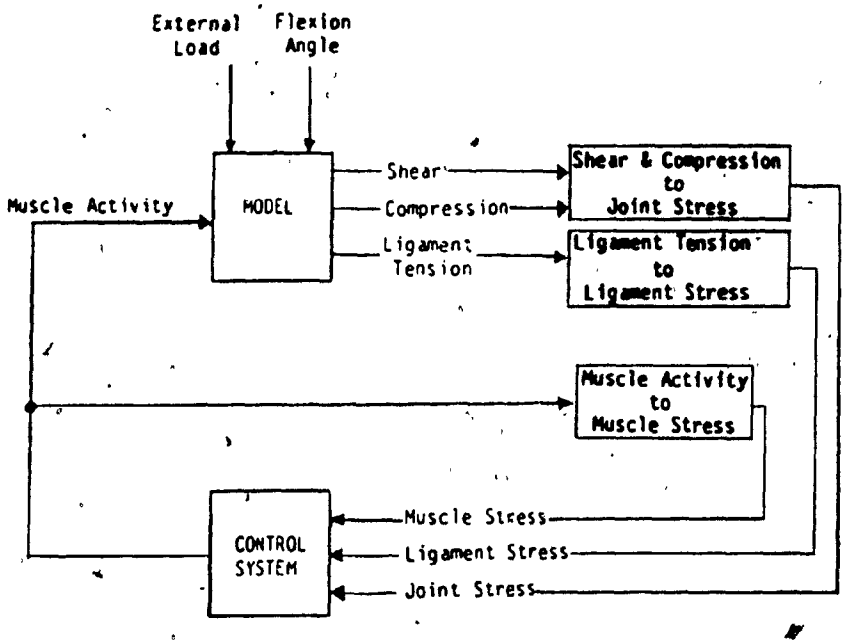

Closed Loop System

Figure 7.2

compression. Without any loss of generality and to simplify the mathematics, the square of the joint stress is used. This quantity is the joint shear squared plus the joint compression squared.

Formulation of the objective function is achieved by summing these components together after multiplying them by arbitrary scaling factors. The result is a quadratic fuction of the muscle activity.

$$O(\underline{K}) = \sum_{L=1}^{5} (P_1 \cdot S_L)^2 + \sum_{L=1}^{5} (P_2 \cdot C_L)^2 + \sum_{L=1}^{5} (P_3 \cdot T_{N_L})^2 + \sum_{i=1}^{6} (P_4 \cdot K_i)^2 + (P_5 \cdot K_7)^2 \qquad (7.1)$$

where:

S_L is the resultant shear at lumbar level 'L' as a function of muscle activity

C_L is the resultant compression at lumbar level 'L' as a function of muscle activity

T_{N_L} is the resultant ligament tension at lumbar level 'L' as a function of muscle activity

K_i is the muscle group activity for group 'i'

P_1 to P_3 are scaling factors for the shear, compression and ligament tension

P_4 is the scaling factor for muscle groups 1 to 6

P_5 is the scaling factor for muscle group 7

The scaling factors are used to modify the contributions of the various components to the overall objective function. This feature is used to tune the model to simulate physiological muscle activity. The tuning of the model is discussed in chapter 8. Separation of the muscle group scaling factors permits the manipulation of group 7 independently of groups 1 to 6.

With some algebraic manipulation this equation can be written in the standard quadratic form:

$$O(\underline{K}) = \tfrac{1}{2}\underline{K}^t G \underline{K} + \underline{C}^t \underline{K} + A \qquad (7.2)$$

The full derivation of the objective function and its transformation to the standard quadratic form is given in APPENDIX C.

7.3) System Constraints

Muscles exert force when contracting. A muscle can only pull, not push. The method used to model the muscle force vectors interprets pos-

itive muscle activity levels as a pull and negative muscle activity levels as a push. Thus the muscle activity level must be constrained to be greater than or equal to zero. Similarly, ligaments can support tension but not compression, just like a cable. In the ligament tension equations, a negative tension implies a compression. Thus the net ligament tension must be greater than or equal to zero. An upper bound on the magnitude of the ligament tension, T_{LIM}, can also be imposed. These three sets of constraints define a range of feasible muscle activity levels in which a minima of the objective function is to be found.

7.4) Minimization of the Objective Function

The optimization problem is stated as the minimization of a quadratic function

$$O(\underset{\sim}{K}) = \tfrac{1}{2}\,\underset{\sim}{K}^t\, G\, \underset{\sim}{K} + \underset{\sim}{C}^t\, \underset{\sim}{K} + A \qquad (7.2)$$

subject to the following linear constraints:

$$K_i > 0, \qquad i = 1,\ldots,7 \qquad (7.3)$$

$$\sum_{j=1}^{7} HMTN_{L,j} \cdot K_j + HMTNK_L > 0, \qquad L = 1,\ldots,5 \qquad (7.4)$$

$$\sum_{j=1}^{7} -HMTN_{L,j} \cdot K_j + T_{LIM} - HMTNK_L > 0, \qquad L = 1,\ldots,5 \qquad (7.5)$$

Equation 7.3 constrains the muscle activity levels of all the 7 groups to be greater than or equal to zero.

Equation 7.4 constrains the net ligament tension at all levels to be greater than or equal to zero.

Equation 7.5 constrains the net ligament tension at all levels to be less than or equal to some upper bound, T_{LIM}.

The algorithm employed to obtain solutions is specifically designed for positive definite quadratic programming problems. Thus the only restriction on using this algorithm is that matrix G is positive definite. This algorithm is described in APPENDIX D.

Chapter 8 Experimental Results and Computer Simulations

8.1) Introduction

It was beyond the mandate of this thesis work to design experiments for and collect data from subjects performing weightlifting tasks. However, another study at Concordia called for a preliminary investigation of the muscle activity patterns for a small number of subjects performing dead lifts with low weights. Thus the opportunity presented itself to compare the experimental results from the study to computer simulation results. Although the number of subjects tested was not large enough to make conclusive statements about muscle activity patterns during the performance of dead lifts, some common patterns did emerge.

Section 8.2 describes the data acquisition procedure used in the study. Section 8.3 presents the common muscle activity patterns observed in the experimental data. Section 8.4 describes tuning the model to yield similar results. Section 8.5 deals with equalizing the compression stress in the spine over a range of weights.

8.2) Data Acquisition

Muscle activity was monitored on subjects performing simple weightlifting tasks. The tasks required a subject to bend forward, grasp a weight and pick it up. The weights lifted ranged from 0 to 50 pounds. EMG signals from the Erector Spinae, Multifidus, Rectus Abdominis and External Obliques were acquired with surface micro electrodes. The electrodes were placed symmetrically on the left and

right sides of the subject.

The EMG signals were analog bandpass filtered with the passband between 10 and 250 Hz. The resulting signals were digitized at a 1kHz rate with 12 bits accuracy (1 part in 4096) and recorded on a mass storage computer disk. Once the task was completed, the acquired signals were processed to remove artifacts and smooth the data to yield an envelope of the monitored muscle activity (Figure 8.1).

The position of the subject during the task is synchronized with the EMG signal acquisition by using stop action photography at 4 frames per second. The hips and shoulders of the subject are identified with markers so an accurate measurement of the flexion angle as a function of time can be obtained.

This experimental procedure allows the envelope of the muscle activity to be plotted versus the subject's forward flexion angle.

8.3) Experimental Results

The muscle activity of a number of subjects was acquired. The experimental results were scrutinized to establish similar patterns of muscle activity across the subjects. Aberrant muscle activities for isolated cases were not considered when establishing the patterns. All the subjects demonstrated activity in the Erector Spinae and Multifidus. The level of activity increased as the size of the weight lifted increased. The Rectus Abdominis and External Obliques were silent for most subjects, slightly active for some subjects and showed sporadic activity in isolated cases.

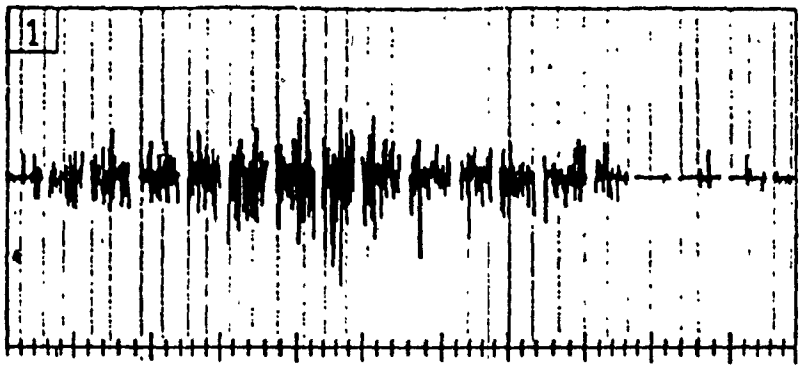

A) Bandpass filtered EMG signal vs Time

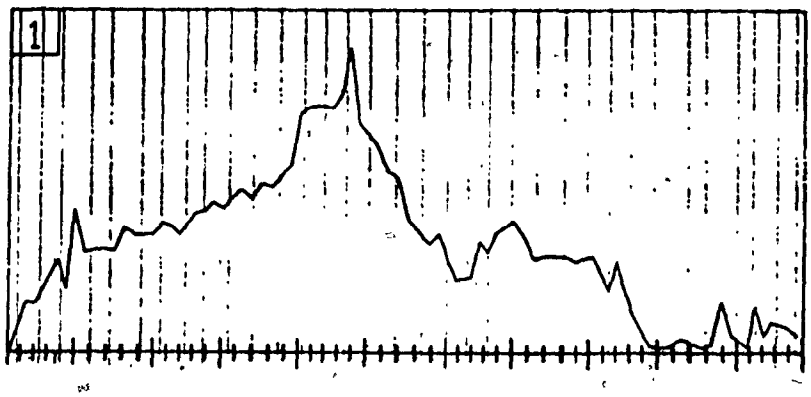

B) Processed EMG signal vs Time

Raw and Processed EMG Signals

Figure 8.1

Typical muscle activity of the Erector Spinae and the Multifidus for a lift of 25 pounds plotted against the forward flexion angle is given in figure 8.2.

Several subjects exhibited the Floyd and Silver [15] response in their Erector Spinae activity. The muscle group activity would peak for some flexion angle, then fall off and begin to rise again as the flexion angle increased. This is shown in figure 8.3.

8.4) Simulation of Experimental Results

The model yields muscle activities by finding the minima of equation 7.1 subject to the constraints imposed upon the range of solutions. For a given set of P_i's, a unique set of muscle activities is computed. Once a task is defined by the weight lifted and the spinal geometry, the P_i's are the only degrees of freedom with which to tune the model.

The model was tuned to simulate the muscle activity of the Erector Spinae and Multifidus of figure 8.2. Setting P_4 and P_5 to unity and imposing no upper limit on the ligament tension value, the values $P_1 = .1$, $P_2 = .23$ and $P_3 = .2$ yield the muscle activities for the Erector Spinae and Multifidus shown in figure 8.4a. The shapes of the curves agree in the region from 0 to 50 degrees, but after 50 degrees the experimental curves have an inflection point whereas the computed curves continue to rise. Using the same P_i's for the range 0 to 50 degrees, but making $P_3 = .19$ at 60 degrees and $P_3 = .18$ at 70 degrees causes the computed curves to exhibit the same type of

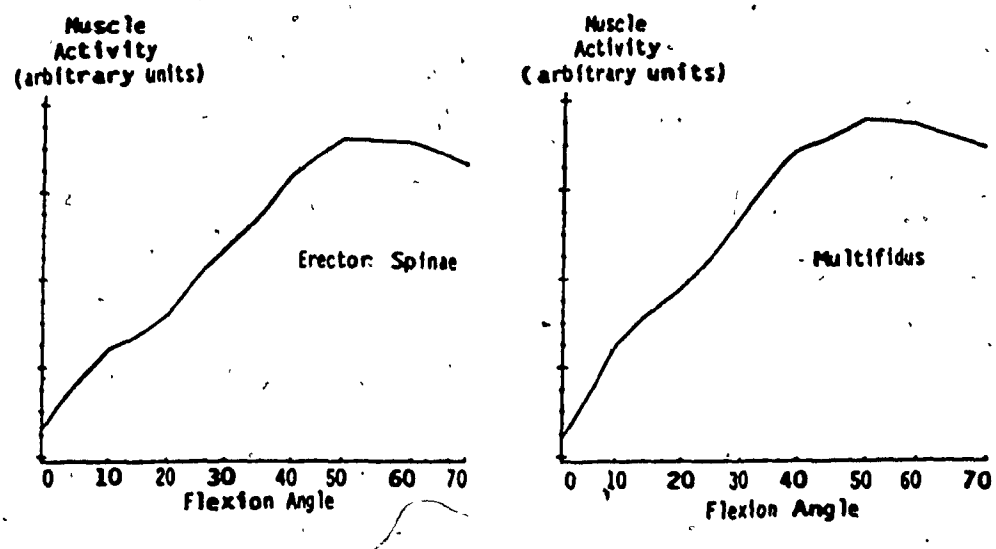

Typical Experimental Data for
Erector Spinae and Multifidus

Figure 8.2

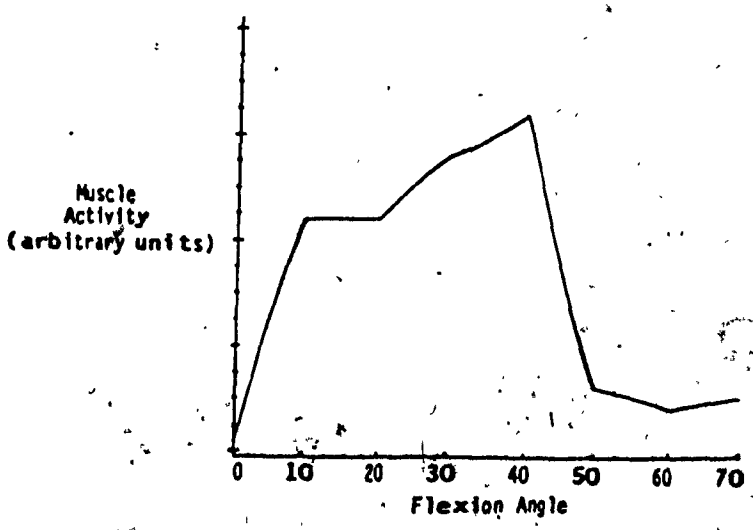

Experimental observation of Floyd & Silver, shutoff

Figure 8.3

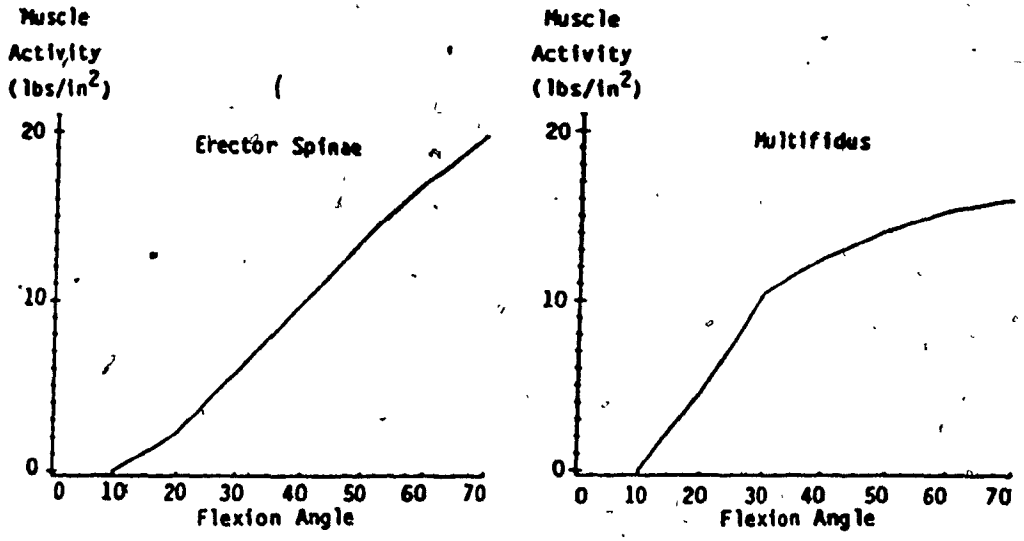

Simulation of Erector Spinae & Multifidus activity

Figure 8.4a

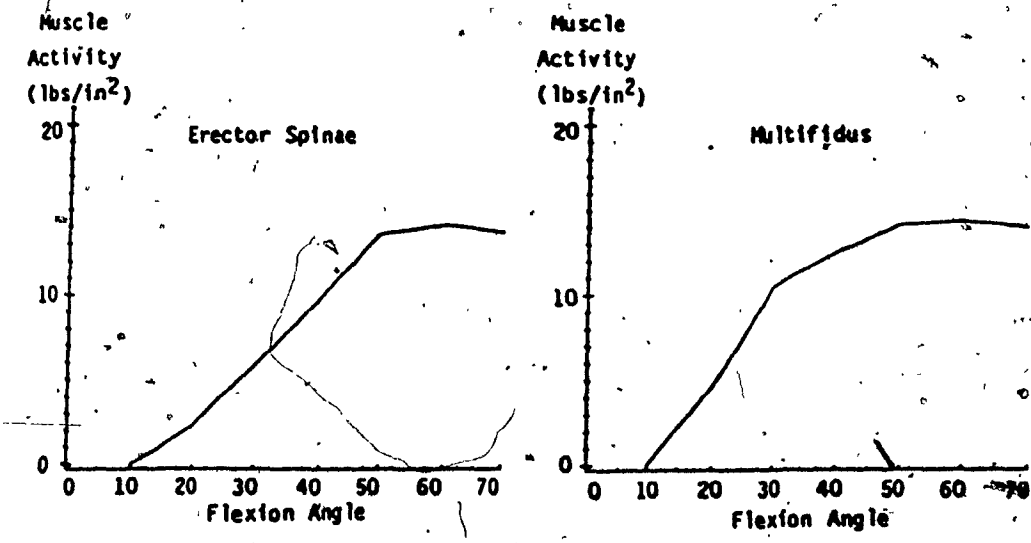

Simulation with modified scaling factors to produce inflection points

Figure 8.4b

The Floyd & Silver muscle activity pattern for the Erector Spinae has been simulated by imposing an upper bound on the net ligament tension of 130 pounds until a flexion angle of 48 degrees is attained and by setting $P_1 = .35$, $P_2 = .35$, $P_3 = .24$, $P_4 = P_5 = 1.0$. The computed curve is plotted in figure 8.5.

8.5) Equalization of Compression Stress

Wolff's law [43] states that bone grows when subjected to stress. The stress a bone experiances can be inferred from the size of the bone. The lumbar vertebrae increase in size from L1 to L5. The ratio of the centrum area of L5 to L1 is 1.2:1. That is, L5 has 20% more centrum area than L1. Since the vertebrae experience a greater magnitude of compression stress than shear stress on the centrum, it is reasonable to assume from Wolff's law that L5 experiences 20% more compression than L1 at any flexion angle for any weight.

Lifts of 0, 25, 50, 100, 200, 300 and 400 pounds have been simulated to yield a spread of compression between L1 and L5 of 20% $\pm$ .05% for all angles. The parameters used for each weight and the salient results are presented in table 8.1. For the 400 pound simulation, the maximum muscle moment at L5 was computed to be 2137 inch-pounds, the maximum muscle activity was 69.7 pounds/inch^2 and the maximum compression at L5 was 3101 pounds. These values conform to the limits for a maximum lift put forward by Gracovetsky et al [18].

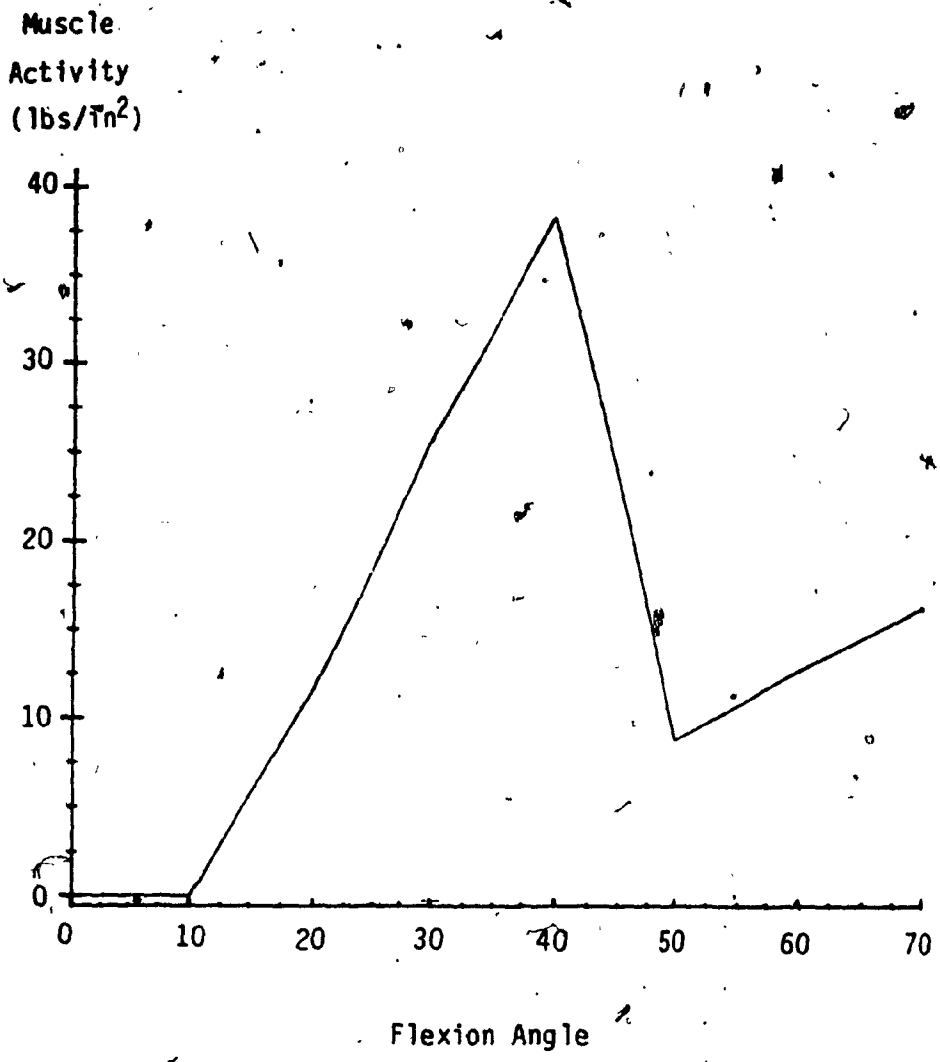

Simulation of Floyd & Silver shutoff

Figure 8.5

Weight	P_1	P_2	P_3	$Alpha_0$	C_5	L_5	M_5	Act.
400.	.0555	.0555	.0555	8.	3101.	6526.	2137.	69.7
300.	.0555	.0555	.0555	12.	2421.	5121.	1638.	53.4
200.	.0555	.0555	.0555	15.5	1762.	3750.	1162.	37.9
100.	.0555	.0555	.0625	29.	1119.	2107.	951.	31.0
50.	.0555	.0555	.0740	38.5	820.	1242.	941.	30.6
25.	.0555	.0555	.0860	46.25	675.	810.	947.	30.8
0.	.0555	.0555	.1090	48.	532.	402.	937.	30.4

$P_4 = P_5 = 1.0$

With:

C_5 The resultant compression at L_5 (lbs).

L_5 The ligament moment at L_5 (in-lbs).

M_5 The muscle moment at L_5 (in-lbs).

Act. The maximum muscle activity (lbs/in^2).

Input parameters and results for equalized compression stress simulations.

Table 8.1

The maximum muscle moments computed for weights of 0, 25, 50 and 100 pounds are similar. This may seem contradictory at first, for as the weight increases the muscle moment stays relatively constant. What must be taken into account however is the the $ALPHA_0$ angle. As the weight increases, the $ALPHA_0$ angle is seen to decrease. This implies that the ligaments are balancing any additional moment due to the extra weight that is not being balanced by the muscles. Examining the ligament moment column in table 8.1, we see that this is indeed the case. As the weight gets heavier, the muscle moment increases and the $ALPHA_0$ angle decreases until at 400 pounds the muscle moment is at its maximum and the $ALPHA_0$ angle is at its minimum.

The degrees of freedom offered by the P_i's and the $ALPHA_0$ angle proved insufficient to generate the spread of compression equal to 20% for all weights and at all levels. An additional 5 degrees of freedom are available by the choice of the location of the center of reaction at each lumbar level. As stated in chapter 6, the centers of reaction can arbitrarily be placed within the disc at a distance of $\pm$40% the size of the disc from the center of the disc. The center of reaction at L5 was fixed at the most anterior portion (+.4). The center of reaction at L1 was chosen at each angle for every weight so as to give a spread of compression of 20%. The locations of the centers of reaction at L2, L3 and L4 were computed through the use of linear interpolation based on the locations of the centers of reaction of L1 and L5.

The location of the center of reaction of L1 for every weight plotted against the flexion angle is given in figure 8.6. From the family of curves plotted, it can be seen that as the flexion angle increases, the center of reaction moves towards the posterior portion of the disc. Interrestingly enough, this migration towards the posterior portion of the disc occurs at smaller flexion angles for lower weights.

Displacing the center of reaction so as to yield the desired result of a 20% spread of compression may seem like an artificial method to get that result. But there is a reason for considering the displacement of the centers of rotation as a valid tuning mechanism, it is the action of the Psoas muscle.

The Psoas has unique attachments to the individual vertebrae of the lumbar spine (Figure 5.5). It is in a perfect position to modulate the location of the centers of reaction of the vertebrae. Thus it is proposed that the function of the Psoas is to modulate the centers of reaction of the individual vertebrae in such a fashion that any task an individual performs subjects his/her spine to equal stress per unit area at all levels.

In this thesis the Psoas has not been modelled to function as a modulator of the centers of rotation, but rather as a 'weightlifting' muscle. As a 'weightlifting' muscle it fares poorly, being the only muscle that the model never recruits. But it has been shown in the literature [7] that the Psoas exhibits constant activity when an

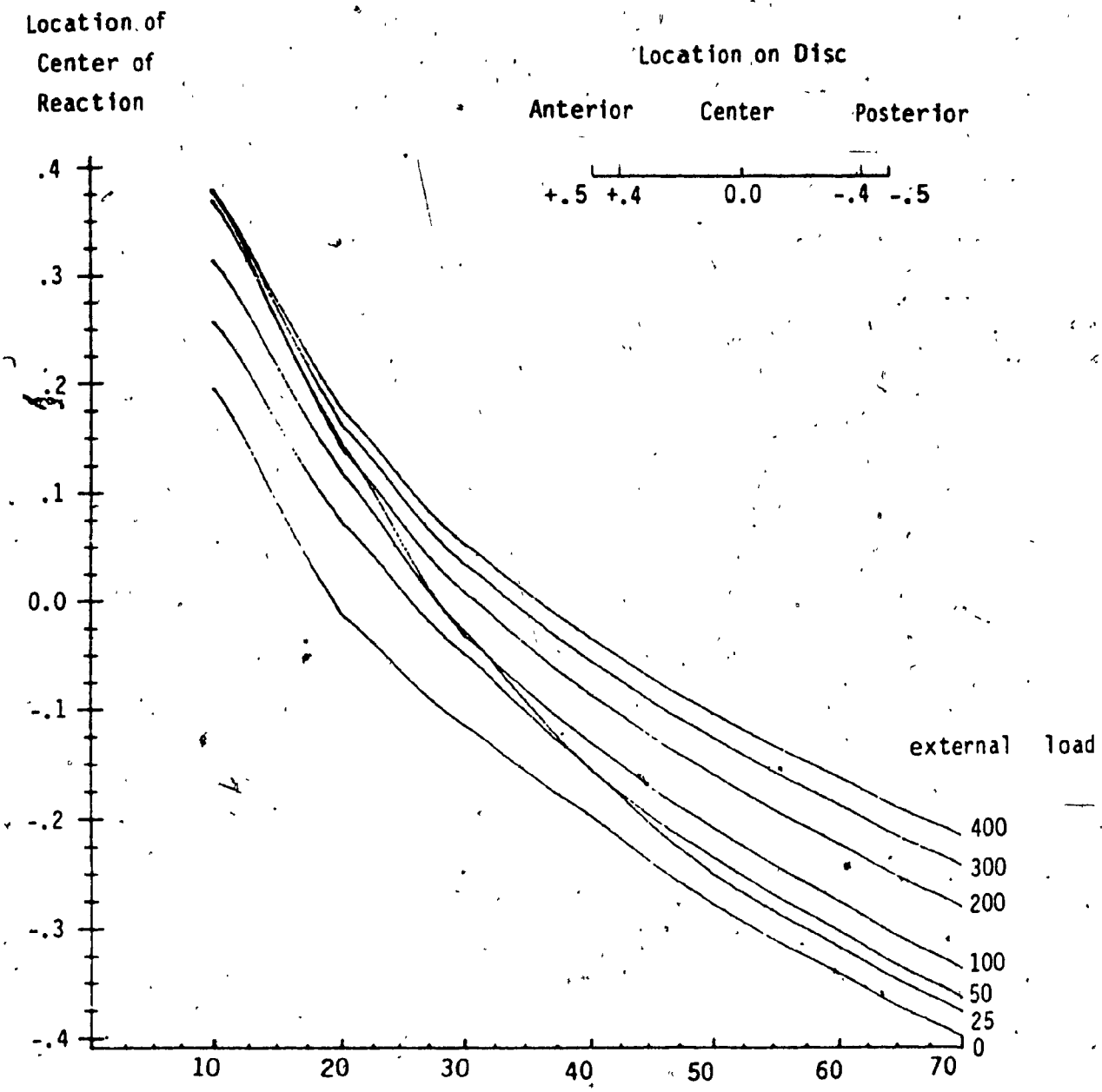

Migration patterns of center of reaction of L1

Figure 8.6

individual moves his/her torso. It can be concluded that the Psoas is improperly modelled as a 'weightlifting' muscle and must be modelled in another capacity. Following this train of thought, the closed loop system illustrated in figure 7.2 can be expanded so that stress is minimized by the muscles best suited to do so and stress is equalized by the Psoas modulating the locations of the centers of reaction of the lumbar vertebrae (Figure 8.7)

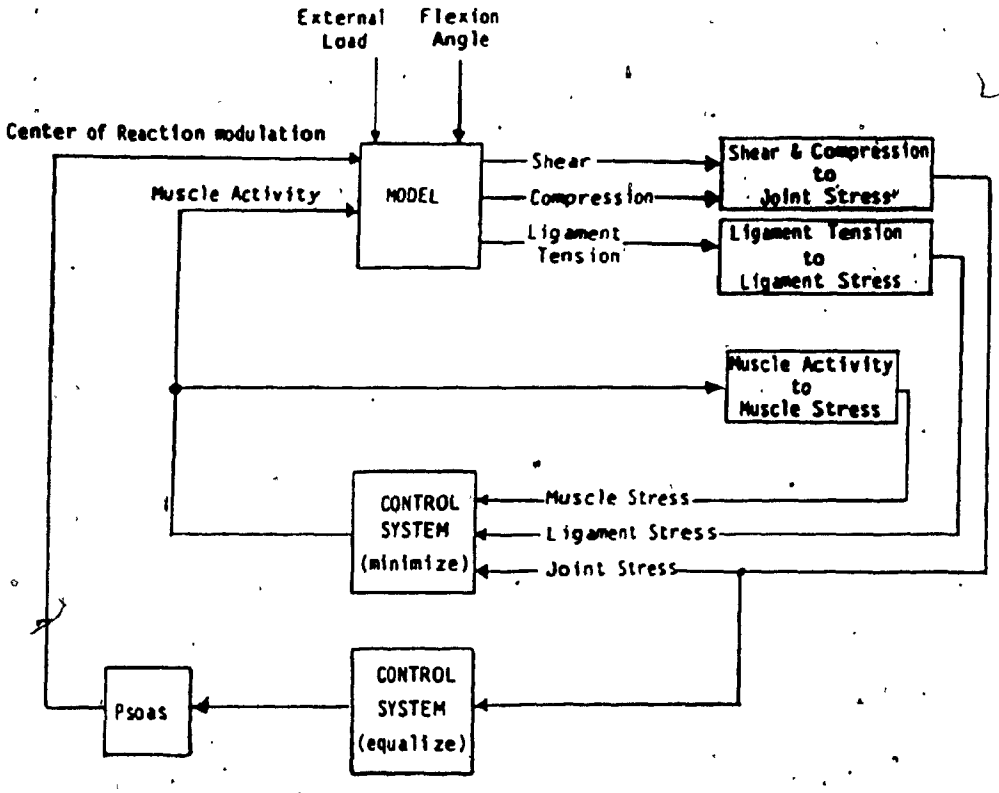

Closed loop system with stress minimization and equalization

Figure 8.7

Chapter 9 Conclusions

The relevant anatomy of the lumbar spine in the performance of a dead lift has been represented mathematically to form a model which computes the resultant forces acting on the various spinal components as a function of muscle activity. A control criterion which expresses the musculo - skeletal stress as a function of these resultant forces has been formed mathematically as an objective function. The objective function is minimized with respect to muscular activity to predict the muscle activity patterns during the performance of a dead lift. A comparison of experimental data from subjects performing light weight dead lifts and model - predicted muscle activity patterns shows the model capable of simulating muscle activity patterns common to a number of subjects. Also simulated is the Floyd & Silver shutoff. It should be noted however that the experimental data came from a small group of test subjects. Before any conclusive statements are made about the model's ability to predict muscle activity patterns, a more detailed study involving the collection and classification of muscle activity patterns is required.

The model has been tuned to predict the muscle activity patterns required for a series of dead lifts ranging from 0 to 400 pounds so that the compression stress at all levels could be equalized. It was discovered that the scaling factors (P_i's) did not offer enough degrees of freedom to obtain the desired stress equalization. The additional degrees of freedom necessary were attained by modulating the locations of the centers of reaction of the five lumbar levels. The

modulation patterns for different weights and different angles formed a non-random family of nested curves. Given that the modulation patterns exhibited non-random behavior, the Psoas was proposed as the mechanism through which the centers of reaction are modulated. A system in which 'weightlifting' muscles are controlled by a stress minimization subsystem and the Psoas is controlled by a stress equalization subsystem is presented.

The model demonstrated, based on the assumption that the centers of reaction could be modulated, that it was possible to find sets of locations for the centers of reaction and muscle activity patterns such that the compression stress in the spine could be equalized at all levels for all weights and angles. Furthermore, the predicted muscle activity patterns indicated that for equalized compression stress to be achieved some minimum level of muscle activity must be maintained regardless of the weight.

Future work based on this model could be to reasses the role of the Psoas muscle, change its mathematical description to make it modulate the locations of the centers of reaction and introduce the stress equalization loop in the overall model.

References

[1] Ahmad, R.; "Patient Assistance in Reduction of Medical Costs for Backache"; J. of Occupational Medicine, Vol. 21, no. 6, June 1979.

[2] Andersson, G.; "Epidemiologic Aspects on Low Back Pain in Industry"; Spine, Vol. 6, #1, Jan/Feb. 1981.

[3] Andersson, G.; "The Relation IAP / weight lifted"; presented to the ISSLS, Göteborg, June 1979.

[4] Andersson, G.; Herberts, T. N.; Ortengren, R.; "Quantitative electromyographic studies of back muscle activity related to posture and loading"; Orthop Clin North Am, Vol. 8, 1977.

[5] Aquino, C. F.; "A Dynamic Model of the Lumbar Spine"; Journal of Biomechanics, Vol. 3, 1970.

[6] Arvikar, R. J.; Seireg, A.; "Distribution of Spinal Disk Pressure in the Seated Posture Subjected to Impact"; Aviation, Space and Environmental Medicine, Vol. 49, Jan. 1978.

[7] Basmajian, J. V.; Muscles Alive; Williams & Wilkins Publishers, Baltimore, 1967.

[8] Belytschko, T.; Schwer, L.; Privitzer, E.; "Theory and applications of a 3-dimensional model of the lumbar spine"; Aviation, Space and Environmental Medicine, Vol.49, Jan. 1978.

[9] Blitzer, C.; "An Ounce of Prevention Eases Back Pain"; Business Insurance.

[10] Chadwick, P.; "Advising Patients on Back Care"; Physiotherapy, Vol. 65, #9, Sept. 1979.

[11] Eycleshymer, A. C.; Schoemaker, D. M.; A Cross - Section Anatomy; Appleton - Century - Crofts, New York, 1970.

[12] Farfan, H. F.; "The biomechanical advantage of lordosis and hip extension for upright activity in man as compared with other anthropoids"; Spine, Vol. 4, 1978.

[13] Farfan, H. F.; "Prospective Study."; Accepted for publication in Spine.

[14] Farfan, H. F.; Cossette, J.; Robertson, G.; Wells, R.; Kraus, H.; "The effects of torsion on the intervertebral joint; the role of torsion in the production of disc degeneration"; Journal of Bone and Joint Surgery, Vol. 52A, 1970.

[15] Floyd, W. F.; Silver, P. H. S.; "The function of the erector spinae muscles in certain movements and postures in man"; J. Physiology, Vol. 129, 1955.

[16] Frymoyer et. al.; "Epidemiologic Studies of Low Back Pain"; Spine, Vol. 5, #5, 1980.

[17] Gracovetsky, S.; Farfan, H. F.; Helleur, C.; "The Abdominal Mechanism"; accepted for publication in Spine.

[18] Gracovetsky, S.; Farfan, H. F.; Lamy, C.; "The Mechanism of the Lumbar Spine"; Spine, Vol. 6, #3, 1981.

[19] Gunterberg, B.; "Effects of major resection of the Sacrum, Clinical Studies on Urogenital and Anorectal function and a Biomechanical study on pelvic strength"; Thesis, Uno Lundgren Tryckeri, A. B., Göteborg, 1975.

[20] Hadler, N. M.; "Legal Ramifications of the Medical Definition of Back Disease"; Annuals of Internal Medicine, Vol. 84, #6, December 1978.

[21] Hadler, N. M.; "The Sociopolitical Climate Surrounding Low Back Pain"; J. of Occupational Medicine, Vol. 21, #10, October 1979.

[22] Helleur, C.; "Modelling of the Muscular Response of the Human Cervical Spine subjected to Acceleration"; Ph. D. Thesis, Concordia University, Montreal, 1983.

[23] Hess, J. L.; Lombard, C. F.; "Theoretical Investigation of Dynamic Response of Man to High Vertical Acceleration"; Journal of Aviation Medicine, Vol. 29, 1958.

[24] Hirsh, J.; "The Billion Dollar Backache"; National Safety News, May 1977.

[25] Hollinshead, W. H.; Anatomy for Surgeons: The Back and Limbs; Volume 3, Harper & Row, New York, 1969.

[26] Kelsey, J. L.; White, A. A.; "Epidemiology & Impact of Low Back Pain"; Spine, Vol. 5, #2, 1980.

[27] Kirkaldy-Willis, W.; Farfan, H. F.; "The present status of spinal fusion."; Clin. Ortho. & Rel. Res., 1981.

[28] Latham, F.; "A Study of Ballistics: Seated Ejections"; Proc. Royal Society B - 147, 19[illegible].

[29] Lucas, D.; Bresler, B.; "Stability of Ligamentous Spine"; Biomechanics Lab, Report 40, University of California, San Francisco, 1961.

[30] McClintic, J. R.; Basic Anatomy and Physiology of the Human Body; John Wiley & Sons, Inc., New York, 1975.

[31] McNeill, T.; Addison, R.; Andersson, G.; Schultz, A.;"Trunk strength in attempted flexion, extension and lateral bending in healthy subjects and low back patients"; Presented at the International Society for the Study of the Lumbar Spine, Göteborg, Sweden, May 1979.

[32] Nachemson, A.; "Lumbar intradiscal pressure"; Acta Orthop Scand Supp, 1960.

[33] National Health Survey, "Prevalence of Selected Impairments"; DHHS Publication 81.

[34] Nordby, E. J.; "Epidemiology & Diagnosis in Low Back Injury"; Occupational Health & Safety, January 1981.

[35] Quinet, R. J.; Hadler, N. M.; "Diagnosis and Treatment of Backache"; Seminars in Arthritis and Rheumatism, Vol. 8, #4, May, 1979.

[36] Rolander, S.; Blair, W.E.; "Deformation and fracture of the lumbar vertebral end-plate"; Ortho. Clin. North Am. Vol. 6, #1, Jan 1975.

[37] Spence, A. P.; Mason, E. B.; Human Anatomy and Physiology; Benjamin / Cummings, Menlo Park, 1979.

[38] Toth, R.; "Multiple Degree - of - Freedom Nonlinear Spinal Model"; 19th Ann. Conf. on Eng. in Med. and Biol.; San Francisco, California, 1967.

[39] Toufexis, A.; "The Aching Back!"; Time, July 14, 1980.

[40] Ustby, R. J.; "Pre-employment Back X-Rays - An Unnecessary Practice: Try Another Approach"; Occupational Health Nursing, July 1981.

[41] Week, B. D.; "How to Avoid that Aching BACK"; Am. J. of Nursing, May, 1980.

[42] White, A. A.; Panjabi, M. M.; Clinical Biomechanics of the Spine; J. B. Lippincott Comp., Philadelphia, 1978.

[43] Wolff, J.; "Das Gesetz der Transformation der Knochen"; Berlin, Hirschwald, 1892.

Appendix A: Computation of the Motion of the Spine

A.1) Description of Spinal Motion

The task simulated in this thesis is a sagittal plane dead lift. The motion of a dead lift is modelled by eight images of the spine at flexion angles of 0 to 70 degrees, in increments of 10 degrees (Figure 5.20). From a sagittal plane X-Ray of a subject in the upright position, it is possible to estimate the coordinates of the five centers of rotation of the Lumbar IV joints (cx_i, cy_i) (Figure 5.16), the disc inclination angles (DA_i) (Figure 5.17) and the initial disc wedge angles (DWI_i) (Figure 5.18). The centers of rotation are taken to be located at the intersection of the line through the posterior third of the disc and the disc bisector. Calculation of the motion of the spine also requires the flexion angle ($ALPHA_0$) which delimits the transition between the two arcs of motion of the lumbar spine: spine flexion and hip flexion. At the $ALPHA_0$ angle, the spine is fully flexed. This results in a near linear spinal lordosis. The straightening of the lumbar curve is modelled by assuming all the centers of rotation to be collinear at a flexion angle of $ALPHA_0$ degrees (Figure A.1).

Disc deformation due to compression is ignored, thus the distance between the individual centers of rotation does not change. The distances are calculated from the initial coordinates and are maintained throughout the computations. Let the distance between the center of rot-

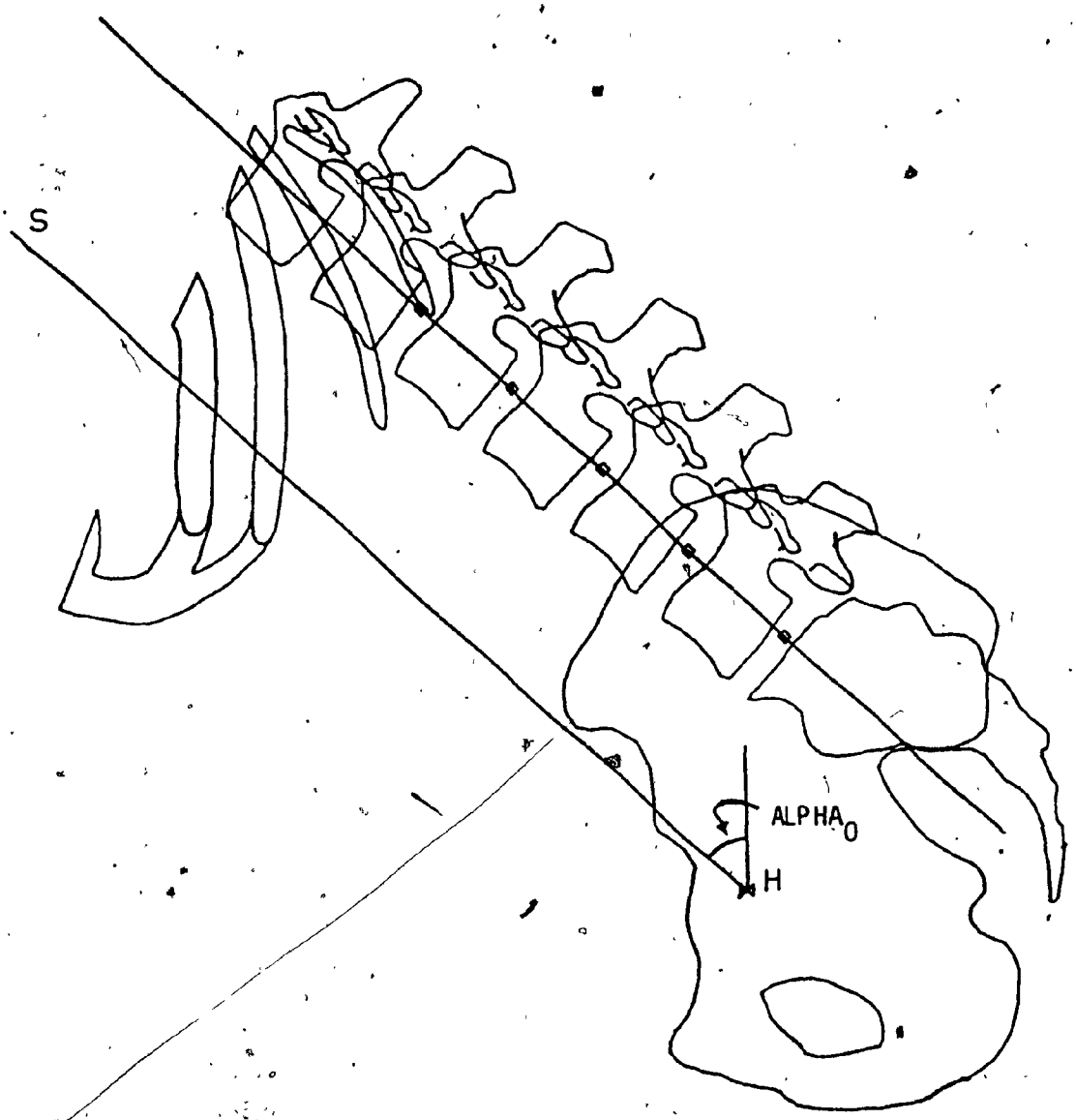

At a flexion angle of ALPHA$_0$ degrees
the centers of rotation are assumed collinear.

Figure A.1

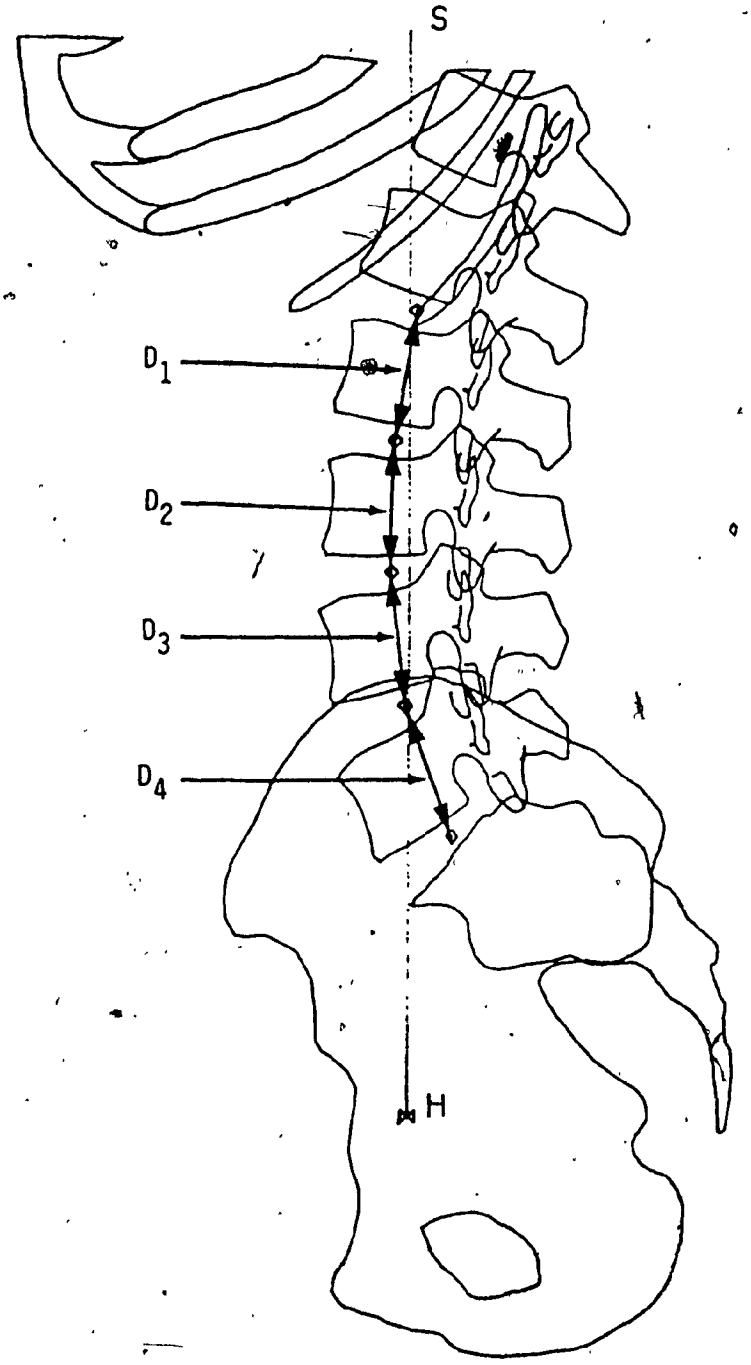

Determination of the distance between adjacent centers of rotation

Figure A.2

ation of L_i and the center of rotation of L_{i+1} be D_i (Figure A.2). The equation defining D_i is:

$$D_i = ((cx_i - cx_{i+1})^2 + (cy_i - cy_{i+1})^2)^{\frac{1}{2}} \qquad (A.1)$$

Once these distances are calculated the locations of the centers of rotation at $ALPHA_0$ can be calculated. L_5 is fixed, hence its coordinate at $ALPHA_0$ is its location in the upright position. Let the coordinates of the center of rotation for L_i at $ALPHA_0$ be (ltx_i, lty_i). Thus we have:

$$ltx_5 = cx_5 \qquad (A.2)$$

$$lty_5 = cy_5 \qquad (A.3)$$

The location of the center of rotation of L_4 can now be determined: it is on a line intersecting (ltx_5, lty_5) that has been rotated $ALPHA_0$ degrees from the upright position and is at a distance D_4 from (ltx_5, lty_5). The equations defining the location of (ltx_4, lty_4) are:

$$ltx_4 = ltx_5 - D_4 * SIN(ALPHA_0) \qquad (A.4)$$

$$lty_4 = lty_5 + D_4 * COS(ALPHA_0) \qquad (A.5)$$

In general, the equations defining the location of the center of rotation of L_i are:

$$ltx_i = ltx_{i+1} - D_i * SIN(ALPHA_0) \qquad (A.6)$$

$$lty_i = lty_{i+1} + D_i * COS(ALPHA_0) \qquad (A.7)$$

A.2) Spine Flexion

This arc of motion corresponds to a flexion angle between 0 and $ALPHA_0$ degrees. When the spine flexes, the center of rotation of L_5 is assumed not to move. L_4 rotates about L_5, L_3 rotates about L_4, L_2 about L_3 and L_1 about L_2. Let the location of the center of rotation of L_i be (ufx_i, ufy_i). For any ALPHA:

$$ufx_5 = cx_5 \tag{A.8}$$

$$ufy_5 = cy_5 \tag{A.9}$$

Before calculating the locations of L_1 to L_4, the angle ($BETA_i$) through which level 'i' must rotate about level 5 to go from its initial position to its fully flexed position at $ALPHA_0$ must be computed for levels 1 to 4. $BETA_i$ is the angle between the level 'i' vector going from (cx_5, cy_5) to (cx_i, cy_i) and the unit vector at (cx_5, cy_5) describing the fully flexed limit of motion of the spine at $ALPHA_0$ (Figure A.3). The unit vector is given by:

$$\hat{V} = (-SIN(ALPHA_0), COS(ALPHA_0))^t \tag{A.10}$$

The level 'i' vector is given by:

$$V_i = ((cx_i - cx_5), (cy_i - cy_5))^t \tag{A.11}$$

The angle between the two vectors is given by the dot product relationship:

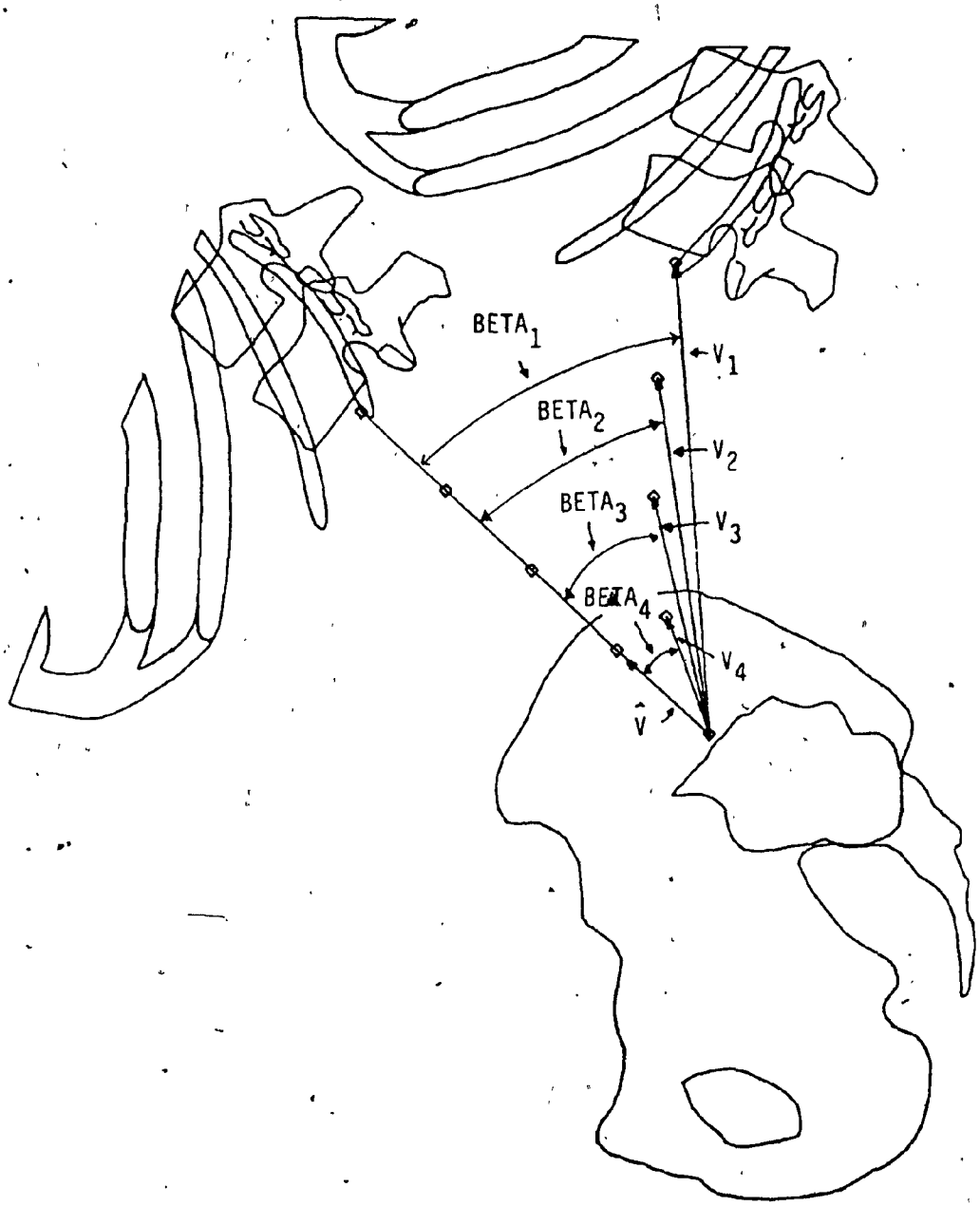

Determination of $BETA_i$.

Figure A.3

$$BETA_i = \cos^{-1}\left[\frac{\hat{v}\cdot v_i}{\|v_i\|}\right] \qquad (A.12)$$

The fraction of forward flexion is defined as:

$$frac = (ALPHA) / (ALPHA_0) \qquad (A.13)$$

The flexed locations of levels 1 to 4 are calculated by applying steps 1 to 3 with 'i' going from 4 to 1:

STEP 1) The location of level 'i' is calculated by determining the intersection of a circle with a radius equal to D_i centered at (ufx_{i+1}, ufy_{i+1}) with a line passing through (cx_5, cy_5) that has a slope angle given by:

$$\text{slope angle} = 90 + BETA_i * (frac - 1.0) + ALPHA_0 \qquad (A.14)$$

The line with this slope angle represents the rotation of level 'i' about L_5 proportional to the total angle level 'i' must rotate through to reach its position at $ALPHA_0$ (Figure A.4).

STEP 2) The intersection between the line and the circle is determined as follows.

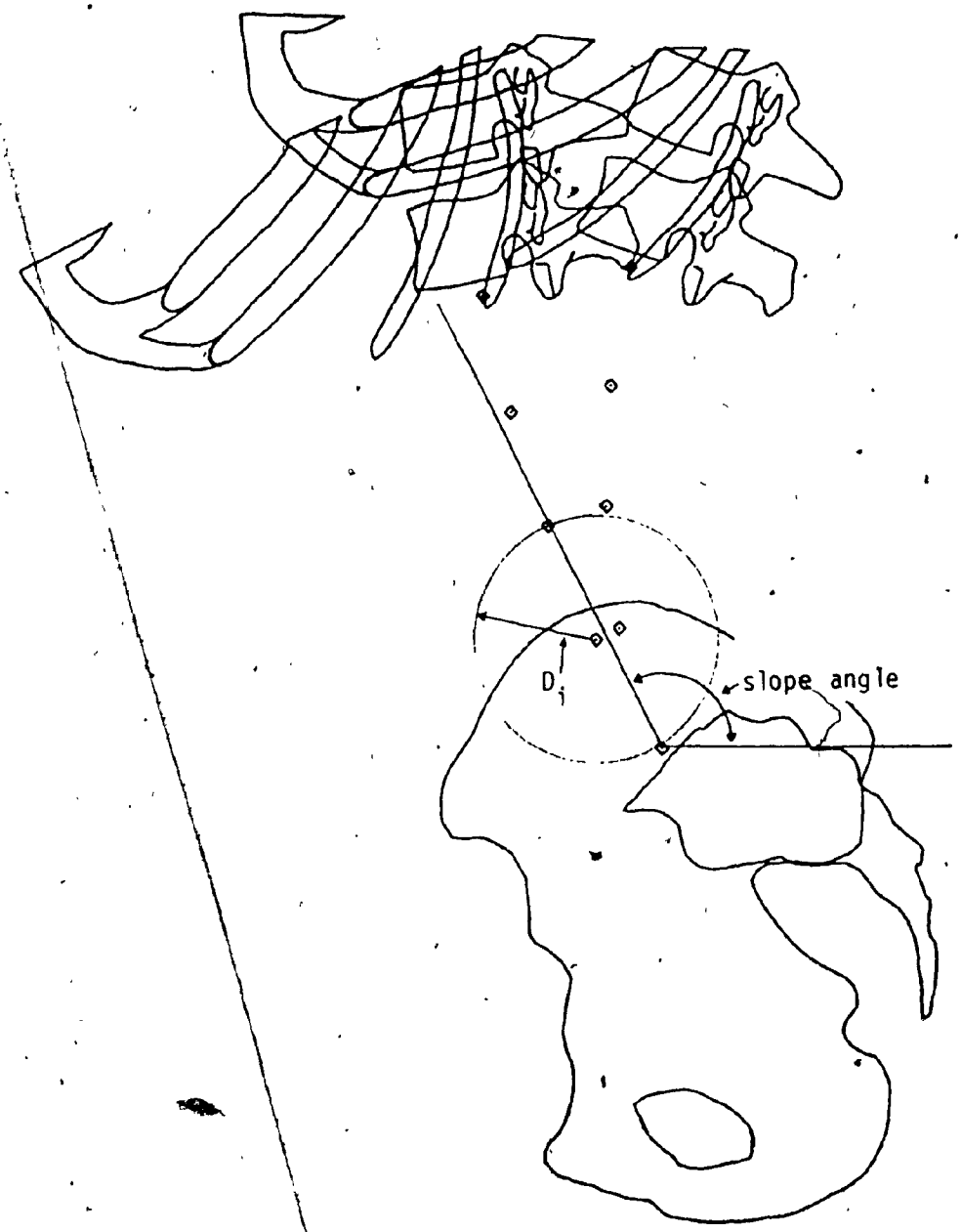

Line and Circle Intersection for determination of location of center of rotation

Figure A.4

2.1) The differentials of the slope are computed:

$$DX = \text{COS}(\text{ slope angle }) \qquad \text{(A.15)}$$

$$DY = \text{SIN}(\text{ slope angle }) \qquad \text{(A.16)}$$

If the absolute value of DX is less than .001 then the line is near vertical through L_5 and this is treated as a special case: go to step 2.6.

2.2) The slope and Y - intercept of the line are computed:

$$\text{SLOPE} = DY / DX \qquad \text{(A.17)}$$

$$\text{YINT} = cy_5 - \text{SLOPE} * cx_5 \qquad \text{(A.18)}$$

We now have the slope - intercept form of the line, i.e.

$$Y = \text{SLOPE} * X + \text{YINT} \qquad \text{(A.19)}$$

The equation of the circle is

$$(X - ufx_{i+1})^2 + (Y - ufy_{i+1})^2 = D_i^2 \qquad \text{(A.20)}$$

2.3) Substituting 'Y' in equation A.20 with equation A.19 yields the following quadratic equation:

$$A * X^2 + B * X + C = 0 \qquad \text{(A.21)}$$

with:

$$A = 1.0 + SLOPE^2 \qquad (A.22)$$

$$B = 2.0*(SLOPE * (YINT - ufy_{i+1}) - ufx_{i+1}) \qquad (A.23)$$

$$C = ufx^2_{i+1} + (YINT - ufy_{i+1})^2 - D_i^2 \qquad (A.24)$$

2.4) Solving the quadratic equation gives two solutions, X_1 and X_2. These two X - values are used in equation A.19 to compute two Y - values:

$$Y_1 = SLOPE * X_1 + YINT \qquad (A.25)$$

$$Y_2 = SLOPE * X_2 + YINT \qquad (A.26)$$

The intersection of the circle and the line is at two points - (X_1, Y_1) and (X_2, Y_2). The proper point must be determined. As stated earlier, given the upright position of the spine (0 degrees flexion) the path of the lumbar spine is computed in flexion angle increments of 10 degrees, from 10 to 70 degrees. Thus when computing the current position of level 'i' the previous position of level 'i' is available. The point that is chosen is the one that is the closest to the previous position of level 'i'.

2.5) Let the previous position of level 'i' be at point (PX_i, PY_i). The distances between this point and the two intersections are given by:

$$DST_1 = ((X_1 - PX_i)^2 + (Y_1 - PY_i)^2)^{\frac{1}{2}} \qquad (A.27)$$

$$DST_2 = ((X_2 - PX_i)^2 + (Y_2 - PY_i)^2)^{\frac{1}{2}} \qquad (A.28)$$

If DST_1 is greater than DST_2 then set

$$ufx_i = X_2 \quad (A.29)$$

$$ufy_i = Y_2 \quad (A.30)$$

else if DST_2 is greater than DST_1 then set

$$ufx_i = X_1 \quad (A.31)$$

$$ufy_i = Y_1 \quad (A.32)$$

Go to Step 3.

2.6) The special case of a vertical line through L_5 is easily dealt with. Since it is a vertical line, the X - coordinate does not change. All that needs to be computed is the location of the Y - coordinate on the circle. There are two solutions, but the proper one is the Y - coordinate closest to the previous position of level 'i'. From geometric considerations, it is the Y - coordinate with the largest value. Thus:

$$ufx_i = cx_5 \quad (A.33)$$

$$ufy_i = ufy_{i+1} + (D_i^2 - (cx_5 - ufx_{i+1})^2)^{\frac{1}{2}} \quad (A.34)$$

STEP 3) Having computed ufx_i and ufy_i, the previous location variables are updated:

$$PX_i = ufx_i \quad (A.35)$$

$$PY_i = ufy_i \quad (A.36)$$

A.3) Hip Flexion

When the flexion angle ALPHA is greater than $ALPHA_0$, the entire spine and pelvis rotate about the hips as a rigid body (Figure A.5). The lumbar spine is locked in its completely flexed position with all the centers of rotation assumed to be collinear. The net rotation angle about the hips is equal to the flexion angle minus $ALPHA_0$:

$$ANG = ALPHA - ALPHA_0 \qquad (A.37)$$

The locations of the centers of rotation are determined by rotating the coordinates of the centers of rotation at $ALPHA_0$ (ltx_i, lty_i) by ANG degrees. Let the location of the center of rotation of L_i be (xr_i, yr_i). The equations defining (xr_i, yr_i) are:

$$xr_i = ltx_i * COS(ANG) - lty_i * SIN(ANG) \qquad (A.38)$$

$$yr_i = ltx_i * SIN(ANG) + lty_i * COS(ANG) \qquad (A.39)$$

A.4) Disc Inclination Angle

The disc inclination angles describe the orientations in space of the five lumbar intervertebral joints with respect to the Hip - Shoulder line. Each joint has associated with it an imaginary line that bisects the disc and intersects the center of rotation for that joint. The disc inclination angle is defined as the angle between a line perpendicular to the Hip - Shoulder line and the bisector of that disc (Figure 5.17).

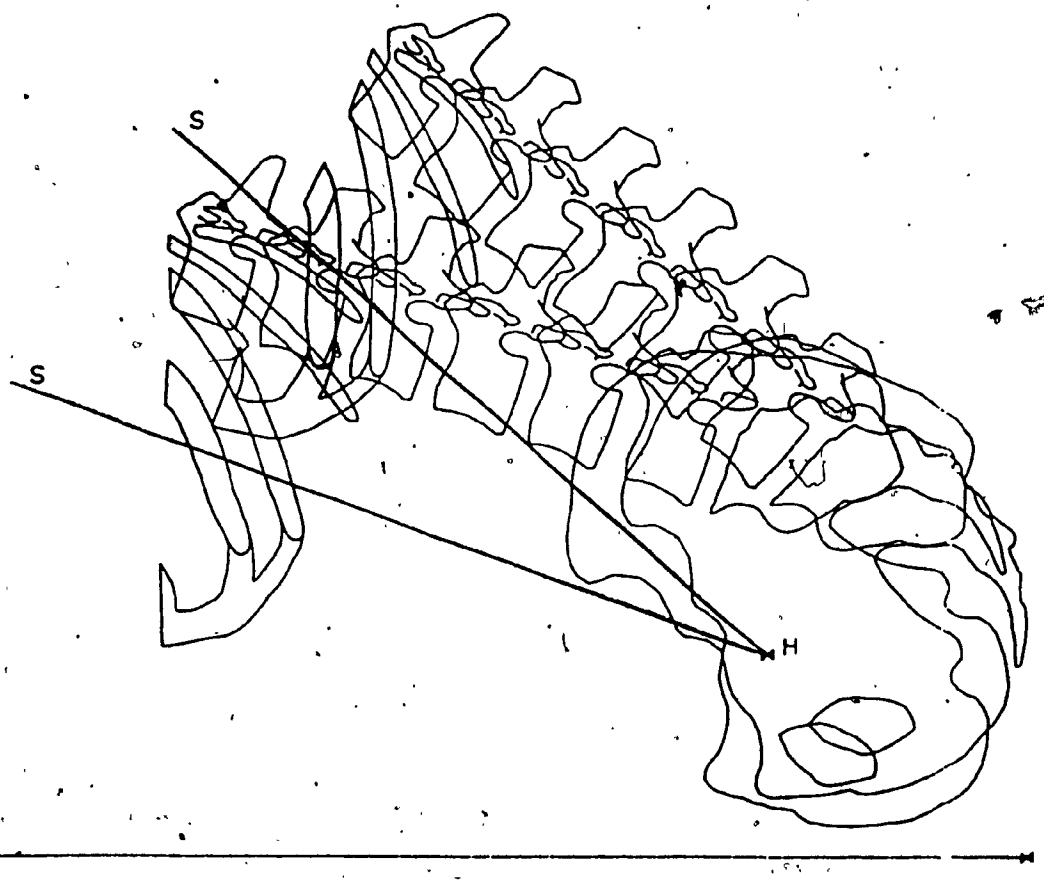

Spinal rotation about the hips as a rigid body for flexion angles greater than $ALPHA_0$

Figure A.5

Computation of the disc inclination angle for any flexion angle ALPHA is based upon three assumptions: 1) For a flexion angle of $ALPHA_0$ degrees, all the disc inclination angles are zero. This implies that at $ALPHA_0$ all the discs are perpendicular to the Hip - Shoulder line (Figure 5.18). 2) For all flexion angles greater than $ALPHA_0$, the disc inclination angles remain zero. This implies that the spine is locked in its fully flexed position relative to the pelvis. 3) For flexion angles less than $ALPHA_0$, the disc inclination angle goes to zero linearly proportional to ALPHA divided by $ALPHA_0$.

Let the disc inclination angle in the upright position for level 'i' be $GAMMA_i$. The equations defining the disc inclination angle relative to a line normal to the Hip - Shoulder line for any ALPHA are:

$$DAr_i = GAMMA_i * (1 - frac) \qquad ALPHA < ALPHA_0 \qquad (A.40)$$

$$DAr_i = 0 \qquad ALPHA \geq ALPHA_0 \qquad (A.41)$$

To transform this angle to the reference coordinate system it need only be rotated by the given flexion angle.

$$DA_i = DAr_i + ALPHA \qquad ALPHA < ALPHA_0 \qquad (A.42)$$

$$DA_i = ALPHA \qquad ALPHA \geq ALPHA_0 \qquad (A.43)$$

A.5) Disc Wedge Angle

When in the upright position, the endplates of any given vertebral body in the lumbar region are usually not quite parallel to those of the vertebral body either above or below it. Rather, they make some small angle with respect to the disc bisector. This angle is defined as the disc wedge angle (Figure 5.18). As the spine unfolds to its $ALPHA_0$ position, the disc wedge angle decreases to some terminal value at the $ALPHA_0$ position (Figure A.6). For flexion angles greater than $ALPHA_0$, the disc wedge angle remains at its terminal value (the spine is fully flexed). Compression of the disc causes it to deform, but the change is small for the range of compression forces considered in this study and is thus ignored. For flexion angles less than $ALPHA_0$ the disc wedge angles are assumed to vary linearly from their initial to terminal values proportional to ALPHA divided by $ALPHA_0$. Let DWI_i and DWT_i be the initial and terminal values of the disc wedge angle for level 'i'. The disc wedge angle, DW_i, is given by:

$$DW_i = DWI_i + (DWT_i - DWI_i) * \text{frac} \quad ALPHA < ALPHA_0 \qquad (A.44)$$

$$DW_i = DWT_i \qquad ALPHA \geq ALPHA_0 \qquad (A.45)$$

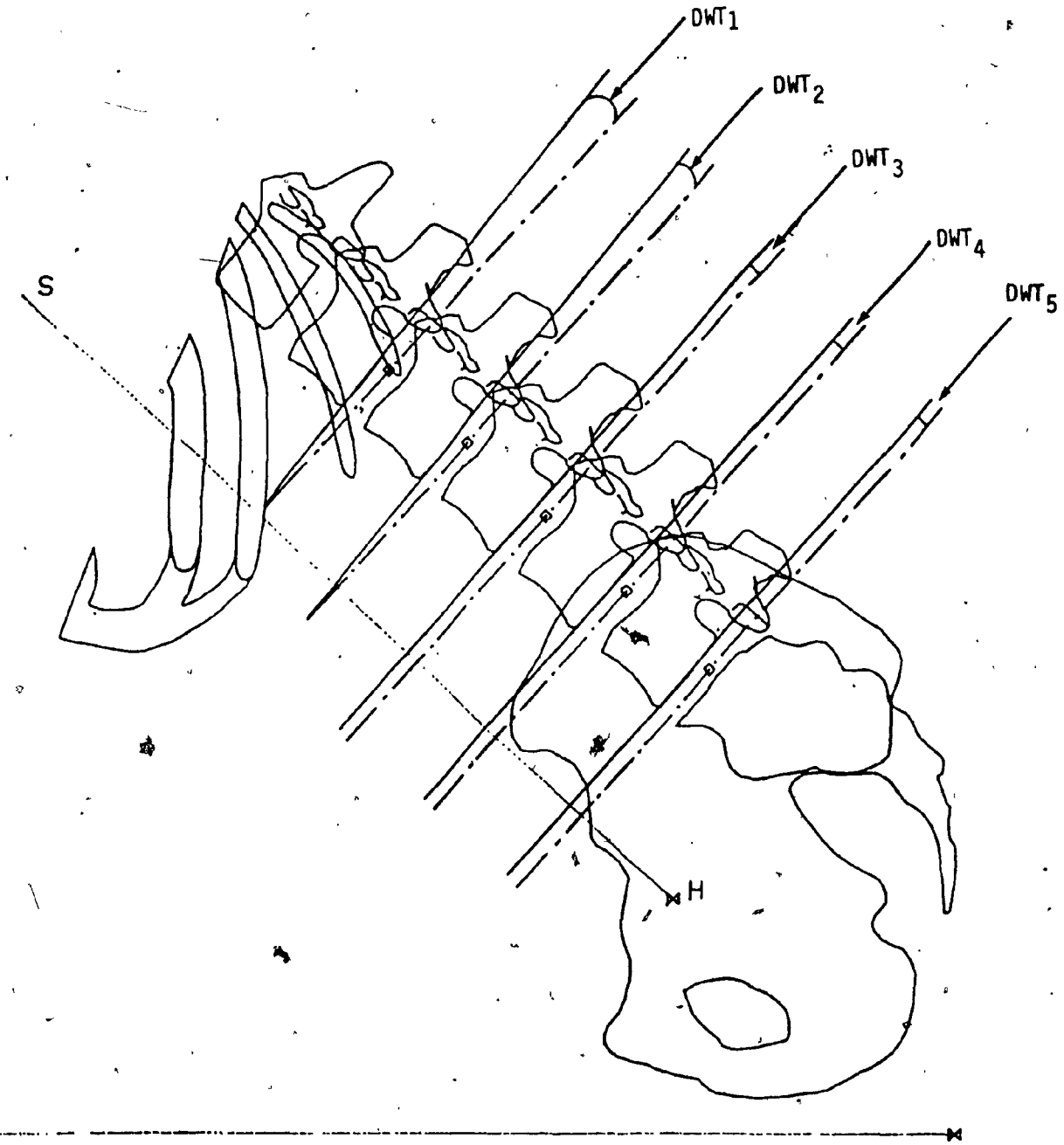

The Terminal Disc Wedge Angle

Figure A.6

Appendix B: Derivation of the System Equations.

In this section the resultant shear and compression at the five lumbar intervertebral joints and the ligament tension are derived as a function of muscle activity and external load. The forces and moments induced by the individual muscles are derived. The muscle grouping described in chapter 5 is used to assemble a muscle moment matrix. Given the external load and muscle moment matrix, the ligament tension equations are derived. Finally the resultant shear and compression equations are derived.

B.1) Muscle Force and Muscle Moment

Muscle activity produces muscle force. The muscle force vector is defined by its direction (a unit vector along the muscle strand line of action) and its magnitude (the product of muscle activity and muscle strand cross sectional area) (Figure B.1).

$$\vec{F}_M = K \cdot A \cdot \hat{F}_M \qquad (B.1)$$

where:

$\vec{F}_M$ is the muscle force vector

K is the muscle activity

A is the muscle strand cross sectional area

$\hat{F}_M$ is the unit vector along the muscle strand line of action

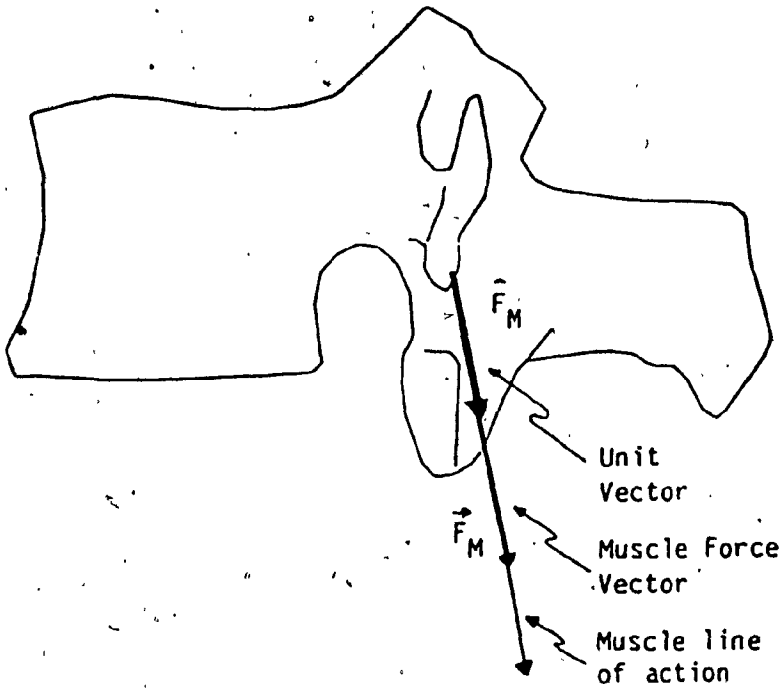

$$\vec{F}_M = K \cdot A \cdot \hat{F}_M$$

where:

$\vec{F}_M$ is the muscle force vector

K is the muscle activity

A is the muscle strand cross sectional area

$\hat{F}_M$ is the unit vector along the muscle strand line of action

Muscle Force Vector

Figure B.1

By combining the muscle strand cross sectional area and the unit vector, the muscle force vector can be written as the product of the muscle activity and a muscle activity to force scaling vector.

$$\vec{FA} = A \cdot \hat{F}_M \tag{B.2}$$

$$\vec{F}_M = K \cdot \vec{FA} \tag{B.3}$$

where:

$\vec{FA}$ is the muscle activity to force scaling vector

A is the muscle strand cross sectional area

$\hat{F}_M$ is the unit vector along the muscle strand line of action

K is the muscle activity

$\vec{F}_M$ is the muscle force vector

Modelling an individual muscle will yield muscle force equations like equation B.3 for each lumbar IV joint. The resultant muscle force at an IV joint is often the summed forces of several strands of that muscle. Thus the resultant muscle force vector can be written as the product of the muscle activity and a net muscle activity to force scaling vector.

$$\vec{FN}_i = \sum_{j=1}^{N_S} \vec{FA}_j \tag{B.4}$$

$$\vec{F}_{M_{Ri}} = K \cdot \vec{FN}_i \tag{B.5}$$

where:

$\vec{FN}_i$ is the net muscle activity to force scaling vector for level 'i'

$\vec{FA}_j$ is the muscle activity to force scaling vector for muscle strand 'j' acting on level 'i'

N_s is the number of muscle strands acting on level 'i'

K is the muscle activity

$\vec{F}_{M_{Ri}}$ is the resultant muscle force on level 'i'

The moment about a particular center of reaction is given by the vector cross product of the lever arm distance vector (running from the center of reaction to the origin of the muscle strand line of action) and the muscle strand force vector (Figure B.2)

$$\vec{M} = \vec{D}_{i,j} \times \vec{F}_{M_j} \qquad (B.6)$$

where:

$\vec{M}$ is the moment induced by the muscle activity

$\vec{D}_{i,j}$ is the lever arm distance vector from center of reaction 'i' to the origin of the line of action of muscle strand 'j'

$\vec{F}_{M_j}$ is the force vector of muscle strand 'j'

The muscle strand cross sectional area is constant. The distance vector and line of action unit vector are constant for any given flexion angle. Furthermore, all the vectors lie in the saggital plane with only X & Y components. The cross product of these vectors will

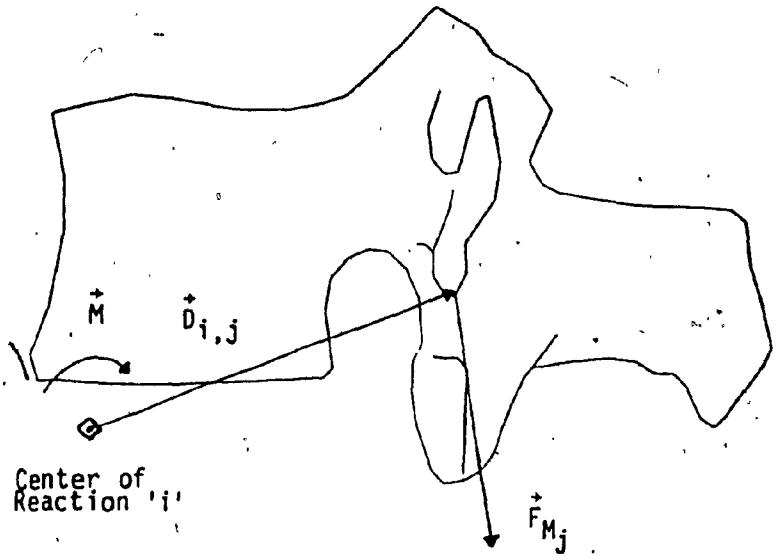

$$\vec{M} = \vec{D}_{i,j} \times \vec{F}_{M_j}$$

$\vec{M}$ is the moment induced by the muscle activity

$\vec{D}_{i,j}$ is the lever arm distance vector from center of reaction 'i' to the origin of the line of action of muscle strand 'j'

$\vec{F}_{M_j}$ is the force vector of muscle strand 'j'

Moment induced by the muscle force vector.

Figure B.2

yield a vector in the Z direction. The sign of the Z direction component indicates its orientation. To simplify the mathematics, the result of the cross product will be written as a scaled triple product preserving the Z direction component. This simplification is valid only because of the two dimensional nature of the model. Extending the model to three dimensions would modify the equilibrium conditions stated in chapter 5 and would necessitate rewriting the equations.

Factoring out the muscle activity, the moment can be written as the scalar product of the muscle activity and a muscle activity to moment scaling factor denoted MSF.

$$M = K \cdot MSF \tag{B.7a}$$

$$MSF = [\vec{D}_{i,j} \times \vec{FA}_j] \bullet \hat{Z} \tag{B.7b}$$

In the reference coordinate system, a positive moment is counter-clockwise and a negative moment is clockwise.

Modelling an individual muscle will yield a moment equation like equation B.7a for each lumbar IV joint. The resultant moment at an IV joint is often due to several strands of the muscle each inducing moments at the IV joint. Thus the resultant moment can be written as the product of the muscle activity and a net muscle activity to moment scaling factor. The five net scaling factors can be assembled in a [5 X 1] vector. Multiplying this vector by the muscle activity yields

a [5 x 1] vector of the resultant moments induced by the muscle at the IV joints.

$$\begin{bmatrix} M_1 \\ M_2 \\ M_3 \\ M_4 \\ M_5 \end{bmatrix} = K \cdot \begin{bmatrix} MSF_1 \\ MSF_2 \\ MSF_3 \\ MSF_4 \\ MSF_5 \end{bmatrix} \qquad (B.8)$$

where:

M_i is the moment induced at level 'i'

MSF_i is the net muscle activity to moment scaling factor for level 'i'

K is the muscle activity

These results will be used to derive the net muscle activity to force scaling vectors and the net muscle activity to moment scaling factors for all the muscles.

PSOAS

Refer to figure B.3 for the numbering and directions of the muscle strands.

CENTER OF REACTION R_i (i = 1 to 4)

$$\vec{FN}_i = \sum_{j=1}^{i+1} \vec{FA}_j \qquad (B.9)$$

$$MSF_i = \left[\sum_{j=1}^{i+1} (\vec{D}_{i,j} \times \vec{FA}_j)\right] \cdot \hat{Z} \qquad (B.10)$$

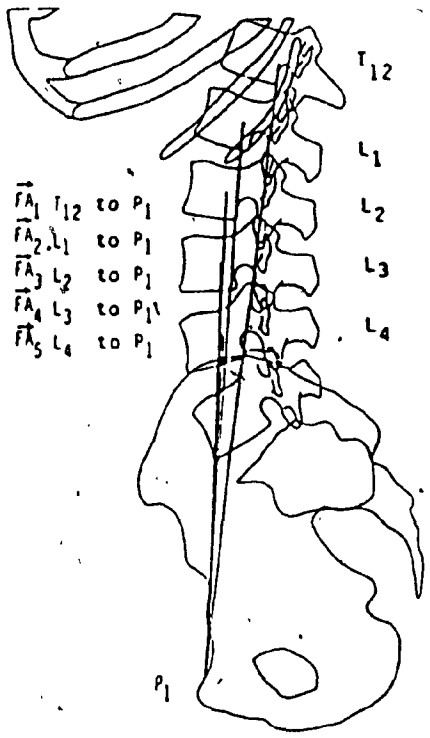

Psoas
Figure B.3

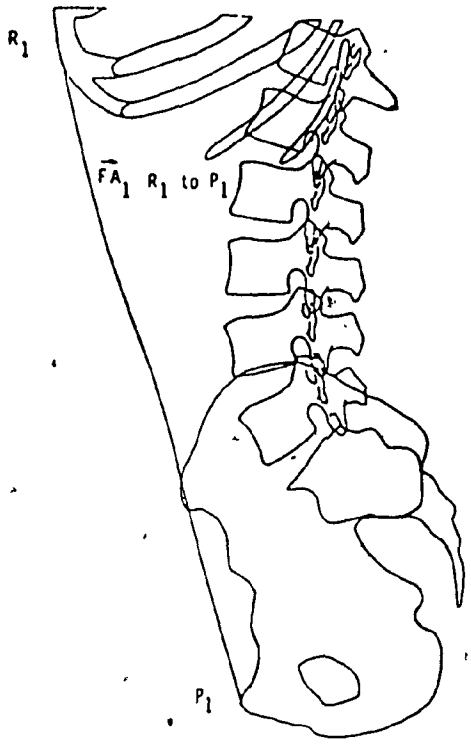

Rectus Abdominis
Figure B.4

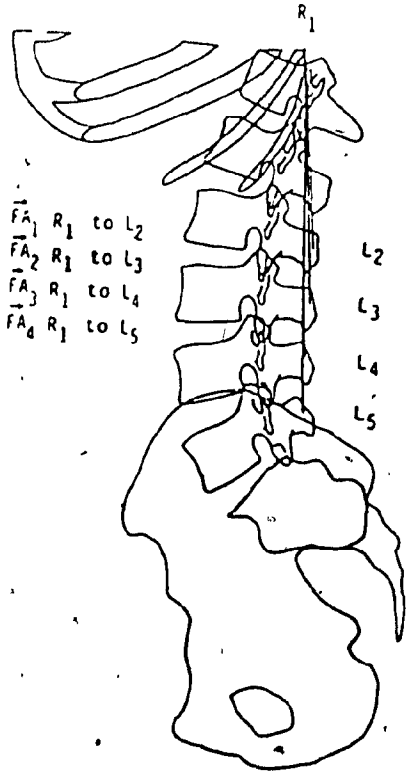

Medialis Spinalis
Figure B.5

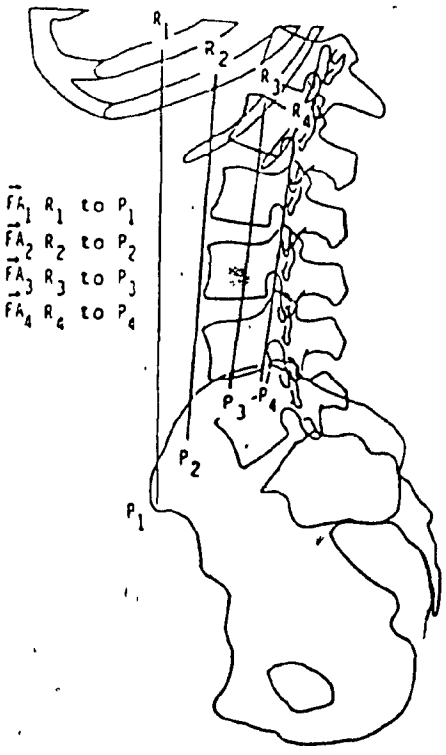

External Obliques
(Posterior part)
Figure B.6

CENTER OF REACTION R_5

$$\vec{FN}_5 = \sum_{j=1}^{5} \vec{FA}_j \qquad (B.11)$$

$$MSF_5 = [\sum_{j=1}^{5} (\vec{D}_{5,j} \times \vec{FA}_j)] \bullet \hat{Z} \qquad (B.12)$$

RECTUS ABDOMINIS

Refer to figure B.4 for the direction of the muscle strand.

CENTER OF REACTION R_i (i = 1 to 5)

$$\vec{FN}_i = \vec{FA}_1 \qquad (B.13)$$

$$MSF_i = [\vec{D}_{i,1} \times \vec{FA}_1] \bullet \hat{Z} \qquad (B.14)$$

MEDIALIS SPINALIS

Refer to figure B.5 for the numbering and directions of the muscle strands.

CENTER OF REACTION R_i (i = 1 to 4)

$$\vec{FN}_i = \sum_{j=i}^{4} \vec{FA}_j \qquad (B.15)$$

$$MSF_i = [\sum_{j=i}^{4} (\vec{D}_{i,j} \times \vec{FA}_j)] \bullet \hat{Z} \qquad (B.16)$$

CENTER OF REACTION R_5

As it has been modelled, Medialis Spinalis does not exert any force nor induce any moment on center of reaction R_5.

$$\vec{FN}_5 = (0,0,0)^t \qquad (B.17)$$

$$MSF_5 = 0 \qquad (B.18)$$

EXTERNAL OBLIQUES (Posterior part)

Refer to figure B.6 for the numbering and directions of the muscle strands.

CENTER OF REACTION R_i (i = 1 to 5)

$$\vec{FN}_i = \sum_{j=1}^{4} \vec{FA}_j \qquad (B.19)$$

$$MSF_i = \left[\sum_{j=1}^{4} (\vec{D}_{i,j} \times \vec{FA}_j)\right] \bullet \hat{Z} \qquad (B.20)$$

ILIOCOSTALIS LUMBORUM (Superficial part)

Refer to figure B.7 for the numbering and directions of the muscle strands.

CENTER OF REACTION R_i (i = 1 to 5)

$$\vec{FN}_i = \sum_{j=1}^{3} \vec{FA}_j \qquad (B.21)$$

$$MSF_i = \left[\sum_{j=1}^{3} (\vec{D}_{i,j} \times \vec{FA}_j)\right] \bullet \hat{Z} \qquad (B.22)$$

QUADRATUS LUMBORUM

Refer to figure B.8 for the direction of the muscle strand.

CENTER OF REACTION R_i (i = 1 to 5)

$$\vec{FN}_i = \vec{FA}_1 \qquad (B.23)$$

$$MSF_i = [\vec{D}_{i,1} \times \vec{FA}_1] \bullet \hat{Z} \qquad (B.24)$$

LATISSIMUS DORSI

Refer to figure B.9 for the numbering and directions of the muscle strands.

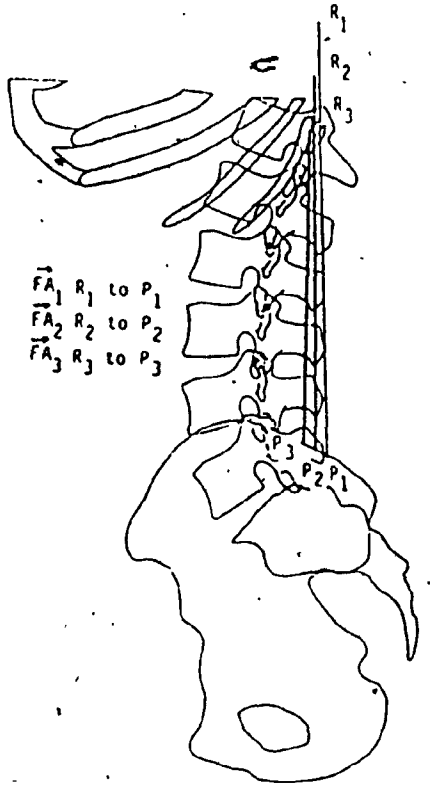

Iliocostalis Lumborum
(Superficial part)
Figure B.7

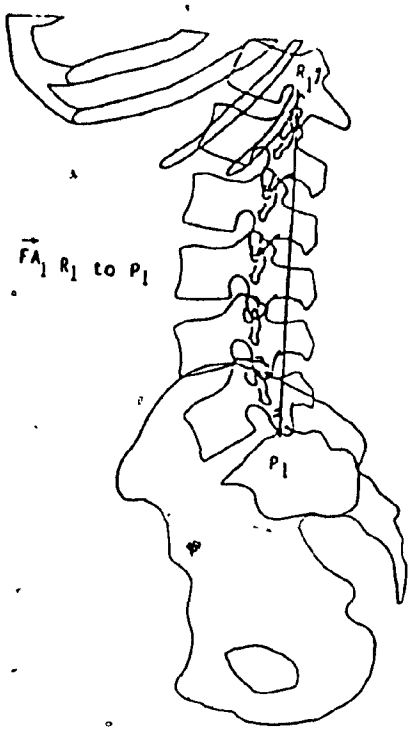

Quadratus Lumborum
Figure B.8

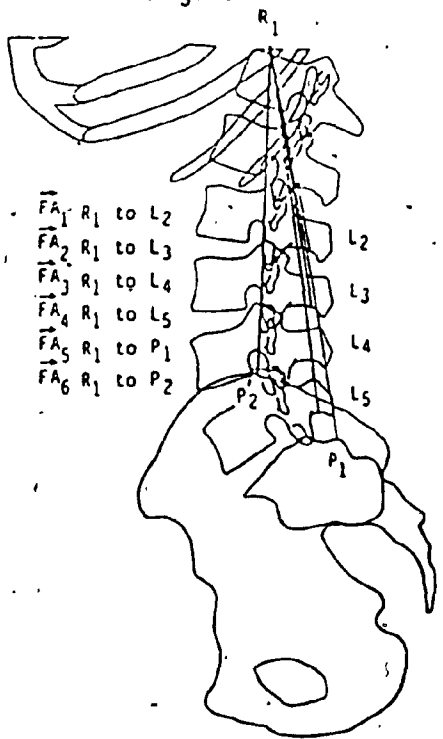

Latissimus Dorsi
Figure B.9

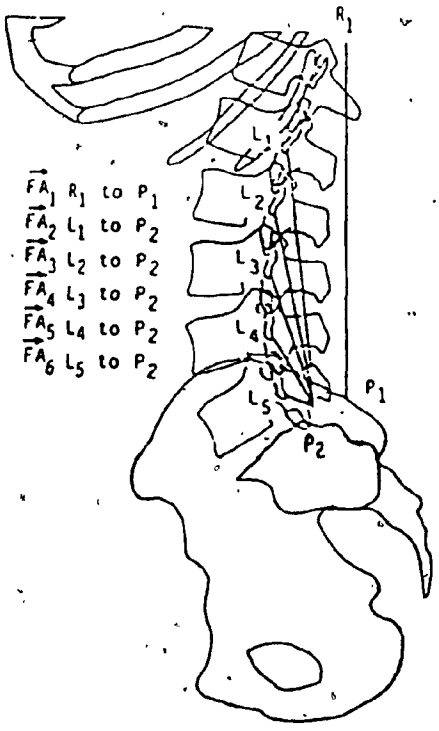

Sacrospinalis
Figure B.10

CENTER OF REACTION R_i (i = 1 to 5)

$$\vec{FN}_i = \sum_{j=i}^{6} \vec{FA}_j \qquad (B.25)$$

$$MSF_i = \left[\sum_{j=i}^{6} (\vec{D}_{i,j} \times \vec{FA}_j)\right] \bullet \hat{Z} \qquad (B.26)$$

SACROSPINALIS & DEEP ILIOCOSTALIS LUMBORUM

Refer to figure B.10 for the numbering and direction of the muscle strands.

CENTER OF REACTION R_i (i = 1 to 5)

$$\vec{FN}_i = \sum_{j=1}^{i+1} \vec{FA}_i \qquad (B.27)$$

$$MSF_i = \left[\sum_{j=1}^{i+1} (\vec{D}_{i,j} \times \vec{FA}_j)\right] \bullet \hat{Z} \qquad (B.28)$$

MULTIFIDUS

This is a complex muscle. Levels 1 to 4 have six muscle strands acting on each level. Level 5 has five muscle strands acting on it. The muscle strands are defined in table B.1 by their attachment points. Refer to figure B.11 for the location of the attachment points.

CENTER OF REACTION R_i (i = 1 to 4)

$$\vec{FN}_i = \sum_{j=1}^{6} \vec{FA}_j \qquad (B.29)$$

$$MSF_i = [(\vec{D}_1 \times \vec{FA}_1)+(\vec{D}_2 \times (\vec{FA}_2+ \vec{FA}_4))+(\vec{D}_3 \times (\vec{FA}_3+ \vec{FA}_5+ \vec{FA}_6))] \bullet \hat{Z} \qquad (B.30)$$

CENTER OF REACTION R_5

$$\vec{FN}_5 = \sum_{j=1}^{5} \vec{FA}_j \qquad (B.31)$$

$$MSF_5 = [\vec{D}_1 \times \vec{FN}_5] \bullet \hat{Z} \qquad (B.32)$$

	LUMBAR LEVEL									
	1		2		3		4		5	
MUSCLE STANDS	FROM	TO	FROM	TO	FROM	TO	FROM	TO	FROM	TO
$\vec{FA}_1$	T_{11}	V_{22}	T_{12}	V_{32}	V_{11}	V_{12}	V_{21}	V_{52}	V_{51}	P_1
$\vec{FA}_2$	T_{12}	V_{22}	V_{11}	V_{32}	V_{21}	V_{42}	V_{31}	V_{52}	V_{51}	P_2
$\vec{FA}_3$	V_{11}	V_{22}	V_{21}	V_{32}	V_{31}	V_{42}	V_{41}	V_{52}	V_{51}	P_3
$\vec{FA}_4$	T_{12}	V_{32}	V_{11}	V_{42}	V_{21}	V_{52}	V_{31}	P_1	V_{51}	P_4
$\vec{FA}_5$	V_{11}	V_{32}	V_{21}	V_{42}	V_{31}	V_{52}	V_{41}	P_1	V_{51}	P_5
$\vec{FA}_6$	V_{11}	V_{42}	V_{21}	V_{52}	V_{31}	P_1	V_{41}	P_2	--	--
LEVER ARM										
$\vec{D}_1$	R_1	T_{11}	R_2	T_{12}	R_3	V_{11}	R_4	V_{21}	R_5	V_{51}
$\vec{D}_2$	R_1	T_{12}	R_2	V_{11}	R_3	V_{21}	R_4	V_{31}	--	--
$\vec{D}_3$	R_1	V_{11}	R_2	V_{21}	R_3	V_{31}	R_4	V_{41}	--	--

Muscle strand and lever arm distance vectors for Multifidus

Table B.1

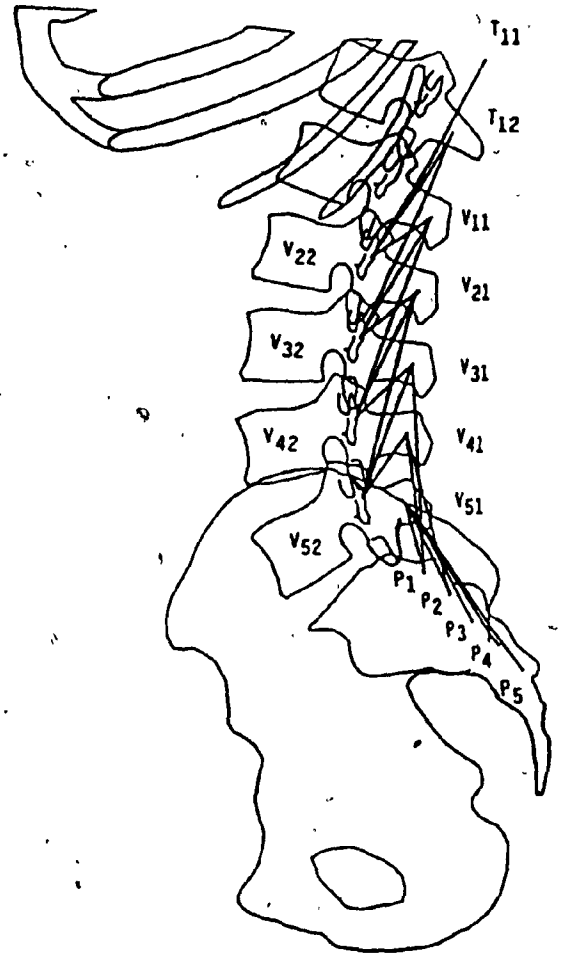

Multifidus

Figure B.11

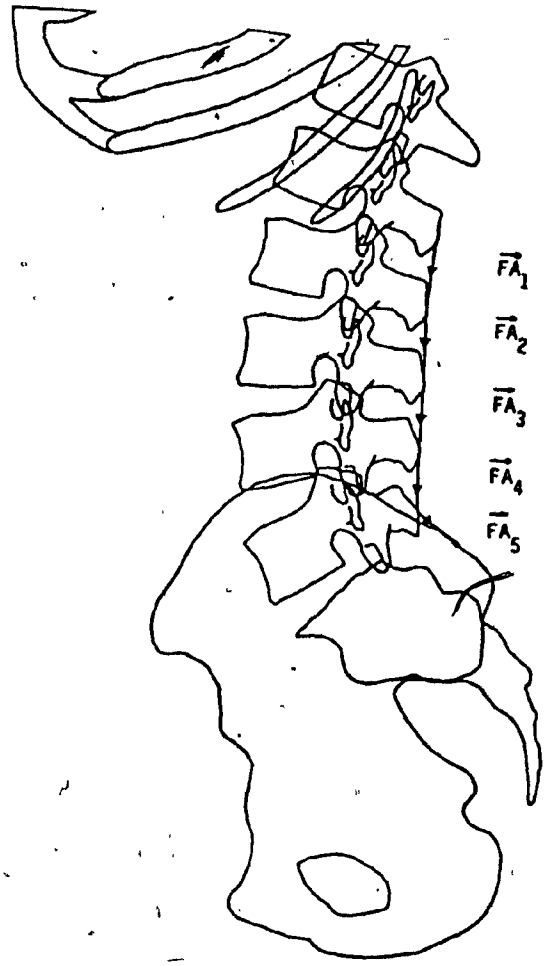

Fascia

Figure B.12

FASCIA (INTERNAL OBLIQUES & TRANSVERSUS ABDOMINIS)

Refer to figure B.12 for the numbering and directions of the Fascia strands. A unit force pull on the edges of the Fascia at a given level by the Internal Obliques & Transversus Abdominis is assumed to induce a unit force along the Fascia strand at that level. The Fascia strands at levels 3 & 4 are rotated in the saggital plane by ϵ degrees. This models the Fascia's angled insertion at those levels due to its wrapping around the bulk of the Erector Spinae muscle bundle. For an individual with a large Erector Spinae muscle bundle, ϵ can vary between 10 & 20 degrees.

CENTER OF REACTION R_i

$$\vec{FN}_i = \vec{FA}_i \tag{B.33a}$$

$$\vec{FN}_i = \begin{bmatrix} \cos(\epsilon) & -\sin(\epsilon) & 0 \\ \sin(\epsilon) & \cos(\epsilon) & 0 \\ 0 & 0 & 1 \end{bmatrix} \vec{FN}_i \quad i = 3, 4 \tag{B.33b}$$

$$MSF_i = [\vec{D}_{i,i} \times \vec{FN}_i] \bullet \hat{Z} \tag{B.34}$$

B.2) Muscle Moment Matrix

The eleven muscles described can be divided into seven independent groups. The muscles constituting a group are assumed to have the same muscle activity. Thus the equivalent net muscle activity to force scaling vectors and net muscle activity to moment scaling factors for muscles within a group can be summed. Given that the moments are calculated for 5 IV joints and that there are 7 independent muscle groups, a [5 x 7] muscle moment matrix can be constructed. The

i,j^{th} entry in the matrix is the net muscle group activity to moment scaling factor for level 'i' of group 'j'. Multiplying the muscle moment matrix by a [7 x 1] vector of muscle group activities yields a [5 x 1] vector of the resultant muscle moment at each IV joint of the lumbar spine.

$$\begin{bmatrix} GM_{1,1} & \cdots & GM_{1,7} \\ \vdots & & \vdots \\ GM_{5,1} & \cdots & GM_{5,7} \end{bmatrix} \begin{bmatrix} K_1 \\ K_2 \\ K_3 \\ K_4 \\ K_5 \\ K_6 \\ K_7 \end{bmatrix} = \begin{bmatrix} RM_1 \\ RM_2 \\ RM_3 \\ RM_4 \\ RM_5 \end{bmatrix} \qquad (B.35)$$

where:

$GM_{i,j}$ is the net muscle group activity to moment scaling factor for level 'i' of group 'j'

K_j is the muscle group activity of group 'j'

RM_i is the resultant muscle moment at level 'i'

Group 1 is comprised of three muscles: Medialis Spinalis, Illiocostalis Lumborum and Sacrospinalis. Thus the first column of the muscle moment matrix is formed by summing the components of equations B.16, B.18, B.22 and B.28 corresponding to the same level 'i'. Group 2 is the Multifidus only, so the second column of the matrix is formed with equations B.30 for levels 1 to 4 and equation B.32 for level 5. Group 3 is the Latissimus Dorsi only. The third column of the matrix is formed wih equation B.26. Group 4 is the Quadratus Lumborum only. The fourth

column of the matrix is formed with equation B.24. Group 5 is the Psoas only, thus the fifth column of the matrix is formed with equation B.10 for levels 1 to 4 and equation B.12 for level 5. Rectus Abdominis is the sole muscle in group 6. The sixth column of the matrix is formed with equation B.14. Group 7 is comprised of three muscles, the External Obliques (Posterior part), the Internal Obliques and the Transversus Abdominis. The seventh column of the matrix is formed by summing the components of equations B.20 and B.34 corresponding to the same level 'i'. The muscle groups and the constituent equations are summarized in table B.2.

B.3) Ligament Tension Matrix

There are essentially three forces inducing moments at any lumbar IV joint: the external forces (comprising of the external load and body weight), the muscle force and the ligament force. Static equilibrium dictates that the resultant moment at all IV joints be zero.

$$EM_i + RM_i + LM_i = 0 \qquad (B.36)$$

Where:

EM_i is the external moment induced by an external load and the body weight at level 'i'

RM_i is the resultant muscle moment at level 'i'

LM_i is the ligament moment at level 'i'

GROUP NUMBER	MUSCLES IN GROUP	EQUATIONS
1	Medialis Spinalis	B.16, B.18
	Illiocostalis Lumborum	B.22
	Sacrospinalis	B.28
2	Multifidus	B.30, B.32
3	Latissimus Dorsi	B.26
4	Quadratus Lumborum	B.24
5	Psoas	B.10, B.12
6	Rectus Abdominis	B.14
7	External Obliques (Posterior part)	B.20
	Internal Obliques Transversus Abdominis	B.34

Equations defining the net muscle activity to
to moment scaling factors for the Muscle Groups

Table B.2

Isolating the ligament moment in equation B.36 yields

$$LM_i = - (EM_i + RM_i) \tag{B.37}$$

The desired result is the ligament tension in each strand 'i'. The ligament line of action unit vectors are defined in figure B.13. The ligament force vector for strand 'i' is given by the product of the ligament tension in strand 'i' and the ligament line of action unit vector for strand 'i'.

$$\vec{T}_{L_i} = T_i \cdot \hat{T}_{L_i} \tag{B.38}$$

where:

$\vec{T}_{L_i}$ is the ligament force vector for strand 'i'

T_i is the ligament tension in strand 'i'

$\hat{T}_{L_i}$ is the ligament line of action unit vector for strand 'i'

The ligament moment at each level 'i' can be computed. $\vec{D}_{i,j}$ is the level arm distance vector from center of reaction 'i' to unit vector 'j'.

$$L_{M_1} = T_1 \cdot [\vec{D}_{1,1} \times \hat{T}_{L_1}] \bullet \hat{Z} \tag{B.39}$$

$$L_{M_2} = T_2 \cdot [\vec{D}_{2,2} \times \hat{T}_{L_2}] \bullet \hat{Z} \tag{B.40}$$

$$L_{M_3} = T_3 \cdot [\vec{D}_{3,3} \times \hat{T}_{L_3}] \bullet \hat{Z} \tag{B.41}$$

$$L_{M_4} = (T_3 \cdot [\vec{D}_{4,3} \times \hat{T}_{L_3}] + T_4 \cdot [\vec{D}_{4,4} \times \hat{T}_{L_4}]) \bullet \hat{Z} \tag{B.42}$$

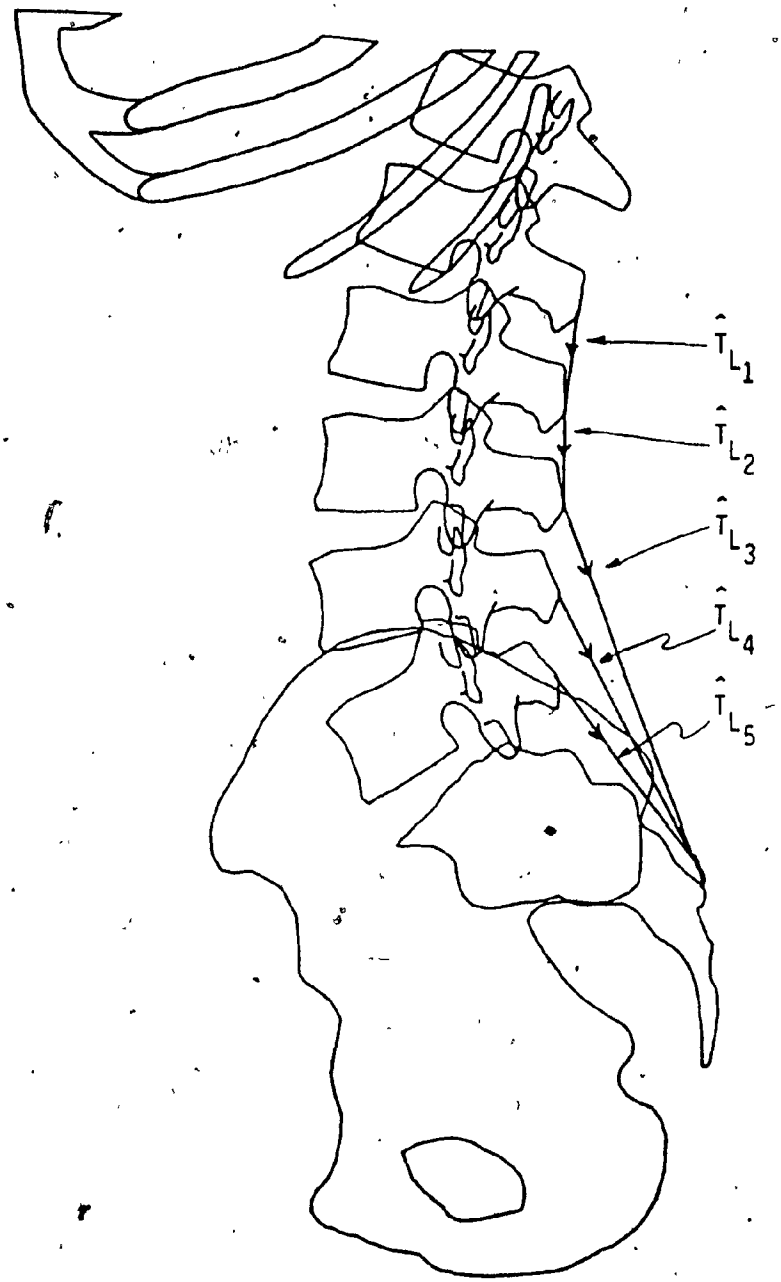

Midline Strand Definitions.

Figure B.13

$$L_{M_5} = (T_3 \cdot [\vec{D}_{5,3} \times \hat{T}_{L_3}] + T_4 \cdot [\vec{D}_{5,4} \times \hat{T}_{L_4}] + T_5 \cdot [\vec{D}_{5,5} \times \hat{T}_{L_5}]) \cdot \hat{Z} \quad \text{(B.43)}$$

The ligament tension is computed by substituting equation B.37 into equations B.39 to B.43. The resultant muscle moment at level 'i' can be written as the dot product of row 'i' of the muscle moment matrix and the muscle group activity vector.

$$RM_i = \sum_{j=1}^{7} GM_{i,j} \cdot K_j \quad \text{(B.44)}$$

where:

RM_i is the resultant muscle moment at level 'i'

$GM_{i,j}$ is the net muscle group activity to moment scaling factor for level 'i' of group 'j'

K_j is the muscle group activity of group 'j'

The ligament tension in strand 1 is given by combining equations B.37, B.39, and B.44.

$$T_1 \cdot [\vec{D}_{1,1} \times \hat{T}_{L_1}] \cdot \hat{Z} = - (EM_1 + \sum_{j=1}^{7} GM_{1,j} \cdot K_j) \quad \text{(B.45)}$$

After some algebraic manipulation, equation B.45 is reduced to

$$T_1 = \sum_{j=1}^{7} MTN_{1,j} \cdot K_j + MTNK_1 \quad \text{(B.46)}$$

where:

$$MTN_{1,j} = - \frac{GM_{1,j}}{[\vec{D}_{1,1} \times \hat{T}_{L_1}] \cdot \hat{Z}} \tag{B.47}$$

$$MTNK_1 = - \frac{EM_1}{[\vec{D}_{1,1} \times \hat{T}_{L_1}] \cdot \hat{Z}} \tag{B.48}$$

The ligament tension in strand 2 is similarly computed. Combining equations B.37, B.40 and B.44 yields

$$T_2 \cdot [\vec{D}_{2,2} \times \hat{T}_{L_2}] \cdot \hat{Z} = - (EM_2 + \sum_{j=1}^{7} GM_{2,j} \cdot K_j) \tag{B.49}$$

Reducing equation B.49 yields

$$T_2 = \sum_{j=1}^{7} MTN_{2,j} \cdot K_j + MTNK_2 \tag{B.50}$$

where:

$$MTN_{2,j} = - \frac{GM_{2,j}}{[\vec{D}_{2,2} \times \hat{T}_{L_2}] \cdot \hat{Z}} \tag{B.51}$$

$$MTNK_2 = - \frac{EM_2}{[\vec{D}_{2,2} \times \hat{T}_{L_2}] \cdot \hat{Z}} \tag{B.52}$$

The ligament tension in strand 3 is formed by combining equations B.37, B.41 and B.44.

$$T_3 \cdot [\vec{D}_{3,3} \times \hat{T}_{L_3}] \cdot \hat{Z} = - (EM_3 + \sum_{j=1}^{7} GM_{3,j} \cdot K_j) \tag{B.53}$$

Reducing equation B.53 yields

$$T_3 = \sum_{j=1}^{7} MTN_{3,j} \cdot K_j + MTNK_3 \tag{B.54}$$

where:

$$MTN_{3,j} = -\frac{GM_{3,j}}{[\vec{D}_{3,3} \times \hat{T}_{L_3}] \bullet \hat{Z}} \qquad (B.55)$$

$$MTNK_3 = -\frac{EM_3}{[\vec{D}_{3,3} \times \hat{T}_{L_3}] \bullet \hat{Z}} \qquad (B.56)$$

The ligament tension in strand 4 is formed by combining equations B.37, B.42 and B.44.

$$T_4 \cdot [\vec{D}_{4,4} \times \hat{T}_{L_4}] \bullet \hat{Z} = -(EM_4 + \sum_{j=1}^{7} GM_{4,j} \cdot K_j + T_3 \cdot [\vec{D}_{4,3} \times \hat{T}_{L_3}] \bullet \hat{Z}) \qquad (B.57)$$

Substituting equation B.54 for T_3 and simplifying yields

$$T_4 = \sum_{j=1}^{7} MTN_{4,j} \cdot K_j + MTNK_4 \qquad (B.58)$$

where:

$$MTN_{4,j} = -\frac{(GM_{4,j} + MTN_{3,j} \cdot [\vec{D}_{4,3} \times \hat{T}_{L_3}] \bullet \hat{Z})}{[\vec{D}_{4,4} \times \hat{T}_{L_4}] \bullet \hat{Z}} \qquad (B.59)$$

$$MTNK_4 = -\frac{(EM_4 + MTNK_3 \cdot [\vec{D}_{4,3} \times \hat{T}_{L_3}] \bullet \hat{Z})}{[\vec{D}_{4,4} \times \hat{T}_{L_4}] \bullet \hat{Z}} \qquad (B.60)$$

The ligament tension in strand 5 is formed by combining equations B.37, B.43 and B.44.

$$T_5 \cdot [\vec{D}_{5,5} \times \hat{T}_{L_5}] \bullet \hat{Z} = -(EM_5 + \sum_{j=1}^{7} GM_{5,j} \cdot K_j + (T_3 \cdot [\vec{D}_{5,3} \times \hat{T}_{L_3}] + T_4 \cdot [\vec{D}_{5,4} \times \hat{T}_{L_4}]) \bullet \hat{Z}) \qquad (B.61)$$

Substituting equation B.54 for T_3 and equation B.58 for T_4 and simplifying yields

$$T_5 = \sum_{j=1}^{7} MTN_{5,j} \cdot K_j + MTNK_5 \qquad (B.62)$$

where:

$$MTN_{5,j} = - \frac{(GM_{5,j} + (MTN_{3,j} \cdot [\vec{D}_{5,3} \times \hat{T}_{L_3}] + MTN_{4,j} \cdot [\vec{D}_{5,4} \times \hat{T}_{L_4}]) \cdot \hat{Z})}{[\vec{D}_{5,5} \times \hat{T}_{L_5}] \cdot \hat{Z}} \qquad (B.63)$$

$$MTNK_5 = - \frac{(EM_5 + (MTNK_3 \cdot [\vec{D}_{5,3} \times \hat{T}_{L_3}] + MTNK_4 \cdot [\vec{D}_{5,4} \times \hat{T}_{L_4}]) \cdot \hat{Z})}{[\vec{D}_{5,5} \times \hat{T}_L] \cdot \hat{Z}} \qquad (B.64)$$

Equations B.46, B.50, B.54, B.58, and B.62 can be arranged in matrix form:

$$\begin{bmatrix} MTN_{1,1} & \cdots & MTN_{1,7} \\ \vdots & & \vdots \\ MTN_{5,1} & \cdots & MTN_{5,7} \end{bmatrix} \begin{bmatrix} K_1 \\ K_2 \\ K_3 \\ K_4 \\ K_5 \\ K_6 \\ K_7 \end{bmatrix} + \begin{bmatrix} MTNK_1 \\ MTNK_2 \\ MTNK_3 \\ MTNK_4 \\ MTNK_5 \end{bmatrix} = \begin{bmatrix} T_1 \\ T_2 \\ T_3 \\ T_4 \\ T_5 \end{bmatrix} \qquad (B.65)$$

where:

$MTN_{i,j}$ is the muscle activity to ligament tension scaling factor for strand 'i' of group 'j'

$MTNK_i$ is the ligament tension in strand 'i' due to an external load and the body weight

K_j is the muscle group activity of group 'j'

T_i is the resultant ligament tension in strand 'i'

The net ligament tension at levels 1, 2 and 3 is simply the tension in the respective ligament strands. Ligament strands 3 and 4 exert force on level 4, thus the net ligament tension at level 4 is the sum of the tension in strands 3 and 4. Similarly ligament strands 3, 4 and 5 exert force on level 5. Thus the net ligament tension at level 5 is the sum of the tension in strands 3, 4 and 5. The net ligament tension equations can be put in a form similar to equation B.65:

$$\begin{bmatrix} HMTN_{1,1} & \cdots & HMTN_{1,7} \\ \vdots & & \vdots \\ HMTN_{5,1} & \cdots & HMTN_{5,7} \end{bmatrix} \begin{bmatrix} K_1 \\ K_2 \\ K_3 \\ K_4 \\ K_5 \\ K_6 \\ K_7 \end{bmatrix} + \begin{bmatrix} HMTNK_1 \\ HMTNK_2 \\ HMTNK_3 \\ HMTNK_4 \\ HMTNK_5 \end{bmatrix} = \begin{bmatrix} T_{N_1} \\ T_{N_2} \\ T_{N_3} \\ T_{N_4} \\ T_{N_5} \end{bmatrix} \tag{B.66}$$

where: T_{N_i} is the net ligament tension at level 'i'

$$HMTNK_i = MTNK_i \qquad i = 1, 2, 3 \tag{B.67}$$

$$HMTNK_i = \sum_{n=3}^{i} MTNK_n \qquad i = 4, 5 \tag{B.68}$$

$$HMTN_{i,j} = MTN_{i,j} \qquad i = 1, 2, 3 \qquad j = 1,\ldots,7 \tag{B.69}$$

$$HMTN_{i,j} = \sum_{n=3}^{i} MTN_{n,j} \qquad i = 4, 5 \qquad j = 1,\ldots,7 \tag{B.70}$$

Equation B.66 is equation 6.3 in chapter 6.

B.4) Resultant Shear and Compression Matricies

The net force acting on any IV joint is the sum of the muscle force, the ligament force, the external load force and the body weight force acting on that joint.

$$\vec{F}_{NET_i} = \vec{F}_{EXT_i} + \vec{F}_{MUS_i} + \vec{F}_{LIG_i} \qquad (B.71)$$

where:

$\vec{F}_{EXT_i}$ is the external load and body weight force at level 'i'

$\vec{F}_{MUS_i}$ is the net muscle force at level 'i'

$\vec{F}_{LIG_i}$ is the net ligament force at level 'i'

$\vec{F}_{NET_i}$ is the resultant force at level 'i'

This net force can be decomposed along shear and compression directions defined by two unit vectors (Figure B.14)

$$S_i = \vec{F}_{NET_i} \bullet \hat{S}_i \qquad (B.72)$$

$$C_i = \vec{F}_{NET_i} \bullet \hat{C}_i \qquad (B.73)$$

where:

$\vec{F}_{NET_i}$ is the resultant force at level 'i'

$\hat{S}_i$ is the unit vector defining the positive shear direction for level 'i'

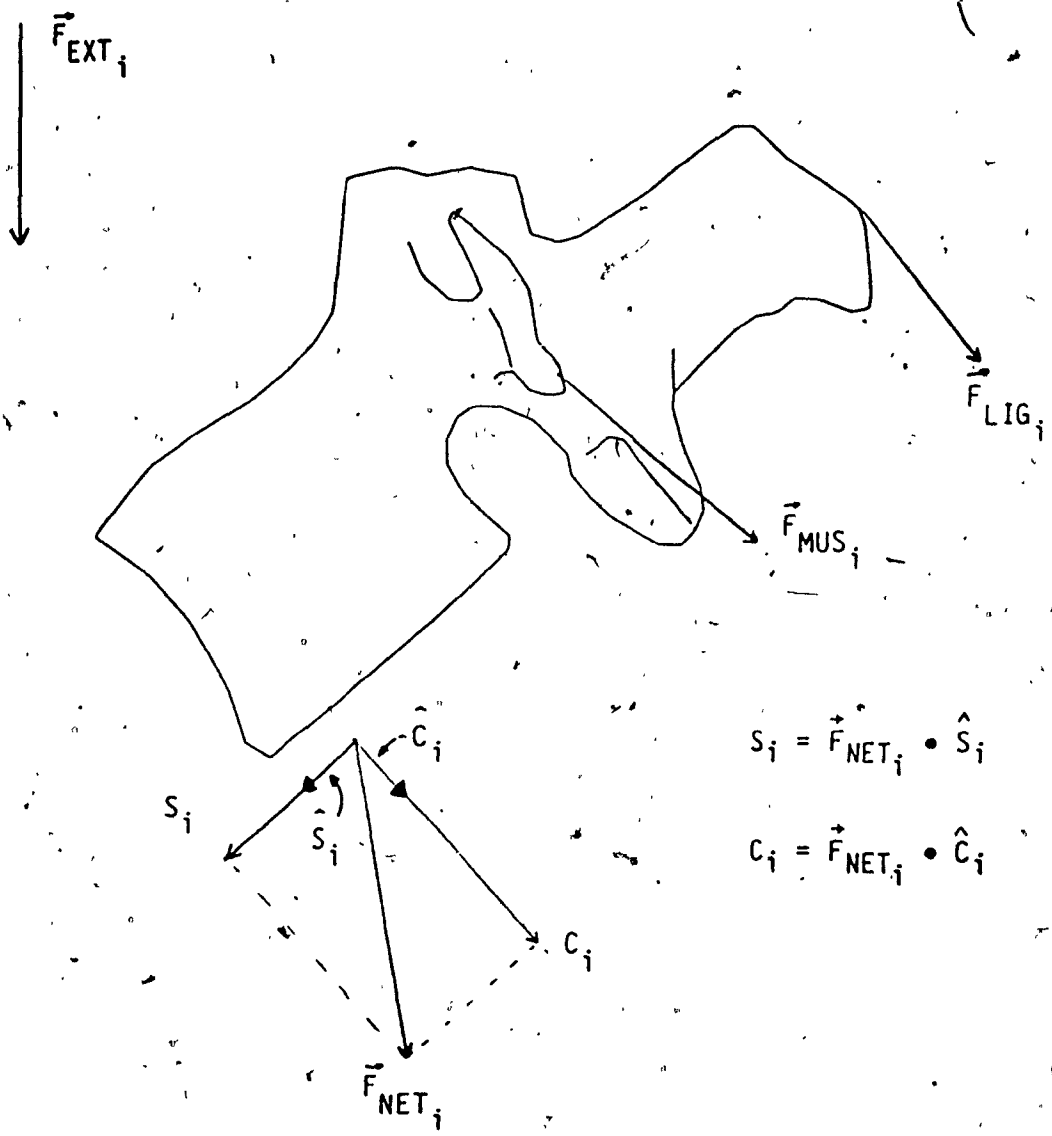

Decomposition of net force into shear & compression components.

Figure B.14

S_i is the projection of $\vec{F}_{NET}$ on S_i

$\hat{C}_i$ is the unit vector defining the positive compression direction for level 'i'

C_i is the projection of $\vec{F}_{NET}$ on C_i

The seven muscle groups each have five net muscle group activity to force scaling vectors associated with them. In a fashion similar to the formation of the muscle moment matrix, the net muscle force at any level is given by

$$\vec{F}_{MUS_i} = \sum_{j=1}^{7} \vec{F}_{MG_{i,j}} \cdot K_j \qquad (B.74)$$

where:

$\vec{F}_{MG_{i,j}}$ is the net muscle group activity to force scaling vector for level 'i' of group 'j' (see Table B.3)

K_j is the muscle group activity of group 'j'

$\vec{F}_{MUS_i}$ is the net muscle force at level 'i'

The ligament force vectors are given by equation B.38.

$$\vec{T}_{L_i} = T_i \cdot \hat{T}_{L_i} \qquad (B.38)$$

where:

$\vec{T}_{L_i}$ is the ligament force vector at level 'i'

T_i is the ligament tension at level 'i'

GROUP NUMBER	MUSCLES IN GROUP	EQUATIONS
1	Medialis Spinalis	B.15, B.17
	Illiocostalis Lumborum	B.21
	Sacrospinalis	B.27
2	Multifidus	B.29, B.31
3	Latissimus Dorsi	B.25
4	Quadratus Lumborum	B.23
5	Psoas	B.9, B.11
6	Rectus Abdominis	B.13
7	External Obliques (Posterior part)	B.19
	Internal Obliques, Transversus Abdominis	B.33a, B.33b

Equations defining the net muscle activity to to force scaling vectors for the Muscle Groups

Table B.3

$\hat{T}_{L_i}$ is the ligament line of action unit vector at level 'i'

The resultant force at level 'i' (for i = 1 to 3) is given by

$$\vec{F}_{NET_i} = \vec{F}_{EXT_i} + \vec{F}_{MUS_i} + \vec{F}_{LIG_i} \qquad (B.71)$$

Substituting equations B.74, B.38, and B.46 (i=1), B.50 (i=2) or B.54 (i=3) into equation B.71 yields

$$\vec{F}_{NET_i} = \vec{F}_{EXT_i} + \sum_{j=i}^{7} \vec{F}_{MG_{i,j}} \cdot K_j + \left(\sum_{j=1}^{7} MTN_{i,j} \cdot K_j + MTNK_i\right) \cdot \hat{T}_{L_i} \qquad (B.75)$$

The resultant shear and compression at level 'i' are given by

$$S_i = \vec{F}_{NET_i} \bullet \hat{S}_i \qquad (B.76)$$

$$C_i = \vec{F}_{NET_i} \bullet \hat{C}_i \qquad (B.77)$$

Substituting equation B.75 into equation B.76 and reducing yields

$$S_i = \sum_{j=1}^{7} SHR_{i,j} \cdot K_j + SHRK_i \qquad (B.78)$$

with:

$$SHR_{i,j} = (\vec{F}_{MG_{i,j}} + MTN_{i,j} \cdot \hat{T}_{L_i}) \bullet \hat{S}_i \qquad (B.79)$$

$$SHRK_i = (\vec{F}_{EXT_i} + MTNK_i \cdot \hat{T}_{L_i}) \bullet \hat{S}_i \qquad (B.80)$$

Substituting equation B.75 into equation B.77 and reducing yields

$$C_i = \sum_{j=1}^{7} CMP_{i,j} \cdot K_j + CMPK_i \qquad (B.81)$$

with:

$$CMP_{i,j} = (\vec{F}_{MG_{i,j}} + MTN_{i,j} \cdot \hat{T}_{L_i}) \bullet \hat{C}_i \qquad (B.82)$$

$$CMPK_i = (\vec{F}_{EXT_i} + MTNK_i \cdot \hat{T}_{L_i}) \bullet \hat{C}_i \qquad (B.83)$$

The resultant force at level 4 is given by

$$\vec{F}_{NET_4} = \vec{F}_{EXT_4} + \vec{F}_{MUS_4} + \vec{F}_{LIG_4} \qquad (B.84)$$

At level 4, the net ligament force is given by

$$\vec{F}_{LIG_4} = T_3 \cdot \hat{T}_{L_3} + T_4 \cdot \hat{T}_{L_4} \qquad (B.85)$$

Substituting equations B.54 and B.58 into equation B.85 and then substituting equation B.85 and B.74 into equation B.84 yields

$$\vec{F}_{NET_4} = \vec{F}_{EXT_4} + \sum_{j=1}^{7} \vec{F}_{MG_{4,j}} \cdot K_j + (\sum_{j=1}^{7} MTN_{3,j} \cdot K_j + MTNK_3) \cdot \hat{T}_{L_3} + (\sum_{j=1}^{7} MTN_{4,j} \cdot K_j + MTNK_4) \cdot \hat{T}_{L_4} \qquad (B.86)$$

The resultant shear and compression at level 4 are given by

$$S_4 = \vec{F}_{NET_4} \bullet \hat{S}_4 \qquad (B.87)$$

$$C_4 = \vec{F}_{NET_4} \bullet \hat{C}_4 \qquad (B.88)$$

Substituting equation B.86 into equation B.87 and reducing yields

$$S_4 = \sum_{j=1}^{7} SHR_{4,j} \cdot K_j + SHRK_4 \tag{B.89}$$

with:

$$SHR_{4,j} = (\vec{F}_{MG_{4,j}} + MTN_{3,j} \cdot \hat{T}_{L_3} + MTN_{4,j} \cdot \hat{T}_{L_4}) \bullet \hat{S}_4 \tag{B.90}$$

$$SHRK_4 = (\vec{F}_{EXT_4} + MTNK_3 \cdot \hat{T}_{L_3} + MTNK_4 \cdot \hat{T}_{L_4}) \bullet \hat{S}_4 \tag{B.91}$$

Substituting equation B.86 into equation B.88 and reducing yields

$$C_4 = \sum_{j=1}^{7} CMP_{4,j} \cdot K_j + CMPK_4 \tag{B.92}$$

with:

$$CMP_{4,j} = (\vec{F}_{MG_{4,j}} + MTN_{3,j} \cdot \hat{T}_{L_3} + MTN_{4,j} \cdot \hat{T}_{L_4}) \bullet \hat{C}_4 \tag{B.93}$$

$$CMPK_4 = (\vec{F}_{EXT_4} + MTNK_3 \cdot \hat{T}_{L_3} + MTNK_4 \cdot \hat{T}_{L_4}) \bullet \hat{C}_4 \tag{B.94}$$

The resultant force at level 5 is given by

$$\vec{F}_{NET_5} = \vec{F}_{EXT_5} + \vec{F}_{MUS_5} + \vec{F}_{LIG_5} \tag{B.95}$$

At level 5, the net ligament force is given by

$$\vec{F}_{LIG_5} = T_3 \cdot \hat{T}_{L_3} + T_4 \cdot \hat{T}_{L_4} + T_5 \cdot \hat{T}_{L_5} \tag{B.96}$$

Substituting equations B.54, B.58 and B.62 into equation B.96 and then substituting equation B.96 and B.74 into equation B.95 yields

$$\vec{F}_{NET_5} = \vec{F}_{EXT_5} + \sum_{j=1}^{7} \vec{F}_{MG_{5,j}} \cdot K_j + \left(\sum_{j=1}^{7} MTN_{3,j} \cdot K_j + MTNK_3\right) \cdot \hat{T}_{L_3} + \left(\sum_{j=1}^{7} MTN_{4,j} \cdot K_j + MTNK_4\right) \cdot \hat{T}_{L_4} + \left(\sum_{j=1}^{7} MTN_{5,j} \cdot K_j + MTNK_5\right) \cdot \hat{T}_{L_5} \quad (B.97)$$

The resultant shear and compression at level 5 are given by

$$S_5 = \vec{F}_{NET_5} \bullet \hat{S}_5 \quad (B.98)$$

$$C_5 = \vec{F}_{NET_5} \bullet \hat{C}_5 \quad (B.99)$$

Substituting equation B.97 into equation B.98 and reducing yields

$$S_5 = \sum_{j=1}^{7} SHR_{5,j} \cdot K_j + SHRK_5 \quad (B.100)$$

with:

$$SHR_{5,j} = \left(\vec{F}_{MG_{5,j}} + MTN_{3,j} \cdot \hat{T}_{L_3} + MTN_{4,j} \cdot \hat{T}_{L_4} + MTN_{5,j} \cdot \hat{T}_{L_5}\right) \bullet \hat{S}_5 \quad (B.101)$$

$$SHRK_5 = \left(\vec{F}_{EXT_5} + MTNK_3 \cdot \hat{T}_{L_3} + MTNK_4 \cdot \hat{T}_{L_4} + MTNK_5 \cdot \hat{T}_{L_5}\right) \bullet \hat{S}_5 \quad (B.102)$$

Substituting equation B.97 into equation B.99 and reducing yields

$$C_5 = \sum_{j=1}^{7} CMP_{5,j} \cdot K_j + CMPK_5 \quad (B.103)$$

with:

$$CMP_{5,j} = (\vec{F}_{MG_{5,j}} + MTN_{3,j} \cdot \hat{T}_{L_3} + MTN_{4,j} \cdot \hat{T}_{L_4} + MTN_{5,j} \cdot \hat{T}_{L_5}) \bullet \hat{C}_5 \quad \text{(B.104)}$$

$$CMPK_5 = (\vec{F}_{EXT_5} + MTNK_3 \cdot \hat{T}_{L_3} + MTNK_4 \cdot \hat{T}_{L_4} + MTNK_5 \cdot \hat{T}_{L_5}) \bullet \hat{C}_5 \quad \text{(B.105)}$$

Equations B.78, B.89, and B.100 can be arranged in matrix form

$$\begin{bmatrix} SHR_{1,1} & \cdots & SHR_{1,7} \\ \vdots & & \vdots \\ SHR_{5,1} & \cdots & SHR_{5,7} \end{bmatrix} \begin{bmatrix} K_1 \\ K_2 \\ K_3 \\ K_4 \\ K_5 \\ K_6 \\ K_7 \end{bmatrix} + \begin{bmatrix} SHRK_1 \\ SHRK_2 \\ SHRK_3 \\ SHRK_4 \\ SHRK_5 \end{bmatrix} = \begin{bmatrix} S_1 \\ S_2 \\ S_3 \\ S_4 \\ S_5 \end{bmatrix} \quad \text{(B.106)}$$

where:

$SHR_{i,j}$ is the muscle activity & ligament tension to shear force scaling factor for level 'i' of group 'j'

$SHRK_i$ is the shear force at level 'i' due to an external load and the body weight

K_j is the muscle group activity of group 'j'

S_i is the resultant shear at level 'i'

Equation B.106 is equation 6.4 in chapter 6.

Equations B.81, B.92 and B.103 can also be arranged in matrix form

$$\begin{bmatrix} CMP_{1,1} & \cdots & CMP_{1,7} \\ \vdots & & \vdots \\ CMP_{5,1} & \cdots & CMP_{5,7} \end{bmatrix} \begin{bmatrix} K_1 \\ K_2 \\ K_3 \\ K_4 \\ K_5 \\ K_6 \\ K_7 \end{bmatrix} + \begin{bmatrix} CMPK_1 \\ CMPK_2 \\ CMPK_3 \\ CMPK_4 \\ CMPK_5 \end{bmatrix} = \begin{bmatrix} C_1 \\ C_2 \\ C_3 \\ C_4 \\ C_5 \end{bmatrix} \quad \text{(B.107)}$$

where:

$CMP_{i,j}$ is the muscle activity & ligament tension to compression force scaling factor for level 'i' of group 'j'

$CMPK_i$ is the compression force at level 'i' due to an external load an the body weight

K_j is the muscle group activity of group 'j'

C_i is the resultant compression at level 'i'

Equation B.107 is equation 6.5 in chapter 6.

B.5) System Equations and Spinal Geometry

The motion of the dead lift is modelled with eight images of the lumbar spine in successive stages of forward flexion. Each image represents some spinal geometry. The attachment points of the ligaments and muscles and the coordinates of the centers of reaction are defined by the spinal geometry. Thus for each image the lever arm distance vectors and muscle and ligament line of action unit vectors can be computed, as well as the shear and compression unit vectors for each lumbar level.

This implies that the system equations are a function of the spinal geometry. When simulating a dead lift, the system equations describing the task must be formed for each flexion angle considered. In the case of this thesis, eight sets of system equations are formed.

Appendix C: Derivation of Quadratic Objective Function.

C.1) Introduction

The objective function representing the control criterion is given by equation 7.1.

$$O(\underline{K}) = \sum_{L=1}^{5} (P_1 \cdot S_L)^2 + \sum_{L=1}^{5} (P_2 \cdot C_L)^2 + \sum_{L=1}^{5} (P_3 \cdot T_{N_L})^2 + \sum_{i=1}^{6} (P_4 \cdot K_i)^2 + (P_5 \cdot K_7)^2 \qquad (7.1)$$

where:

$$S_L = \sum_{j=1}^{7} SHR_{L,j} \cdot K_j + SHRK_L \qquad (C.1)$$

from equation B.106

$$C_L = \sum_{j=1}^{7} CMP_{L,j} \cdot K_j + CMPK_L \qquad (C.2)$$

from equation B.107 and

$$T_{N_L} = \sum_{j=1}^{7} HMTN_{L,j} \cdot K_j + HMTNK_L \qquad (C.3)$$

from equation B.66.

Equation 7.1 can be written in the standard quadratic form:

$$O(\underline{K}) = \tfrac{1}{2}\,\underline{K}^t\,\underline{G}\,\underline{K} + \underline{C}^t\,\underline{K} + A \qquad (C.4)$$

where:

$\underline{G}$ is a [7 x 7] matrix

$\underline{C}$ is a [7 x 1] vector

A is a constant

$\underline{K}$ is a [7 x 1] vector of muscle group activities

Given an arbitrary scalar function

$$f(\underline{x}) = \underline{d}^t\underline{x} + e \qquad (C.5)$$

where:

$\underline{d}$, $\underline{x}$ are [N x 1] vectors and e is a scalar.

it is possible to form

$$F(\underline{x}) = f(\underline{x}) \cdot f(\underline{x}) \qquad (C.6)$$

Expanding C.6 yields

$$F(\underline{x}) = (\underline{d}^t\underline{x} + e) \cdot (\underline{d}^t\underline{x} + e) \qquad (C.7)$$

$$F(\underline{x}) = \underline{d}^t\underline{x}\;\underline{d}^t\underline{x} + 2e\underline{d}^t\underline{x} + e^2 \qquad (C.8)$$

$$F(\underset{\sim}{x}) = \tfrac{1}{2}\underset{\sim}{x}^t G \underset{\sim}{x} + \underset{\sim}{c}^t \underset{\sim}{x} + A \qquad (C.9)$$

where:

$$G = 2\,\underset{\sim}{d}\,\underset{\sim}{d}^t \quad \text{(symmetric matrix)} \qquad (C.10)$$

$$g_{i,j} = 2 \cdot d_i \cdot d_j \qquad (C.11)$$

$$\underset{\sim}{c} = 2e\underset{\sim}{d} \qquad (C.12)$$

$$c_i = 2 \cdot e \cdot d_i \qquad (C.13)$$

$$A = e^2 \qquad (C.14)$$

This result will be used to reduce equations C.1, C.2, and C.3 to their quadratic forms.

C.2) Reduction of Shear Equation to Quadratic Form

Let the shear component of equation 7.1 be given by

$$O_1(\underset{\sim}{K}) = \sum_{L=1}^{5} (P_1 \cdot S_L)^2 \qquad (C.15)$$

Substituting equation C.1 into equation C.15 yields

$$O_1(\underset{\sim}{K}) = P_1^2 \cdot \sum_{L=1}^{5} \left(\sum_{j=1}^{7} SHR_{L,j} \cdot K_j + SHRK_L \right)^2 \qquad (C.16)$$

and with some algebraic manipulation, this can be reduced to

$$O_1(\underline{K}) = \tfrac{1}{2}\,\underline{K}^t\, S_{RM}\,\underline{K} + \underline{S}^t_{RV}\,\underline{K} + S_{RC} \qquad (C.17)$$

where:

S_{RM} is a [7 x 7] symetric matrix with elements $s_{m_{i,j}}$

$$s_{m_{i,j}} = 2P_1^2 \sum_{L=1}^{5} SHR_{L,i} \cdot SHR_{L,j} \qquad (C.18)$$

$\underline{S}_{RV}$ is a [7 x 1] vector with elements s_{v_i}

$$s_{v_i} = 2P_1^2 \sum_{L=1}^{5} SHR_{L,i} \cdot SHRK_L \qquad (C.19)$$

S_{RC} is a constant

$$S_{RC} = P_1^2 \sum_{L=1}^{5} SHRK_L^2 \qquad (C.20)$$

C.3) Reduction of Compression Equation to Quadratic Form

Let the compression component of equation 7.1 be given by

$$O_2(\underline{K}) = \sum_{L=1}^{5} (P_2 \cdot C_L)^2 \qquad (C.21)$$

Substituting equation C.2 into equation C.21 yields

$$O_2(\underline{K}) = P_2^2 \cdot \sum_{L=1}^{5} \left(\sum_{j=1}^{7} CMP_{L,j} \cdot K_j + CMPK_L \right)^2 \qquad (C.22)$$

and with some algebraic manipulation, this can be reduced to

$$O_2(\underline{K}) = \tfrac{1}{2}\underline{K}^t C_{RM}\underline{K} + \underline{C}_{RV}^t\underline{K} + C_{RC} \qquad (C.23)$$

where:

C_{RM} is a [7 x 7] symmetric matrix with elements $c_{m_{i,j}}$

$$c_{m_{i,j}} = 2P_2^2 \sum_{L=1}^{5} CMP_{L,i} \cdot CMP_{L,j} \qquad (C.24)$$

$\underline{C}_{RV}$ is a [7 x 1] vector with elements c_{v_i}

$$c_{v_i} = 2P_2^2 \sum_{L=1}^{5} CMP_{L,i} \cdot CMPK_L \qquad (C.25)$$

C_{RC} is a constant

$$c_{RC} = P_2^2 \sum_{L=1}^{5} CMPK_L^2 \qquad (C.26)$$

C.4) Reduction of Net Ligament Tension Equation to Quadratic Form

Let the net ligament tension component of equation 7.1 be given by

$$O_3(\underline{K}) = \sum_{L=1}^{5} (P_3 \cdot T_{N_L})^2 \qquad (C.27)$$

Substituing equation C.3 into equation C.27 yields

$$O_3(\underline{K}) = P_3^2 \cdot \sum_{L=1}^{5} \left(\sum_{j=1}^{7} HMTN_{L,j} \cdot K_j + HMTNK_L \right)^2 \qquad (C.28)$$

and with some algebraic manipulation, this can be reduced to

$$O_3(\underline{K}) = \tfrac{1}{2}\,\underline{K}^t\, T_{RM}\,\underline{K} + \underline{T}_{RV}^t\,\underline{K} + T_{RC} \qquad (C.29)$$

where:

T_{RM} is a [7 x 7] symmetric matrix with elements $t_{m_{i,j}}$

$$t_{m_{i,j}} = 2P_3^2 \sum_{L=1}^{5} HMTN_{L,i} \cdot HMTN_{L,j} \qquad (C.30)$$

$\underline{T}_{RV}$ is a [7 x 1] vector with elements t_{v_i}

$$t_{v_i} = 2P_3^2 \sum_{L=1}^{5} HMTN_{L,i} \cdot HMTNK_L \qquad (C.31)$$

T_{RC} is a constant

$$T_{RC} = P_3^2 \sum_{L=1}^{5} HMTNK_L^2 \qquad (C.32)$$

C.5) Muscle Stress in the Quadratic Form

Writing the muscle stress, given by

$$O_4(\underline{K}) = \sum_{i=1}^{6} (P_4 \cdot K_i)^2 + P_5^2 \cdot K_7^2 \qquad (C.33)$$

in the form

$$O_4(\underline{K}) = \tfrac{1}{2}\,\underline{K}^t\, M_S\,\underline{K} \qquad (C.34)$$

is straightforward. Matrix M_S is simply

$$M_S = 2 \begin{bmatrix} P_4^2 & & & & \\ & P_4^2 & & & \\ & & P_4^2 & & \\ & & & P_4^2 & \\ & & & & P_4^2 \\ & & & & & P_5^2 \end{bmatrix} \qquad \text{(C.35)}$$

C.6) Assembing the Objective Function

The objective is given by summing the four sub-objective functions

$$O(\underline{X}) = \sum_{i=1}^{4} O_i(\underline{X}) \qquad \text{(C.36)}$$

In the standard form

$$O(\underline{X}) = \tfrac{1}{2} \underline{X}^t G \underline{X} + \underline{C}^t \underline{X} + A \qquad \text{(C.4)}$$

where:

$$G = S_{RM} + C_{RM} + T_{RM} + M_S \qquad \text{(C.37)}$$

$$\underline{C} = \underline{S}_{RV} + \underline{C}_{RV} + \underline{I}_{RV} \qquad \text{(C.38)}$$

$$A = S_{RC} + C_{RC} + T_{RC} \qquad \text{(C.39)}$$

Appendix D: The Optimization Algorithm

D.1) Introduction

The control criterion described in Chapter 7 is the minimization of musculo-skeletal stress. This criterion is expressed mathematically as a quadratic function of muscle activity. The desired result is the minimization of this function with respect to muscle activity. Certain inequality constraints are placed on the range of feasible solutions, such as positive muscle activity, positive net ligament tension and net ligament tension less than or equal to some prescribed maximum. These constraints are all linear functions of the muscle activity. The equality constraints imposed are that the resultant moment at each level be zero. The system equations are structured so that the equality constraints are always satisfied (see equation 6.1).

The optimization algorithm described in this section is modified from the notes of a graduate level course in optimization techniques given at Concordia University.

D.2) Statement of the Problem

The formal statement of the problem is:

$$\underset{\underline{X}\in R^N}{\text{MIN}} \{F(\underline{X}) = \tfrac{1}{2}\, \underline{X}^t\, G\, \underline{X} + \underline{c}^t\, \underline{X} + a\} \qquad \text{(D.1)}$$

$$C_i(\underline{X}) = \underline{a}_i^t\, \underline{X} - b_i = 0 \qquad i = 1, 2, \ldots, R \qquad \text{(D.2)}$$

$$C_i(\underline{X}) = \underline{a}_i^t\, \underline{X} - b_i > 0 \qquad i = R+1, \ldots, M \qquad \text{(D.3)}$$

where:

G is an [N x N] positive definite symmetric matrix

$\underset{\sim}{c}$ is an [N x 1] vector

a is a constant

Equation D.2 expresses the 'R' equality constraints and equation D.3 expresses the 'M-R' inequality constraints.

D.3) Optimality Conditions

A point $\underset{\sim}{x}^*$ is a solution to the problem if and only if:

i) $\underset{\sim}{x}^*$ is a feasible point (it satisfies equations D.2 and D.3)

ii) KUHN-TUCKER multipliers λ_i^* can be found such that

$$\nabla F(\underset{\sim}{x}^*) = \sum_{i=1}^{R} \lambda_i^* \nabla C_i(\underset{\sim}{x}^*) + \sum_{i \epsilon I_1^*} \lambda_i^* \nabla C_i(\underset{\sim}{x}^*) \qquad (D.4)$$

$$\lambda_i^* > 0, \quad i \epsilon I_1^* \qquad (D.5)$$

$$I_1^* = \{i \mid C_i(\underset{\sim}{x}^*) = 0, \quad i = R + 1, \ldots, M\} \qquad (D.6)$$

I_1^* is the set of active inequality constraints.

D.4) Main Steps of the Algorithm

STEP 1

At the current feasible point $\underline{x}^{(k)}$, a feasible direction $\underline{p}^{(k)}$ is obtained such that the point $\underline{x}^{(k)} + \underline{p}^{(k)}$ minimizes $F(\underline{x})$ subject to the condition that the presently active constraints remain active. It is possible that $\underline{p}^{(k)}$ is equal to zero. If this is so, then two cases arise:

i) All the KUHN-TUCKER multipliers of the active inequality constraints are greater than or equal to zero (equation D.5 is satisfied). This means that $\underline{x}^{(k)}$ is $\underline{x}^*$ (the solution).

ii) One or more of the KUHN-TUCKER multipliers of the active inequality constraints is negative. The inequality constraint corresponding to the most negative K-T multiplier is released from the active inequality constraint set. A new feasible direction $\underline{p}^{(k)}$ is obtained such that the point $\underline{x}^{(k)} + \underline{p}^{(k)}$ minimizes $F(\underline{x})$ subject to the condition that the revised active constraints remain active and that it is also a feasible point with respect to the constraint just released.

STEP 2

A line search is performed from $\underline{x}^{(k)}$ along $\underline{p}^{(k)}$ on the function $F(\underline{x})$ to obtain the best feasible point $\underline{x}^{(k+1)}$. Set $k = k + 1$ and go to STEP 1.

D.5) Computation of $\underline{p}^{(k)}$

Let $\underline{x}^{(k)}$ be the present feasible point. The vector $\underline{p}^{(k)}$ that will minimize $F(\underline{x})$ subject to the condition that the present active constraints remain active is the solution to

$$\underset{\underline{p}\in R^N}{\text{MIN}} \{Q(\underline{p}) = F(\underline{x}^{(k)}+\underline{p}) = F(\underline{x}^{(k)}) + \tfrac{1}{2}\,\underline{p}^t G\underline{p} + (G\underline{x}^{(k)}+\underline{c})^t\underline{p}+a\} \quad (D.7)$$

$$C_i(\underline{x}^{(k)}+\underline{p}) = (\underline{a}_i^t\underline{x}^{(k)}-b_i) + \underline{a}_i{}^t\underline{p} = 0 \qquad i = 1,2,\ldots,R \quad (D.8)$$

$$C_i(\underline{x}^{(k)}+\underline{p}) = (\underline{a}_i{}^t\underline{x}^{(k)}-b_i) + \underline{a}_i^t\underline{p} = 0 \qquad i\in I_1 \quad (D.9)$$

Where I_1 is the set of active inequality constraints. Given that $\underline{x}^{(k)}$ is a feasible point and that $C_i(\underline{x}^{(k)})=0$, the problem reduces to

$$\underset{\underline{p}\in R^N}{\text{MIN}} \{ Q(\underline{p}) = \tfrac{1}{2}\,\underline{p}^t G\,\underline{p} + (G\underline{x}^{(k)}+\underline{c})^t\underline{p} + a\} \quad (D.10)$$

$$\underline{a}_i^t\underline{p} = 0 \qquad i = 1, 2,\ldots,R \text{ and } i\in I_1 \quad (D.11)$$

Let

R_1 be equal to the number of elements in set I_1.

$t = R + R_1$ be the total number of active constraints at the point $\underline{x}^{(k)}$.

$A^{(k)}$ be the [N x t] matrix whose columns are the $\underline{a}_i$ vectors corresponding to the active constraints. Assume that the rank of $A^{(k)}$ is equal to t.

S be the t-dimensional subspace generated by the columns of $A^{(k)}$

$S^{\perp}$ be the orthogonal complement of S (dimension N-t)

$Z^{(k)}$ be an [N x (N-t)] orthogonal matrix whose columns form a basis for $S^{\perp}$.

Thus, any vector $\underset{\sim}{p}$ that satisfies equation D.11 must be an element of $S^{\perp}$ and can be generated by the matrix $Z^{(k)}$.

$$\underset{\sim}{p} = Z^{(k)} \underset{\sim}{p}_A \tag{D.12}$$

where:

$\underset{\sim}{p}_A$ is an [(N-t) x 1] column vector.

Using equation D.12 reduces the problem to the equivalent unconstrained problem.

$$\underset{\underset{\sim}{p}_A \in R^{N-t}}{\text{MIN}} \left[Q(\underset{\sim}{p}_A) = \tfrac{1}{2} \underset{\sim}{p}_A^t G_p \underset{\sim}{p}_A + \underset{\sim}{g}_p^t \underset{\sim}{p}_A + a \right] \tag{D.13}$$

where:

$$G_p = Z^{(k)t} G Z^{(k)} \tag{D.14}$$

$$\underset{\sim}{g}_p = Z^{(k)t} (G\underset{\sim}{x}^{(k)} + \underset{\sim}{c}) \tag{D.15}$$

Equation D.14 is the projected Hessian matrix of $F(\underset{\sim}{x})$ and equation D.15 is the projected gradient vector of $F(\underset{\sim}{x})$ at $\underset{\sim}{x}^{(k)}$. The minimum point of equation D.13 is given by $\underset{\sim}{p}_A^*$:

$$\underset{\sim}{p}_A^* = - G_p^{-1} \underset{\sim}{g}_p \tag{D.16}$$

thus $\underset{\sim}{p}^{(k)}$ can be obtained using equation D.12

$$\underset{\sim}{p}^{(k)} = Z^{(k)} \underset{\sim}{p}_A^* \tag{D.17}$$

D.6) Line Search along $\underline{p}^{(k)}$

The point $\underline{x}^{(k)}+\underline{p}^{(k)}$ is the minimum point of $F(\underline{x})$ subject to the conditions that the presently active constraints are satisfied. The point may violate some of the presently inactive constraints. If it satisfies all the constraints, it is $\underline{x}^*$.

To determine the new point $\underline{x}^{(k+1)}$, the largest feasible step α_{MAX} along the direction $\underline{p}^{(k)}$ that can be taken without violating any inactive constraints is calculated. The α_i for inactive constraint 'i' is given by solving:

$$C_i(\underline{x}^{(k)} + \alpha_i \underline{p}^{(k)}) = 0 \qquad (D.18)$$

$$i\epsilon I_2, \quad I_2 = M-I_1 \text{ (set of inactive constraints)} \qquad (D.19)$$

for α_i. Using equation D.3, equation D.18 can be reduced to

$$\alpha_i = -\frac{\underline{a}_i^t \underline{x}^{(k)} - b_i}{\underline{a}_i^t \underline{p}^{(k)}}, \quad i\epsilon I_2 \qquad (D.20)$$

The smallest non-zero α_i is chosen as α_{max}:

$$\alpha_{MAX} = \underset{i|\alpha_i > 0}{\text{MIN}} \{\alpha_i\}, \quad i\epsilon I_2 \qquad (D.21)$$

Any value of a greater than α_{max} will be such that the point $\underline{x}^{(k)} + \alpha \underline{p}^{(k)}$ will violate at least one constraint.

The optimum step size along direction $\underline{p}^{(k)}$ is 1. However, if α_{max} is less than 1, then the step size must be reduced to α_{max}. Thus,

$$\alpha_{OPT} = \text{MIN } \{\alpha_{MAX}, 1\} \qquad (D.22)$$

$$\underline{x}^{(k+1)} = \underline{x}^{(k)} + \alpha_{OPT}\, \underline{p}^{(k)} \qquad (D.23)$$

Note that if α_{max} is less than 1, the new feasible point $\underline{x}^{(k+1)}$ activates the inequality constraint corresponding to α_{max}.

D.7) Determination of $Z^{(k)}$.

The formal statement of the problem assumes the range of feasible solutions to be in N-dimensional space. Active constraints reduce the range of solutions to some subspace less than N-dimensions. The search direction $\underline{p}^{(k)}$ is in this smaller subspace. The matrix $Z^{(k)}$ forms the basis of this subspace.

As stated in section D.5, $A^{(k)}$ is an [N x t] matrix whose columns are the $\underline{a}_i$'s corresponding to the 't' active constraints at $\underline{x}^{(k)}$. Matrix $A^{(k)}$ can be premultiplied by an [N x N] orthogonal matrix $Q^{(k)}$ to yield an [N x t] matrix. $Q^{(k)}$ can be chosen so that the resultant matrix has embedded in it an upper triangular matrix $R^{(k)}$ in its first 't' rows and zeros in its last [N-t] rows.

$$Q^{(k)}\, A^{(k)} = \begin{bmatrix} R^{(k)} \\ \hline 0 \end{bmatrix} \begin{matrix} t \\ N-t \end{matrix} \qquad (D.24)$$

The process whereby $Q^{(k)}$ is determined so as to yield $R^{(k)}$ is called the QR factorization of $A^{(k)}$. This factorization is accomplished by using the Givens transformation to construct orthogonal Givens matrices and then multiplying the matrices together to yield $Q^{(k)}$ and subsequently $R^{(k)}$. Assuming the rank of $A^{(k)}$ to be 't', the matrix $R^{(k)}$ is nonsingular.

The matrix $Z^{(k)}$ is obtained by partitioning $Q^{(k)}$.

$$Q^{(k)} = \begin{bmatrix} Q_1^{(k)} \\ \hline Q_2^{(k)} \end{bmatrix} \begin{matrix} t \\ \\ N-t \end{matrix} \qquad \text{(D.25)}$$

$$Q_1^{(k)} \, Q_2^{(k)^t} = 0 \qquad \text{(D.26)}$$

$$A^{(k)} = Q_1^{(k)^t} \, R^{(k)} \qquad \text{(D.27)}$$

Equation D.26 implies that the column space of $A^{(k)}$ is the same as the column space of $Q_1{}^{(k)^t}$. Equations D.26 and D.27 combined imply that the column space of $Q_2{}^{(k)^t}$ is orthogonal to the column space of $A^{(k)}$. The columns of $Q_2{}^{(k)^t}$ are orthogonal. Thus,

$$Z^{(k)} = Q_2^{(k)^t} \qquad \text{(D.28)}$$

Every time the basis of active constraints is modified, a new $A^{(k)}$ matrix is formed. Thus the QR factorization must be applied to the new $A^{(k)}$ to produce a new $Z^{(k)}$.

D.8) Determination of Kuhn-Tucker Multipliers

Let $\underline{x}^{(k)}$ be a feasible point. Equation D.4 can be written

$$A^{(k)} \lambda^{(k)} = \nabla F(\underline{x}^{(k)}) \tag{D.29}$$

where:

$\lambda^{(k)}$ is the Kuhn-Tucker multiplier vector corresponding to the point $\underline{x}^{(k)}$.

Equation D.29 can be solved by replacing $A^{(k)}$ by its QR factorization

$$A^{(k)} = Q^{(k)t} \begin{bmatrix} R^{(k)} \\ \hline 0 \end{bmatrix} \tag{D.30}$$

Recall that $Q^{(k)}$ is orthogonal so $Q^{(k)^{-1}} = Q^{(k)^t}$. Substituting equation D.30 into equation D.29 yields

$$Q^{(k)t} \begin{bmatrix} R^{(k)} \\ \hline 0 \end{bmatrix} \lambda^{(k)} = \nabla F(\underline{x}^{(k)}) \tag{D.31}$$

partitioning $Q^{(k)^t}$ gives

$$\left[Q_1^{(k)t} \vdots Q_2^{(k)t} \right] \begin{bmatrix} R^{(k)} \\ \hline 0 \end{bmatrix} \lambda^{(k)} = \nabla F(\underline{x}^{(k)}) \tag{D.32}$$

Recalling that $Q_1^{(k)^{t^{-1}}} = Q_1^{(k)}$, equation D.32 becomes

$$R^{(k)} \lambda^{(k)} = Q_1^{(k)} \nabla F(\underline{x}^{(k)}) \qquad (D.33)$$

$R^{(k)}$ is upper triangular and $Q_1^{(k)} \nabla F(\underline{x}^{(k)})$ is a vector, so equation D.33 can be solved by backward substitution.

D.9) Comments

This algorithm is computationally very fast. If the initial point chosen, $\underline{x}^{(0)}$, is fully constrained (i.e. N inequality constraints active), the algorithm will find a solution in at most N iterations. This is due to the fact that every iteration reduces the solution range by one dimension.

An outline of the algorithm is given in figure D.1. The algorithm implemented does not deal with equality constraints, as discussed in section D.1.

Outline of optimization algorithm

Figure D.1

0) INPUTS: G, $\underline{c}$, CON, $\underline{x}^{(0)}$, N, NC

G is the [N x N] matrix

$\underline{c}$ is the [N x 1] vector

$\underline{x}^{(0)}$ is the initial point

N is the dimension of the problem

NC is the number of inequality constaints

CON is the [N x NC] matrix of constraints

1) Determine if G is positive definte.

YES: goto 2 NO: exit

2) Set matrix Q equal to the [N x N] identity matrix.

3) Determine the set of active constraints.

4) Are there any active constraints ?

YES: goto 5 NO: goto 11

5) Build the active constraint matrix and QR factor it

6) Is the number of active constraints less than N ?

Yes: goto 11 NO: goto 7

7) Form $\nabla F(\underline{x}^{(k)})$. Is $||\nabla F(\underline{x}^{(k)})|| < 10^{-4}$?

YES: exit NO: goto 8

8) Are there any active constraints ?

YES: goto 9 NO: goto 11

9) Determine Kuhn-Tucker multipliers.

Are any of them negative ? (see notes)

YES: goto 10 NO: exit

10) Release constraint corresponding to the most negative Kuhn-Tucker multipier.

Update active constraint matrix and QR factor it.

11) Find search direction $\underset{\sim}{p}^{(k)}$.

12) Determine α_{OPT}. Form $\underset{\sim}{x}^{(k+1)} = \underset{\sim}{x}^{(k)} + \alpha_{OPT}\, \underset{\sim}{p}^{(k)}$.

If $\alpha_{OPT} < 1$, activate the corresponding constraint, update the active constraint matrix and QR factor it.

13) Go to 7

NOTES:

If all the K-T multipliers are positive and 'N' constraints are active then the solution has been found.

If all the K-T multipliers are positive and less than 'N' constraints are active then a line search is done to eliminate the possibility of finding a solution with positive K-T mults that can still be minimized.